"EFFECT OF WIND INDUCED ON LOW RISE BUILDINGS WITH MONO-SLOPE ROOF"

A DISSERTATION

SUBMITTED IN PARTIAL FULFILLMENT OF THE
REQUIREMENT FOR THE AWARD OF THE DEGREE OF

MASTER OF TECHNOLOGY

IN

STRUCTURAL ENGINEERING

Submitted by:

NITISH BHARDWAJ
(2K20/STE/16)

Under the Supervision of

DR. RITU RAJ

DEPARTMENT OF CIVIL ENGINEERING

DELHI TECHNOLOGICAL UNIVERSITY

(Formerly Delhi College of Engineering)

Bawana Road, Delhi-110042

JUNE 2022

DEPARTMENT OF CIVIL ENGINEERING

DELHI TECHNOLOGICAL UNIVERSITY

(Formerly Delhi College of Engineering)

Bawana Road, Delhi-110042

CANDIDATE'S DECLARATION

I, Nitish Bhardwaj Roll No. (2K20/STE/16) student of Master of Technology in Structural Engineering hereby declare that the project Dissertation entitled "**Effect of wind-induced on low rise buildings with the mono-slope roof**" which is submitted by me to the Department of Civil Engineering, Delhi Technological University, Delhi in partial fulfillment for the requirement for the award of the degree of Master of Technology is original and not copied from any source without proper citation. This work has not previously formed the basis for the award of any Degree, Diploma Associateship, Fellowship, or other similar title or recognition.

(NITISH BHARDWAJ)

DEPARTMENT OF CIVIL ENGINEERING

DELHI TECHNOLOGICAL UNIVERSITY

(Formerly Delhi College of Engineering)

Bawana Road, Delhi-110042

Date: -

CERTIFICATE

I hereby certify that the project Dissertation entitled, "**Effect of wind induced on low rise buildings with mono-slope roof**", " which is submitted by Nitish Bhardwaj Roll No.(2K20/STE/16) student of Master of Technology in Structural Engineering , Department of Civil Engineering, Delhi Technological University, Delhi in partial fulfillment of the requirements for the award of the degree of Master of Technology , is a record of the project work carried out by the student under my supervision. To the best of my knowledge this work has not been submitted in part or full for any Degree or Diploma to this University or elsewhere.

Place: Delhi **(DR. RITU RAJ)**

Date: **SUPERVISOR**

ABSTRACT

In this research study, we performed a comprehensive analysis of a low rise building at varying roof angles like 10°, 20 ° and 30 ° using ANSYUS CFX software package.

The interference effect is analysed of similar low-rise building placed at different spacing, the spacing was from 0 to 2b with incremental increase in width of b/2 i.e. 0, b/2, b, 3b/2 and 2b. Also, the direction of wind incidence was varied from 0 ° to 180 °.

Ansys CFX fluid flow package has been used to carry out the simulations using a standard k-ε turbulent model. The simulations have been carried out for 5 wind incidence angles at an interval of 45°. The comparison of the roofs is done for the coeffient of pressure .

The value of coeffient of internal and external pressure were also computed. The values of coeffient of pressure were varying with roof angles and considerable increase in the coeffient of pressure can be seen. The coeffient of internal pressure was maximum for the front building.

The coeffient of pressure due to interference effect was seen to be higher for wind direction from 90 ° to 180 ° as compared to 0 ° to 90 ° and coefficient of pressure and coeffient of pressure decreases with increase in spacing.

ACKNOWLEDGEMENTS

This research work is the final output of my two years master's degree in Structural Engineering at the Delhi Technological University (DTU), New Delhi, India. I would therefore like to express my very great appreciation to the staff of Delhi Technological University (DTU) for their steadfast academic and administrative support, without which this work would not have been successful.

I wish to express my deepest gratitude to my research supervisor, Prof, Dr. Ritu Raj, Assistant Professor in the Department of Civil Engineering, Delhi Technological University, Delhi for their invaluable guidance, enduring patience, and nurturing support throughout this research without which successful completion would not have been possible. The knowledge and wisdom I have gained from them will forever guide me in education and life.

I extend my appreciation to my family members for their incessant encouragement and support to complete this course. I am also very much thankful to the wonderful moments and experiences shared with all the friends that I met throughout this study programme. These acknowledgements would be incomplete without mentioning the almighty for bringing this day in my life.

NITISH BHARDWAJ

TABLE OF CONTENTS

LIST OF FIGURES

LIST OF TABLES

CHAPTER-1

INTRODUCTION

1.1 GENERAL

Over the last several years, costly disasters have been particularly destructive, and the cyclone is the most dangerous [1] and table 1 shows the statistics from past reports. Cyclones are dominating not only in the number of deaths, but they are causing about 50 percent of total losses by all-natural disasters [2]. Due to the high cost of cyclone-proof construction, or may be technology is away from the reach of cyclone-prone area residents a vast number of people become homeless. That is why cyclone-proof construction and wind load resistance require more research work in this area.

1.2 TYPES OF STRUCTURES

1.2.1 Based on Height

Based on the height of a structure, building structures can be broadly classified into two types viz. the low-rise structures and the high-rise structures. A low rise structure is primarily a building with a height of less than 20 m, whereas a high-rise structure, generally, has a height of 50 m or more above the mean ground level which is the average horizontal plane of the area enclosed by the boundaries of the structure. Structures with a height between 20 m to 50 m are termed mid-rise buildings. Other sub classifications among high-rise buildings according to their height may also exist like sky-rise buildings (between 150 m to 300 m), super-tall buildings (between 300 m to 600 m), or mega-tall buildings (above 600 m). Depending upon the height of the structure, the load calculations and the design criteria vary. High-rise buildings generally experience higher lateral wind loads on their vertical faces, especially at higher storeys, leading to extreme pressure and high wind forces. However, the low-rise structures are projected well within the earth's atmospheric surface layer where wind flow is difficult to quantify.

1.2.2 Based on usage

Different types of roofed buildings are widely used in coastal areas of India as well as all around the world which need more focus. Most of the low-rise buildings that are built for the residential purpose have simple roof forms such as flat or sloping roofs. Many studies have been done on the different roofs like Flat roofs, mono slope roofs, canopy roofs, gable roofs, hip roofs, pyramidal roofs, saw-tooth roofs, multi-span gable roofs, mansard roofs, troughed roofs, domed roofs, curved roofs, arched roof, and stepped roofs by using various numerical and theoretical approaches.

1.3 LOADS ON STRUCTURE

A structure can be subjected to various types of loads as mentioned in Fig. 1.1 which are described as follows:

1. Dead Load: They are the permanent loads acting on the structures which do not change their position with time. They include the self-weight of the structural members, weight of the fixed components in the buildings, permanent partition walls, etc. The values to be considered for different components are given in IS 875 Part 1 (1987).

2. Imposed Load: Also known as live loads, they consist of the movable components of the loads which can simply move to change their position in the building without any acceleration or impact. The magnitude of the live load to be considered depends on the occupancy and the type of use of the building. The provisions to be adopted for Imposed Loads are given in IS 875 Part 2 (1987).

3. Wind Load: They consist primarily of the lateral load exerted by the wind flow which exerts pressure on the faces of the buildings and their roofs. The provisions for estimation of the Wind loads are given in IS 875 Part 3 (2015).

4. Snow Load: As the name suggests, the snow loads are the loads acting on the structure due to snow. Since snowfall is not a common phenomenon in larger parts of India, the effect of snow load needs to be taken into account only in the regions experiencing snowfalls. The relevant provisions are given in IS 875 Part 4 (1987).

5. Earthquake Load: Earthquakes occur due to the movements of the tectonic plates which generate seismic waves in horizontal as well as vertical planes. The vertical loads exerted by the earthquake are generally not very critical. However, the horizontal forces exerted on the superstructure may cause sudden displacement of the superstructure in the horizontal plane which may lead to failure of the structure.

1.4 VARIOUS FACTORS AFFECTING WIND LOAD

The roof shape, roof slope and the wind direction play an important role in the structural safety of buildings to counter the wind load [2-3]. The pressure distribution generated over a building by wind is determined principally by the shape of the building. For basic building forms there are but four primary shape parameters - height, span, length and roof pitch. Following are the various factors that affect the Wind load-

a) Roof Angle
b) Roof Shape
c) Height of Building
d) Interference Effect
e) Aspect Ratio
f) Direction of Wind

All the buildings are exposed to the atmospheric wind and experience a significant wind load, so it can be considered as one of the most important factors for calculating the interference effect also. Interference effect also depends on the position of the building related to the nearby structures.

1.5 DAMAGES TO STRUCTURE DUE TO WIND LOAD

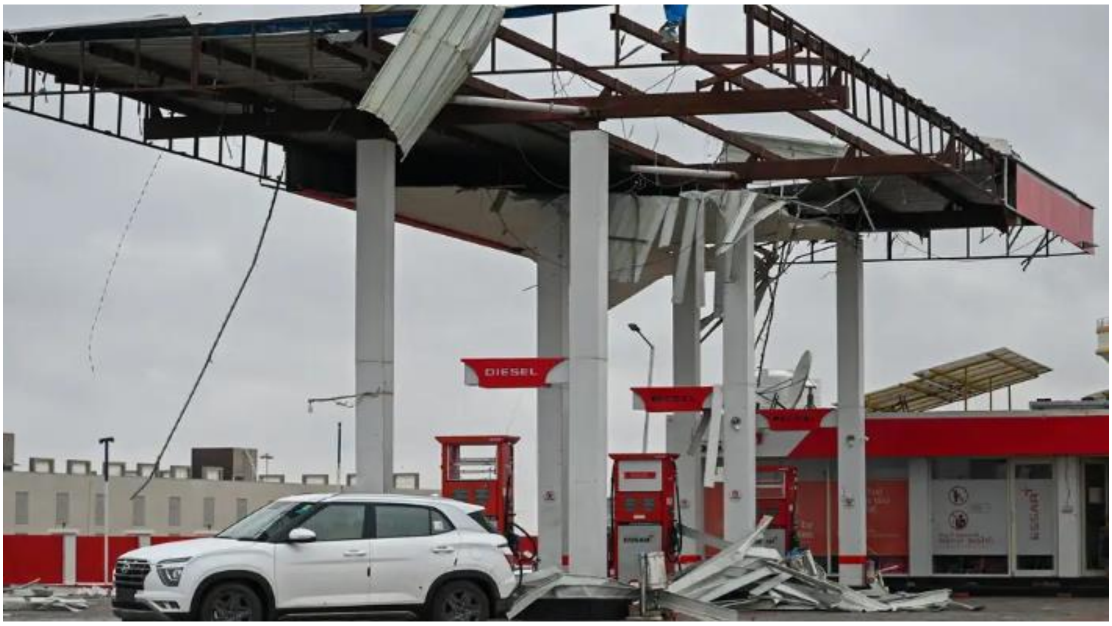

Fig.1.1 A damaged fuel station can be seen after the impact of Cyclone Tauktae near Amreli on May 18, 2021. (Punit Paranjpe/AFP via Getty Images)

Fig. 1.2 Aerial view of damaged roofs due to high-speed wind in Texas, 2022.

Table No.1.1 Billion-dollar events to affect the U.S. from 1980 to 2019* (CPI-Adjusted)[1]

S. N.	Disaster Type	No. of Events	Percent Frequency	CPI-Adjusted Losses (Billions Dollars)	Percent of Total Losses	Average Event Cost (Billions Dollars)	Deaths
1	Draught	26	10.1%	$249.7	14.2%	$9.6	2993
2	Flooding	32	12.4%	$146.5	8.3%	$4.6	555
3	Freeze	9	3.5%	$30.5	1.7%	$3.4	162
4	Severe Storm	113	43.8%	$247.8	14.1%	$2.2	1642
5	Tropical Cyclone	44	17.1%	$945.9	53.9%	$21.5	6502
6	Wildfire	17	6.6%	$84.9	4.8%	$5.0	347
7	Winter Storm	17	6.6%	$49.3	2.8%	$2.9	1048
8	All Disasters Disasters	258	100.0 %	$1754.36	100.0 %	$6.8	13249

The wind-resistant structures can save lives and prevent property damage during the cyclone. Available information in wind codes regarding wind pressure coefficients on roofs in general is very limited. Although there have been many research works conducted to investigate the wind forces on buildings with unconventional plans, there is still a need to fill some research gaps.

1.6 WIND FLOW AROUND THE BODY

The wind is a flow of air over the surface of the earth, and the projections over the earth’s surface, which include natural features, buildings, bridges, etc. are affected by the wind flow. Wind applies pressure and frictional or viscous forces on the buildings and other structures. Due to less density of air, the magnitude of buoyant forces is very less and thus, can be neglected.

1.7 EXTERNAL AND INTERNAL PRESSURE CAUSING MECHANSIM

Due to the modification in the airflow around a building, the wind pressure is developed over the external surfaces of the building. High-pressure regions are developed in the regions where the divergence of streamlines is observed and low-pressure regions are developed where the streamlines converge. Due to the presence of the building as a bluff body, boundary layer separation occurs as discussed above, and generates large eddies, which lead to the development of high local suction, i.e., negative wind pressure in localized areas over the surface.

The wall on the windward side is completely exposed to the wind flow and therefore, positive pressure acts on its surface. Apart from external pressures, wind flow action also exhibits its effect on the internal surfaces of the building. Wind can enter the structure through small vents or gaps through doors or windows and can cause considerable pressure variation on the internal walls.

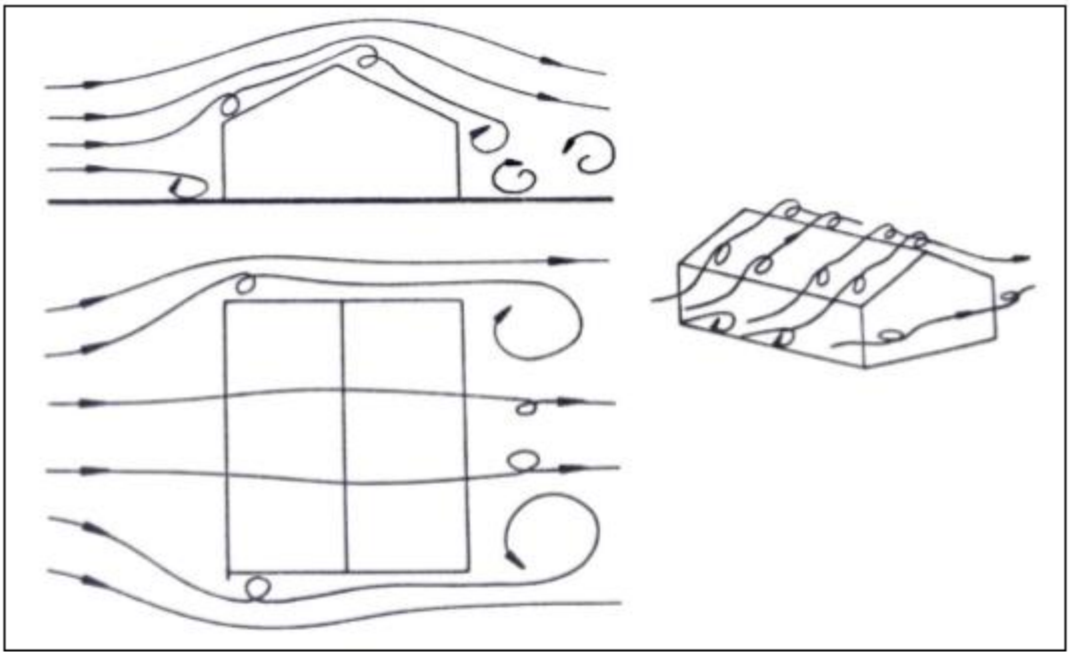

Fig 1.3 Wind Flow over a Low Rise Pitched Roof Type Structure

The structural components of a building are usually designed to resist the wind load acting in the form of a total drag force. However, the design of surface elements like wall tiles/panels or roof cladding panels are affected by the difference in pressures at external and internal surfaces

1.8 WIND PROFILE

Wind profiles are the plots of the flow velocity of wind over a surface of a body obstructing the free stream flow of wind. It gives the variation of wind velocities with height. For the CFD study of wind loads, accurate numerical modeling of the wind profile is necessary to minimize errors. The commonly adopted wind profiles are a power law, uniform flow profile, logarithmic flow profile, etc. The power law is given by

$$u_z = u_{ref} \times (\frac{\mathrm{z}}{\mathrm{zref}})^{\alpha}$$

Where u_z is the wind velocity at height z, u_{ref} is the wind velocity at a reference height of z_{ref}, and α is the power law exponent and its value is different for different terrain conditions. For open terrain conditions, α is usually taken to be equal to 0.143.

Logarithmic law is also used in some cases, to model the wind velocity profile and is given by

$$u_z = u* \; k \times \ln(\frac{z}{z0})$$

where u* is the friction velocity, k is the Von Kármán constant (k ≈ 0.41), z0 is called roughness length, and is a characteristic of the terrain. For open flat terrain, z_0 is in the range of 0.001 m - 0.005 m and for dense urban areas, it can go as high as 5 m.

The logarithmic wind profile matches more closely for modeling wind speeds for lower 10 to 20 m heights and the power-law produces a better profile for structures having over 100 m heights. In the intermediate zones, both power-law and logarithmic law may be used for modeling the wind profile.

The calculation of wind load for a simple shaped building can be done with the help of different national and international wind codes. But these codes generally give the idea of a direct wind attack on the building. If the wind comes from any inequitable angle and the building is not regular, then the calculation of extreme wind load cannot be done properly through the wind codes. CFD simulation gives beneficiary results in the aspect of time and cost.

1.9 NEED FOR THE STUDY

As stated above, there is a need to study about the wind pressure on the low-rise building in a time and cost-efficient manner. And among all available methods of wind load analysis, CFD can provide comprehensive and useful information and has become a common and attractive design tool for calculating wind load. CFD simulation is a multi-functional and exceptionally beneficial apparatus, and is thus the ultimate tool for assessing the unsteady aerodynamic forces on the pulsating roofs in a widespread reduced occurrence range.30 CFD decreases both times and cost in design and investigation, and offers thorough and visualized information.24,81

1.10 AIM OF THE STUDY

This study aims at studying the wind pressure on the low-rise building to prevent property damage in Cyclones. Wind pressure values on a building roof get modified due to the presence of a nearby building, such information is not available in the code of practices.

This work also sets sights on further decreasing both time and cost in design and investigation, and offers thorough and visualized information by using CFD simulation.

1.11 OBJECTIVES

Following are the objectives that formulated for this research work has been outlined as:

i. To evaluate of coefficient of pressure on the mono slope roof.

ii. To evaluate the coefficient of pressure on mono slope roof with different roof angle

iii. To investigate the interference effect when multiple buildings are placed at different spacing.

iv. To study the variation of pressure coefficient distribution at various wind direction angles (0 ° to 90 °).

1.12 OUTLINE OF THE THESIS

A brief description of the major chapters/parts with key points has been outlined below as the blueprint of this research work.

CHAPTER 1: INTRODUCTION deals with the introduction part, which discusses various parameters for calculating the wind load followed by methods to evaluate the wind loads. The last section discusses the aim, followed by the objectives of the present research work.

CHAPTER 2: LITERATURE REVIEW describes the summary of the reviewed literature to find out the research gaps. Firstly, the literature related to pressure and force measurement. The last section presents the summary of reviewed literature about CFD and full-scale measurements.

CHAPTER 3: METHODOLOGY AND VALIDATION MODEL describes the sequential steps that are followed to obtain the results for this experimental study.

CHAPTER 5: RESULTS AND DISCUSSION explains the concepts behind the results of the experimental study related to the pressure measurements on low-rise building models at different interference conditions.

CHAPTER 6: CONCLUSION represents the conclusions drawn from the present study. The future scope of the study is also discussed.

CHAPTER-2 LITERATURE REVIEW

2.1 OVERVIEW AND RESEARCH CARRIED OUT

The review of literature provides a summary of information gathered through consultation of various publications, articles, manuals, reports and tools employed by previous researchers and stakeholders, forming the basis of desk study in any investigation as well as devising appropriate problem-solving methodologies.

Many researchers have used different methods for the investigation of wind forces on roofs of low and high-rise structures.

This chapter discusses the relevant literature to address the research gaps and develop a theoretical framework and methodology for the present research study.

J.D. Holmes (1988) Total forces both horizontal and vertical on the end bay of a low rise industrial building model are consistent.

R P Hoxey et al.,(1993) The pressure distribution generated over a building by wind is determined principally by the shape of the building. For basic building forms there are but four primary shape parameters - height, span, length and roof pitch.

Prem Krishna (1995) that lateral strength is mainly governed by wind loads

T. Stathopoulos et al., (1996) the implementation of the AR model for the design of monoslope roof buildings requires consideration of the influence of wind direction, building height and roof slope on its parameters.

Masanao Nakayama et al., (1998) method is verified through a numerical simulation of the wind response of a spherical dome.

C.W. Letchford et al., (2000) lift forces decrease while for low roof pitches drag forces increase as porosity is increased in the range 0-23%.

P. Montes et al., (2001) Comparison of the behavior of the dome was studied with and without exterior concrete ribs.

Roy, A.K (2010) roof pitches are affected by wind forces most significantly. Also, the corner roof is under high suction pressure.

C.M. Cheng et al., (2010) flow separation is studied for a range of Reynolds Number.

Alireza Fiouz et al., (2012) Wind load leans to pull dome in up-ward direction, and with increase rise-to-span ratio, its value will increase. Wind load leans to induce an overturning moment in the foundation and its value will decrease with an increasing rise-in the to-span ratio of domes.

Xingqian Peng et al., (2012) wind pressure distribution and the influence on roof wind load by wind direction and the high of the hill is determined.

Augusto Poitevin et al., (2013) two independent methodologies were used to obtain pressure coefficients: wind tunnel testing and Computational Fluid Dynamic (CFD) modeling.

M.B. Natalini et al., (2013) mean wind load coefficients on VCRs obtained in boundary layer tunnel tests.

Yan Zhang et al., (2014) the effect of the geometric scale of a model on the mean wind loads in the outburst region is minor when it is within a blockage ratio of 3% as tested in the study.

Astha Verma et al., (2015) Wind pressure values are measured at many points of multi-span cylindrical roofs.

Rocky Patel et al., (2015) Base dimensions of wind ward face obstructing the wind flow govern the domain size.

Astha Verma et al.,(2017) major portions of the domes are subjected to suction and small portions are subjected to pressure under the wind.

Fabio Rizzo et al., (2017) wind loading of buildings provided with a hyperbolic paraboloid roof is different from that of the same building provided with a different roof shape.

Gang Li et al., (2017) for the regular group of low-rise buildings, larger interference effects occurred on the corners or outer parts of the groups.

Mazdi Yousef (2017) one typical tornado parameter was considered for comparison. The tornado force coefficients on the cube and prisms were larger than those on the dome by at least 90% in the x-y direction, and 140% in the z-direction. The tornado pressure coefficients on the cube and prisms were greater than at least 200.

Neelam Rani et al.,(2017) Pressure coefficients are obtained for upper and lower roof surfaces separately.

Bo Chen et al., (2018) increasing the height of the high-rise building or decreasing the spacing induces an increase in positive pressures.

J. Singh et al., (2018) the result reveals that a pyramidal roof has much better chances of survival in comparison with other roof shapes.

Nourhan Sayed Fouad et al., (2018) the structural design of the building includes the calculation of the applied wind loads as one of the major items in the design process.

Jagbir Singh et al., (2019) the pressure coefficients for building models without openings are almost twice or three times that of the pressure coefficients for models with openings.

Zhixiang Liu et al., (2019) The roof shapes remarkably affect the surrounding wind conditions at the pedestrian level.

Juliya Mironova (2020) the pressure affects not only neighboring high-rises, but also it has an impact on low-rise existing ones.

Prasenjit Sanyal et al.,(2020) result shows the variability of wind load and pressure due to changes in the building side ratio.

Suman Kumar Laha et al., (2020) the simulation has been carried out by fixing the inclination angle of the panel at 25 through ANSYS Fluent software. The maximum stress which has been found here is 4196.4 Pa at 260 km/h wind speed when the maximum structural deformation has also been noticed.

Singh Jagbi et al. (2021) effects of roof shape, roof slope, aspect ratio, interference effect, etc are discussed. Post-tornado research has shown that building rooftops are critical elements that often suffer severe damage.

CHAPTER -3 METHODOLOGY AND VALIDATION

Following are the sequential steps that are followed to obtain the results for this Experimental study.

- Design of Geometry of the building
- Selection of Validation Model from IS Code 875 part 3
- Importing the Geometry of Building and Domain consideration
- Validation through IS Code 875 part 3
- Meshing and Inflation for Simulation
- Boundary-Layer Condition and Flow Physics
- Calculation of the coefficients of Pressure (External and Internal)
- Study of Interference effect with various spacing and having different Wind directions

3.1 DESIGN OF GEOMETRY OF THE BUILDING

For the analysis, a rectangular plan of the structure of 100mmx50mm with a height of 50mm, having a column size of 3mmx3mm is to be investigated for the wind-induced pressure and interference effect due to placing more similar structures having different spacing. A scale of 1:100 has been adopted in this study. The roof angle has been varied at an equal interval of 10° up to 30^0.

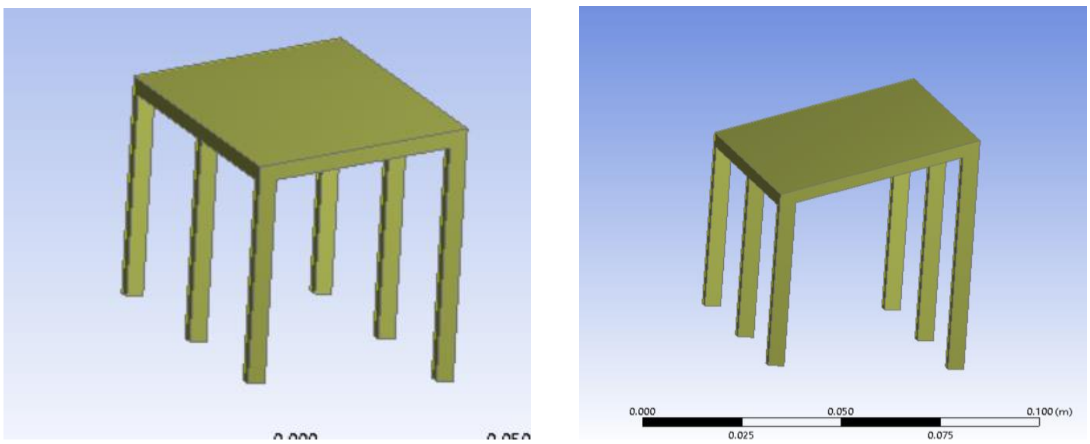

Fig. 3.1 Structure at Roof Angles 10^0 and 20^0

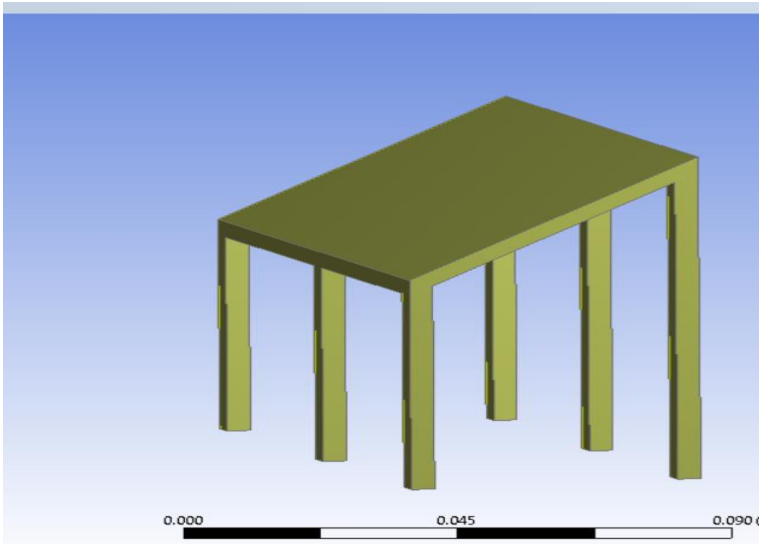

Fig. 3.2 Structure at Roof Angles 30^0

3.2 SELECTION OF VALIDATION MODEL FROM IS CODE 875 PART 3

The meshing and setup in the Ansys CFX need to be validated first with the wind standards of Wind Loads on Building and Structures IS 875 part 3.

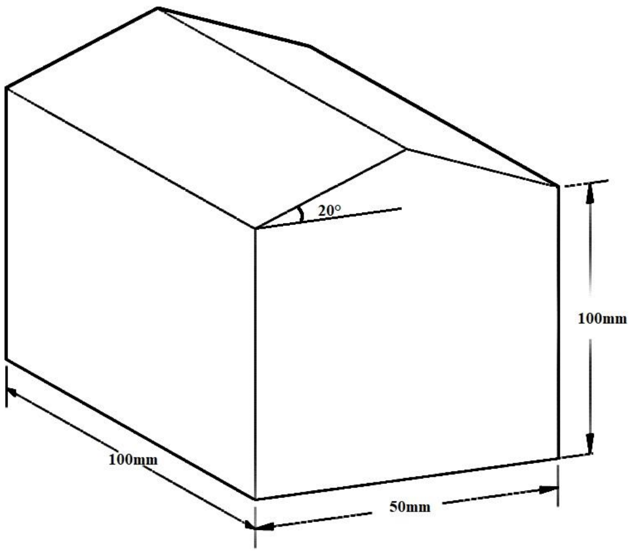

Fig. 3.3 validation model

3.3 IMPORTING THE GEOMETRY OF BUILDING AND DOMAIN CONSIDERATION

Franke et al., (2004) have provided recommendations for CFD applications in wind engineering [42]. The domain size is taken by the recommendations so that the reflection of fluid flow from the domain boundary does not alter the fluid interaction with the model. Accordingly, the inlet and outlet distances were kept as 5H and 15H respectively, where H is the maximum height of the model. The sides of the domain walls and the top clearance from the model roof were kept as 5H each. The domain is shown in Fig.

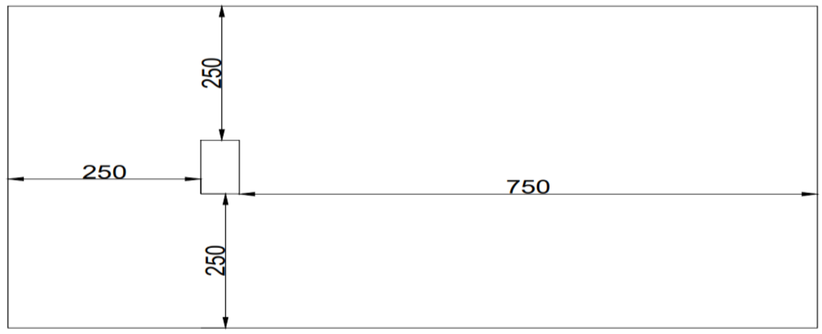

Fig 3.4 plan of Domain

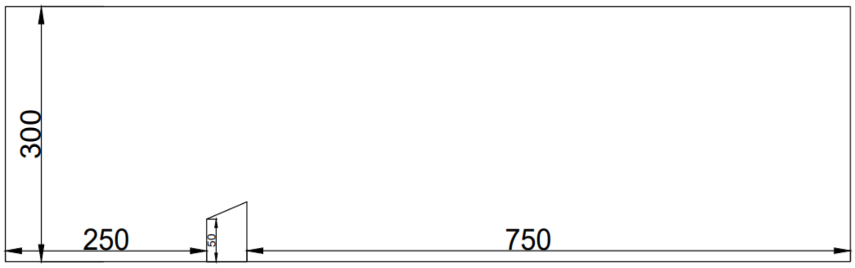

Fig 3.5 Elevation of Domain

3.4 VALIDATION THROUGH IS CODE 875 PART 3

The coefficient of pressure values in various international codes/standards deviate from each other and CFD values are within reasonable bounds of 15 to 20%. A wind pressure coefficient is a dimensionless number which gives describes the relative wind pressure in the wind flow field. The coefficient of pressure values in various international codes/standards deviate from each other and CFD values are within reasonable bounds of 15 to 20%.

$$Cp = \frac{\text{Pressure}}{\frac{1}{2}\,\rho . V2} \qquad \text{Equation 3.1}$$

Where Pressure is the relative pressure acting at a particular point, ρ is the density of air which is equal to 1.225 kg/m^3, and V is the Velocity of wind provided at the building's apex which is equal to 10 m/s.

3.5 MESHING AND INFLATION FOR SIMULATION

The domain volume meshing grid size was finalized as 0.02 m and the model faces and roof meshing sizes as 0.01 m; much smaller as the focus of the present study is to map the pressure effect on the roofs of the model. A mesh diagram showing the variation in the sizes of the tetrahedrons of the mesh for the validation model is shown in Fig. 3.7

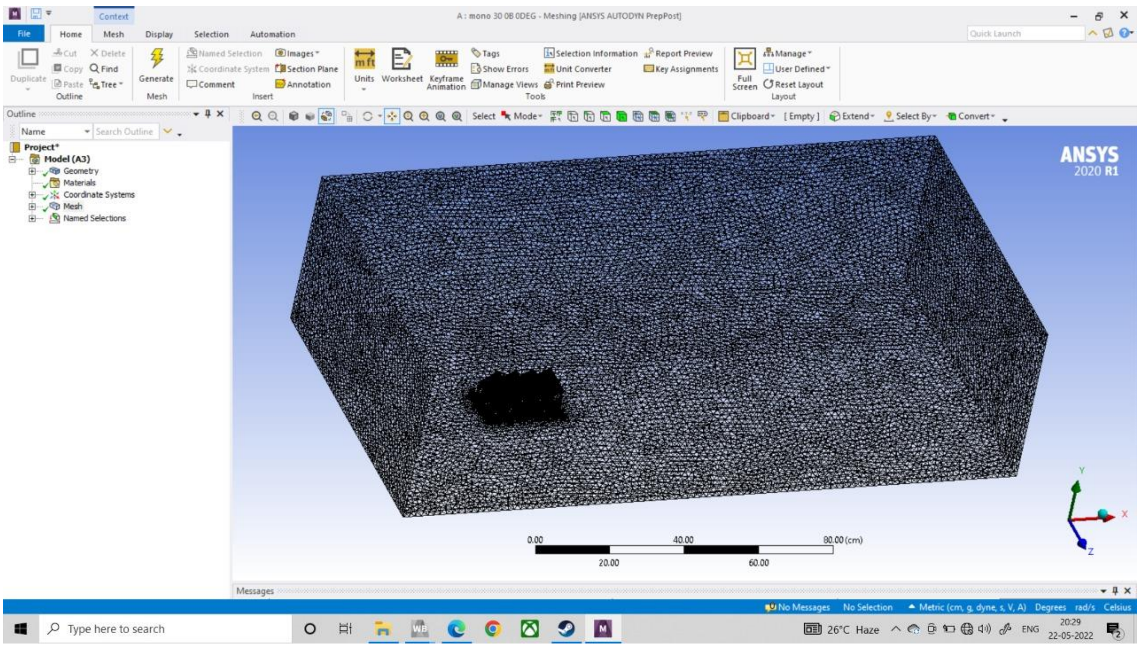

Fig. 3.6 Isometric View of Domain Meshing of Model

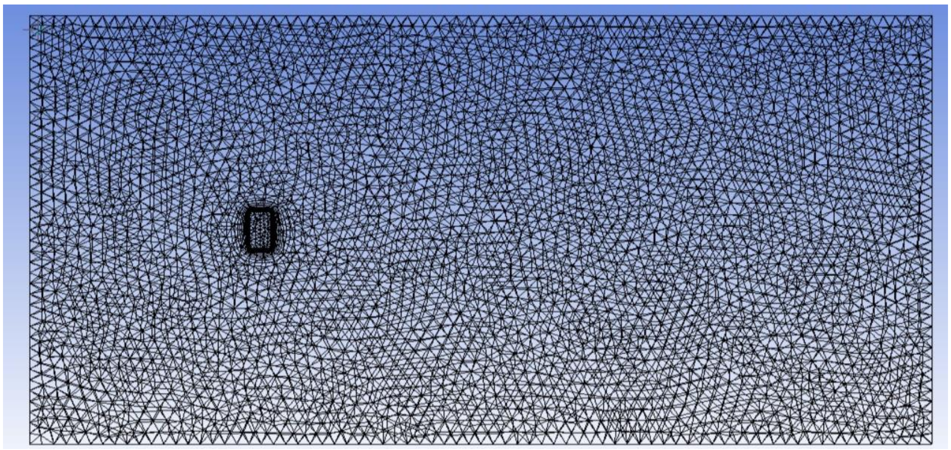

Fig. 3.7 Top View of Domain Mesh of Validation Model

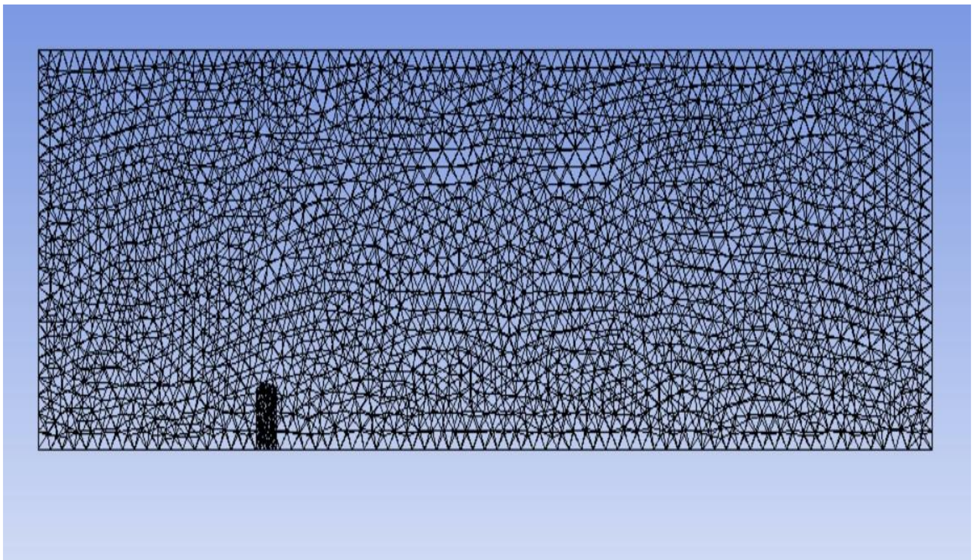

Fig. 3.8 Side View of Domain Mesh of Validation Model

3.6 BOUNDARY LAYER CONDITION AND FLOW PHYSICS

Domain Side Walls- Free Slip Walls

Building walls, Roof, Ground-No Slip Walls

Inlet: Normal Velocity -10m/s

Outlet: Average Static Relative Pressure of 0 Pa

The domain sides and top were defined as free slip walls. The model faces and the ground were defined as no-slip walls (Vwall = 0) which means a component of fluid velocity along the boundary of the wall is zero. Relative pressure at the outlet was defined with 0 Pa. A uniform homogeneous wind flow with a velocity of 10 m/s has been provided at the inlet of the domain.

3.7 CALCULATION OF THE COEFFICIENT OF PRESSURE (EXTERNAL AND INTERNAL)

This section contains a detailed analysis of the pressure coefficient contours. The pressure coefficient over the external and internal surfaces over the rectangular structure is discussed as per equation 3.1. The Pressure Coefficient contours are then validated.

Fig.3.9 External Pressure Coefficients (Cpe) for Pitched Roofs of Rectangular Clad Buildings [IS 875 Part 3]

Building Height Ratio		Roof Angle α	Wind angle θ 0°		Wind angle θ 90°		Local Coefficients			
		Degrees	EF	GH	EG	FH				
$\frac{h}{w} \leq \frac{1}{2}$	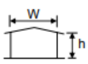	0	-0.8	-0.4	-0.8	-0.4	-2.0	-2.0	-2.0	---
		5	-0.9	-0.4	-0.8	-0.4	-1.4	-1.2	-1.2	-1.0
		10	-1.2	-0.4	-0.8	-0.6	-1.0	-1.4		-1.2
		20	-0.4	-0.4	-0.7	-0.6	-0.8			-1.2
		30	0	-0.4	-0.7	-0.6				-1.1
		45	+0.3	-0.5	-0.7	-0.6				-1.1
		60	+0.7	-0.6	-0.7	-0.6				-1.1
$\frac{1}{2} < \frac{h}{w} \leq \frac{3}{2}$	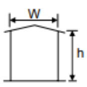	0	-0.8	-0.6	-1.0	-0.6	-2.0	-2.0	-2.0	---
		5	-0.9	-0.6	-0.9	-0.6	-2.0	-2.0	-1.5	-1.0
		10	-1.1	-0.6	-0.8	-0.6	-2.0	-2.0	-1.5	-1.2
		20	-0.7	-0.5	-0.8	-0.6	-1.5	-1.5	-1.5	-1.0
		30	-0.2	-0.5	-0.8	-0.8	-1.0			-1.0
		45	+0.2	-0.5	-0.8	-0.8				
		60	+0.6	-0.5	-0.8	-0.8				
$\frac{3}{2} < \frac{h}{w} < 6$	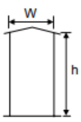	0	-0.7	-0.6	-0.9	-0.7	-2.0	-2.0	-2.0	---
		5	-0.7	-0.6	-0.8	-0.8	-2.0	-2.0	-1.5	-1.0
		10	-0.7	-0.6	-0.8	-0.8	-2.0	-2.0	-1.5	-1.2
		20	-0.8	-0.6	-0.8	-0.8	-1.5	-1.5	-1.5	-1.2
		30	-1.0	-0.5	-0.8	-0.7	-1.5			
		40	-0.2	-0.5	-0.8	-0.7	-1.0			
		50	+0.2	-0.5	-0.8	-0.7				
		60	+0.5	-0.5	-0.8	-0.7				

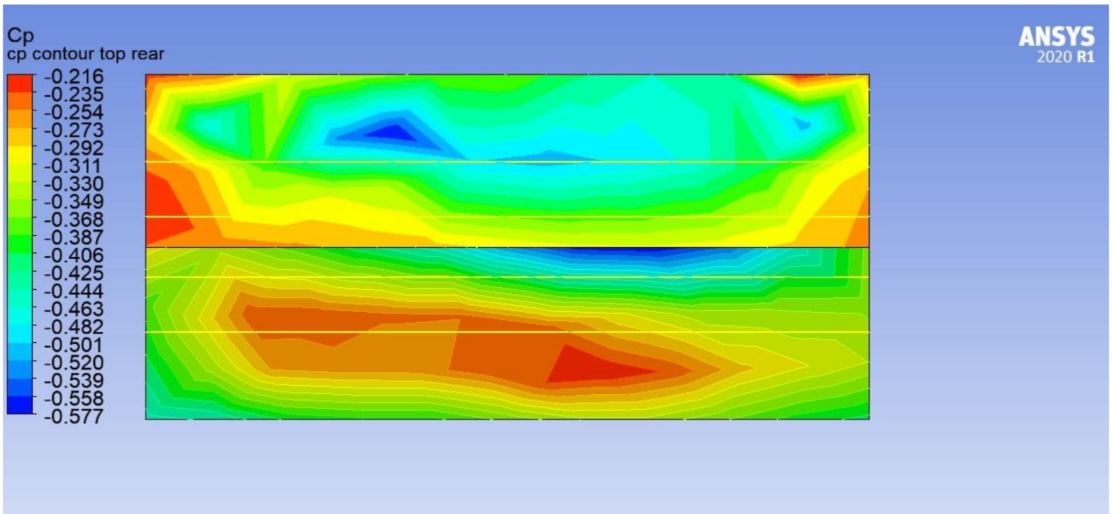

Fig. 3.10 Coefficient of Pressure Contour

The face average value of the pressure coefficient obtained on the validation model was compared with the values given in Indian (IS 875: Part 3, 2015) [3 standards and the average % variation was found to be 16.5 %.

Table 3.1 Validation of Result

Wind Angle	**Cpe for Surface from CFD Simulation**		**Average Value of Cpe for Roof from Simulation**	**Average Value of Cpe for Roof as per IS 875 part 3**	**Average % Error**
0	Roof A	Roof B	-0.585	-0.7	16.4 %
	-0.836	-0.333			

3.8 COEFFIENT OF PRESSURE EXTERNAL (Cpe)

3.8.1 at Roof Angle 10^0

Spacing0

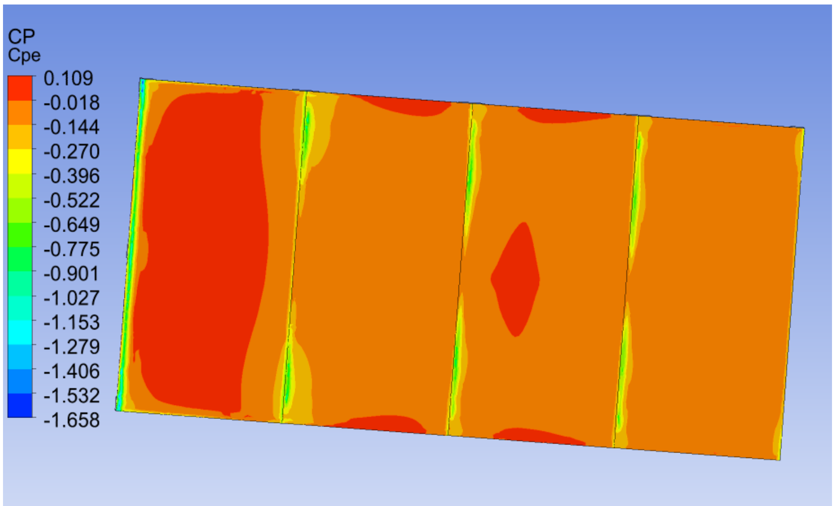

Fig.3.11 External Pressure Coefficient at Wind Direction 0^0

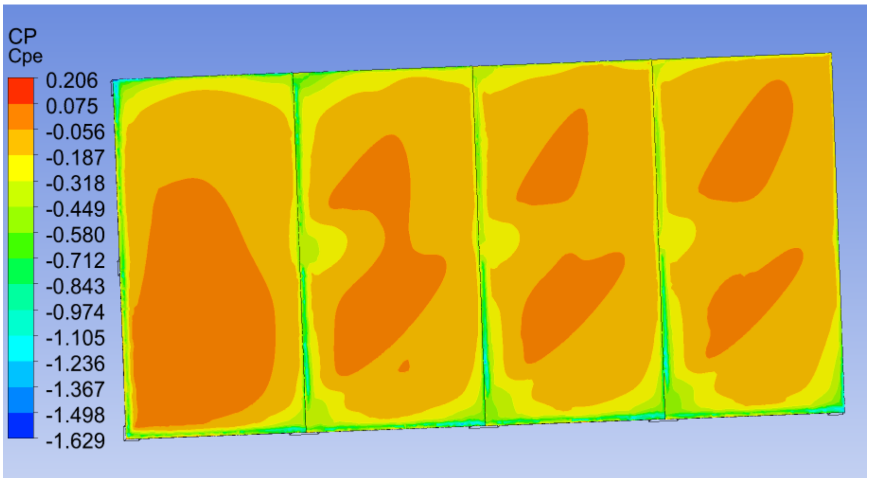

Fig. 3.12 External Pressure Coefficient at Wind Direction 45^0

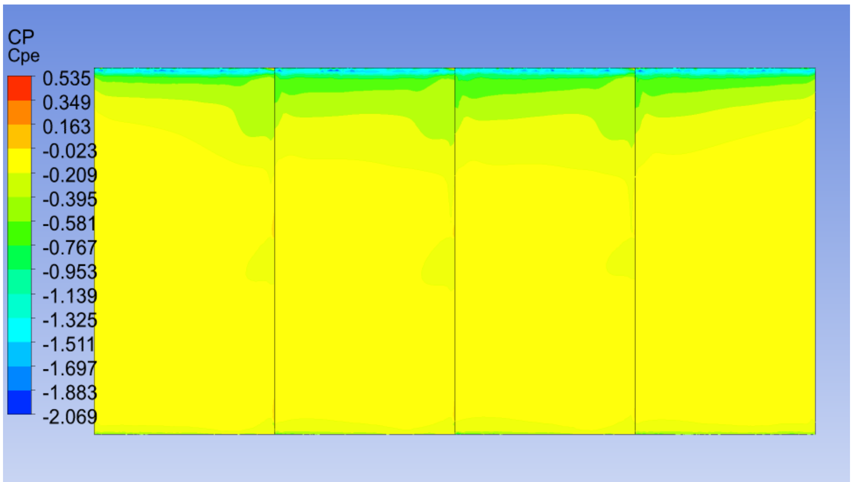

Fig. 3.13 External Pressure Coefficient at Wind Direction 90^0

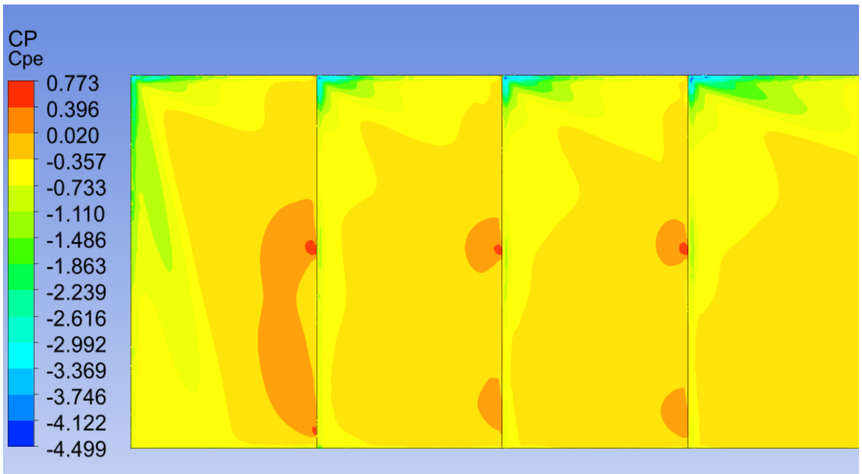

Fig. 3.14 External Pressure Coefficient at Wind Direction 135^0

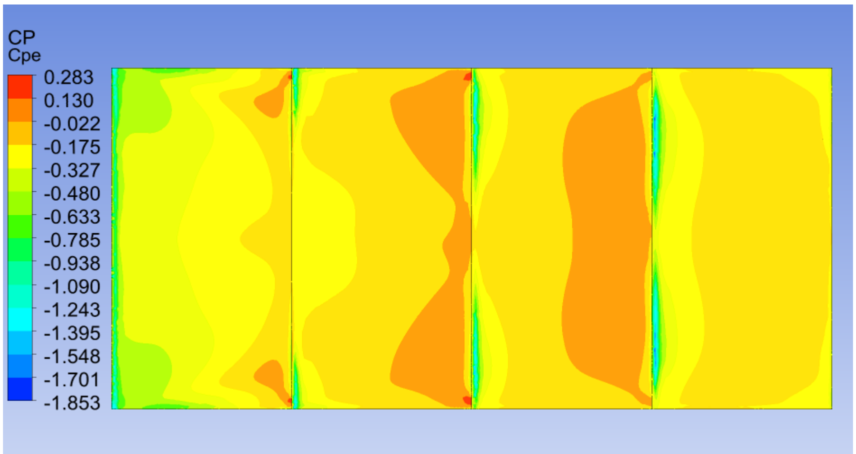

Fig. 3.15 External Pressure Coefficient at Wind Direction 180^0

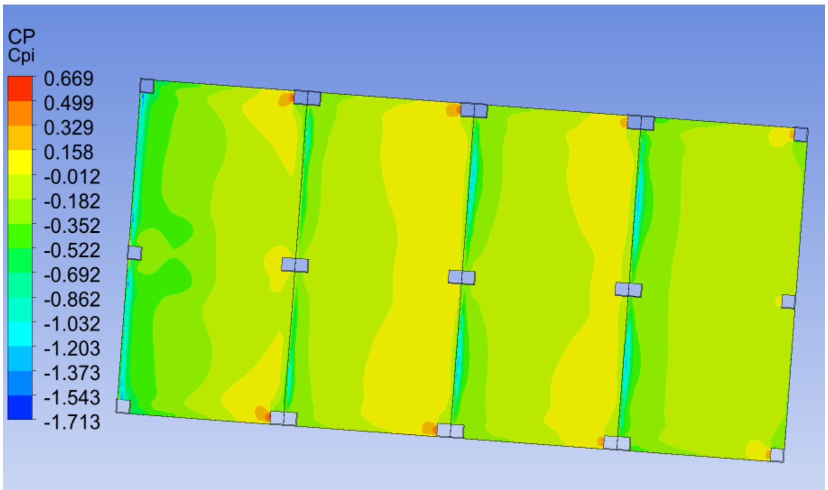

Fig. 3.16 Internal Pressure Coefficient at Wind Direction 0^0

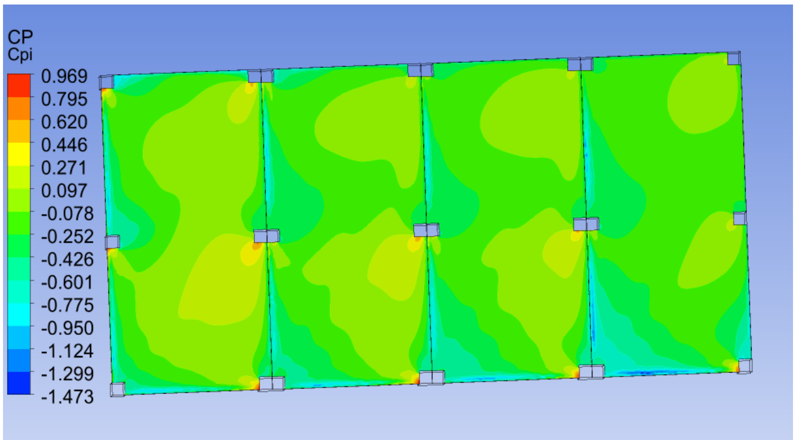

Fig. 3.17 Internal Pressure Coefficient at Wind Direction 45^0

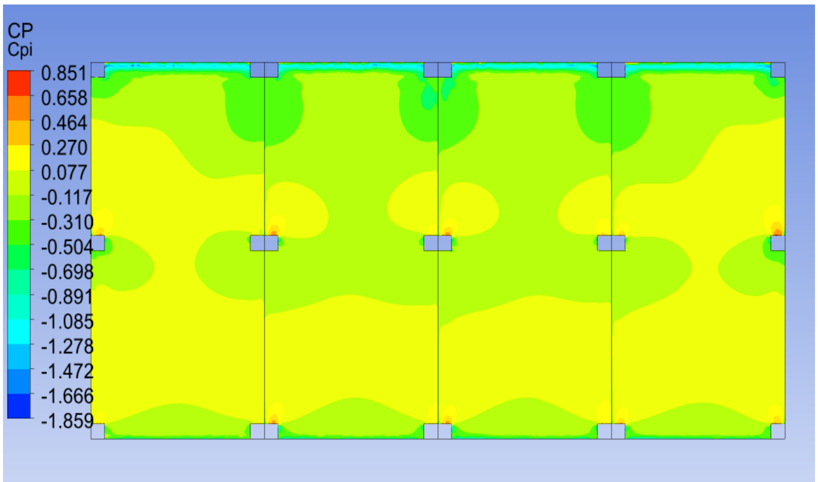

Fig. 3.18 Internal Pressure Coefficient at Wind Direction 90^0

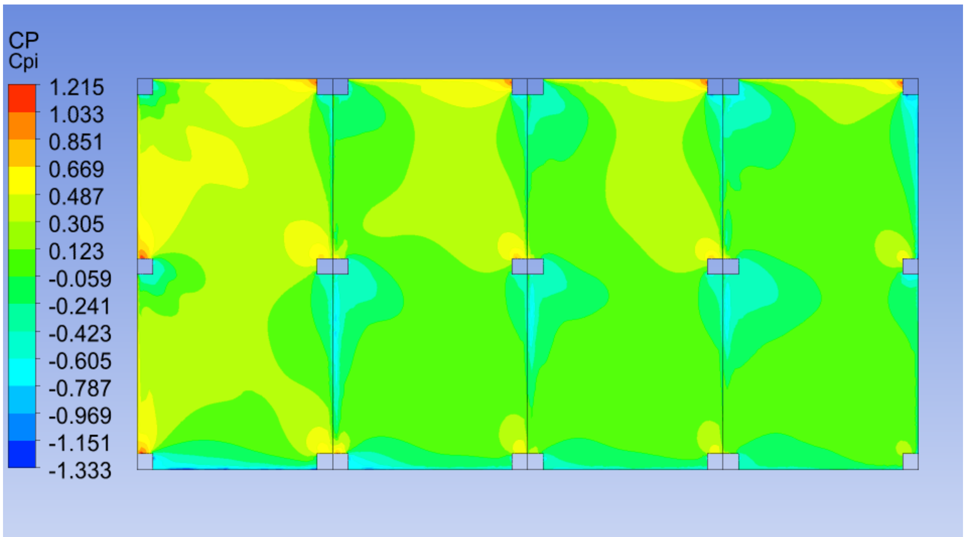

Fig. 3.19 Internal Pressure Coefficient at Wind Direction 135^0

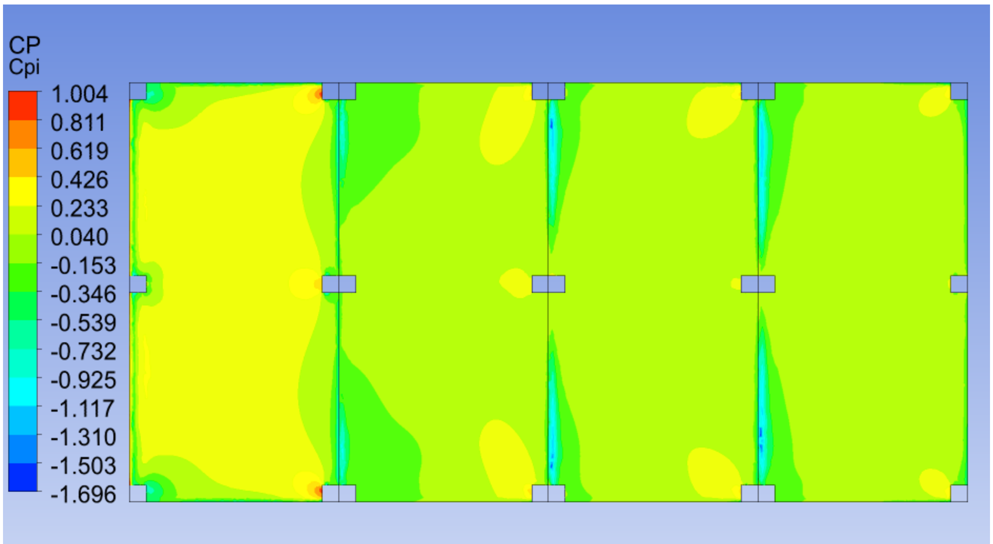

Fig. 3.20 Internal Pressure Coefficient at Wind Direction 180^0

Spacing B = 25

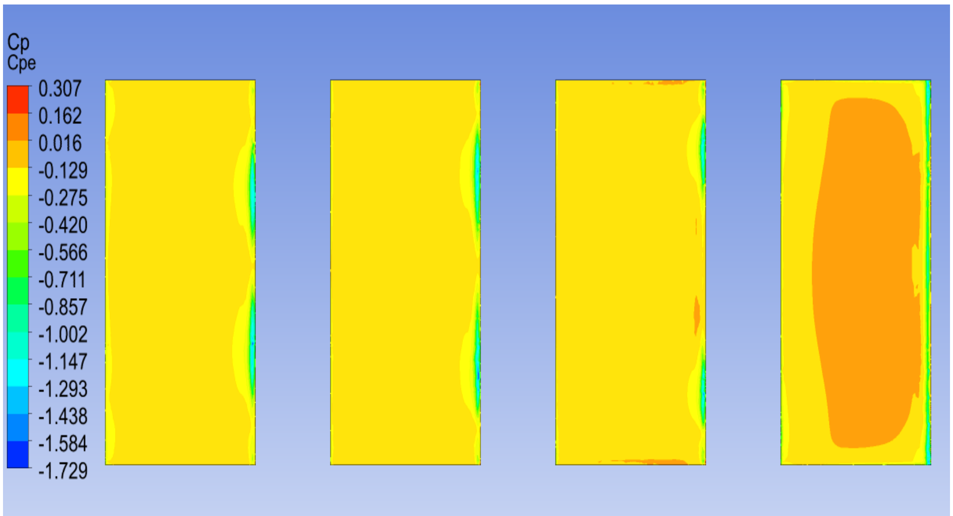

Fig. 3.21 External Pressure Coefficient at Wind Direction 0^0

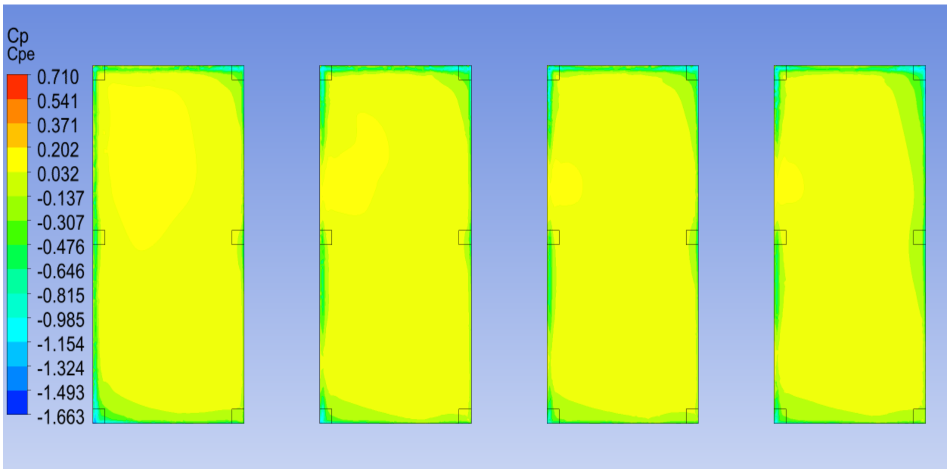

Fig. 3.22 External Pressure Coefficient at Wind Direction 45^0

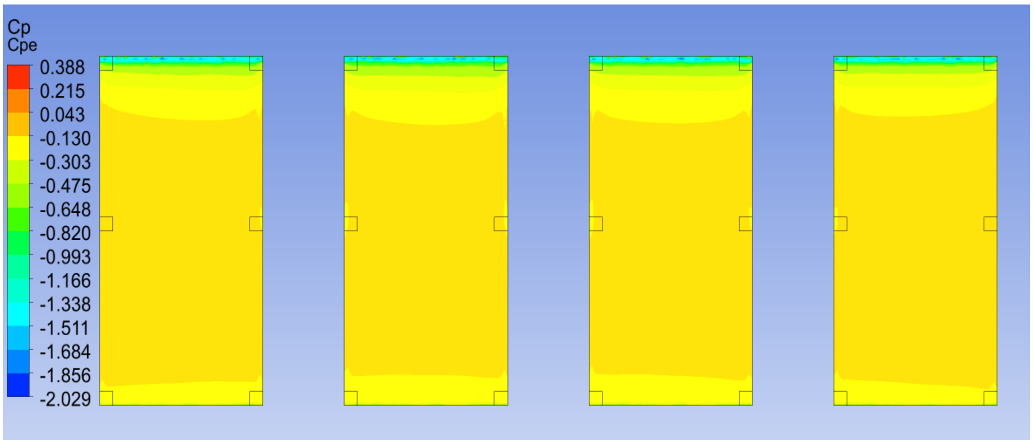

Fig. 3.23 External Pressure Coefficient at Wind Direction 90

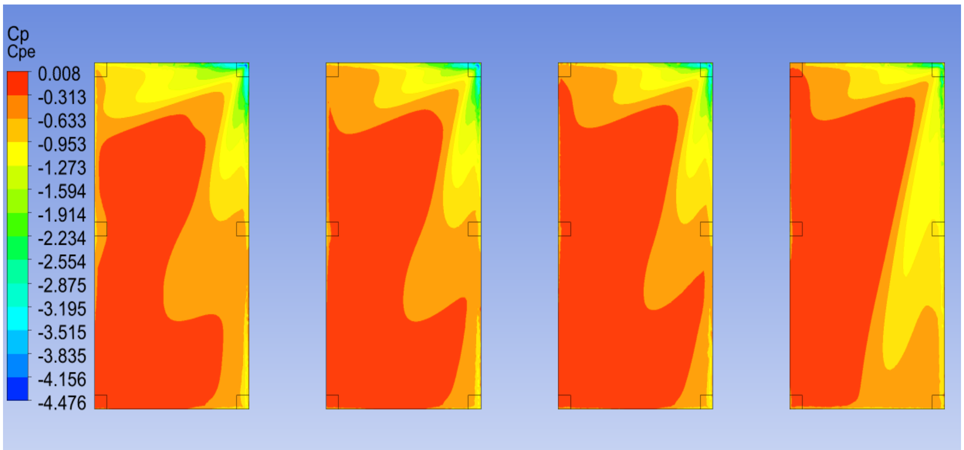

Fig. 3.24 External Pressure Coefficient at Wind Direction 135^0

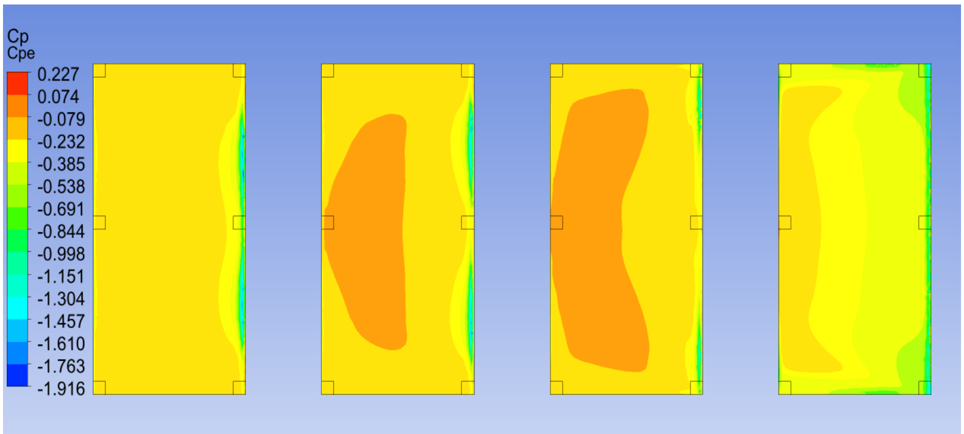

Fig. 3.26 External Pressure Coefficient at Wind Direction 180^0

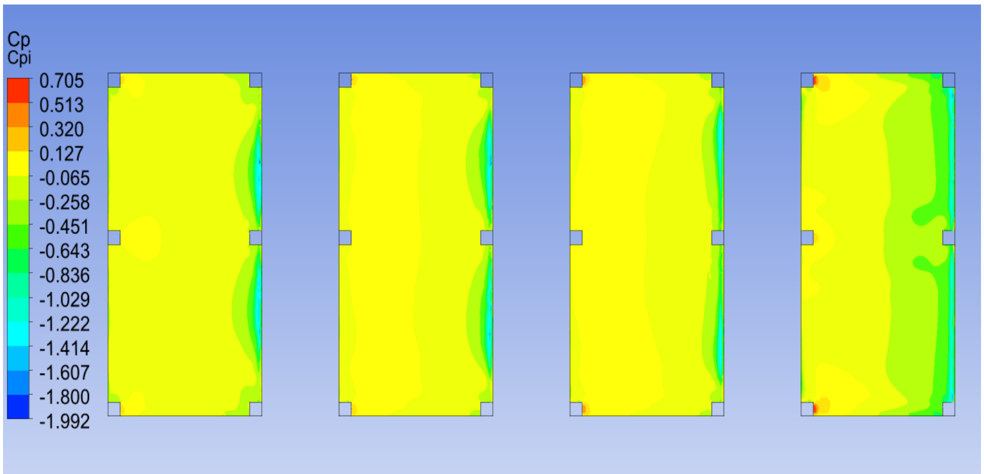

Fig. 3.27 Internal Pressure Coefficient at Wind Direction 0^0

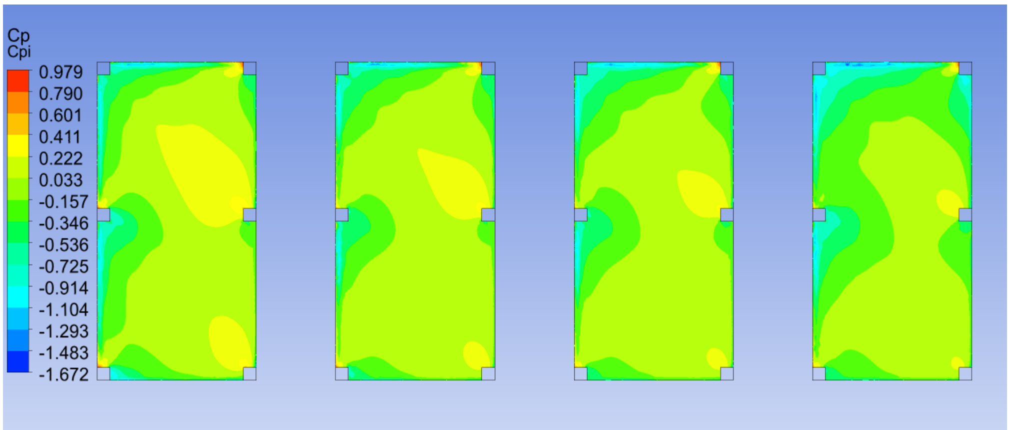

Fig. 3.28 Internal Pressure Coefficient at Wind Direction 45^0

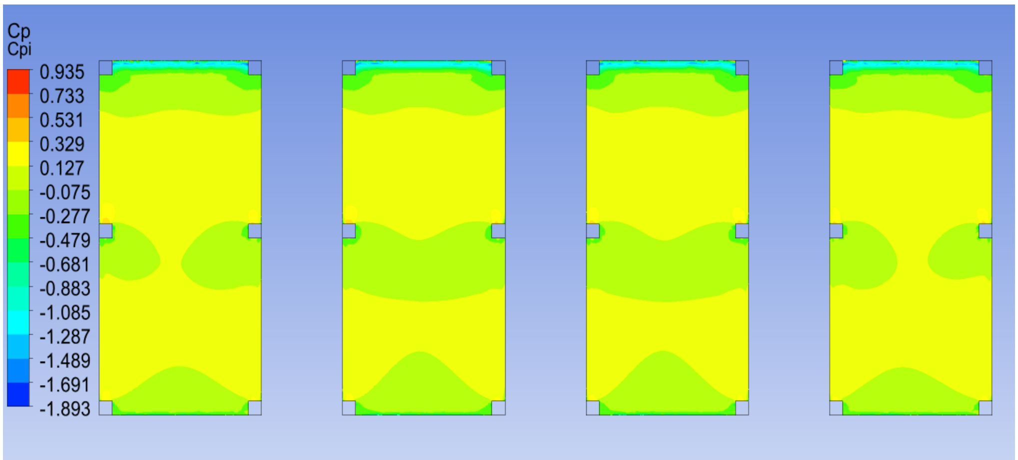

Fig. 3.29 Internal Pressure Coefficient at Wind Direction 90^0

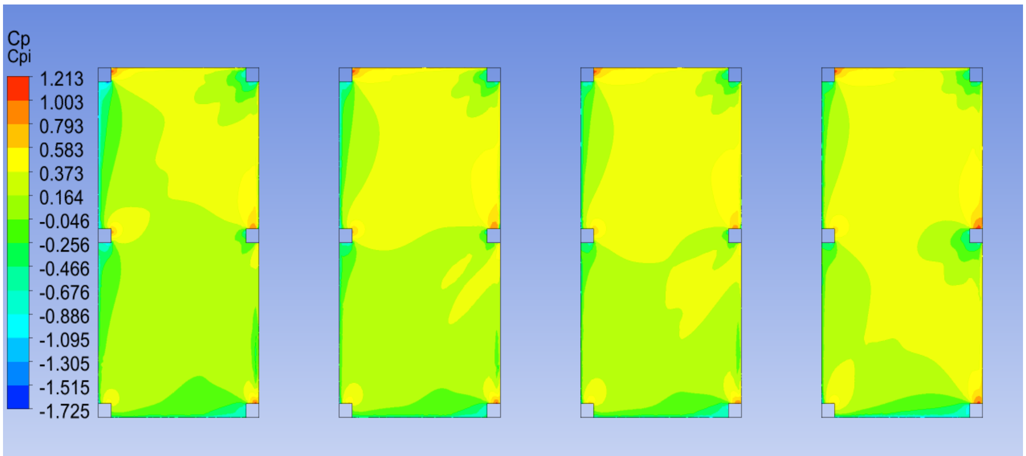

Fig. 3.30 Internal Pressure Coefficient at Wind Direction 135^0

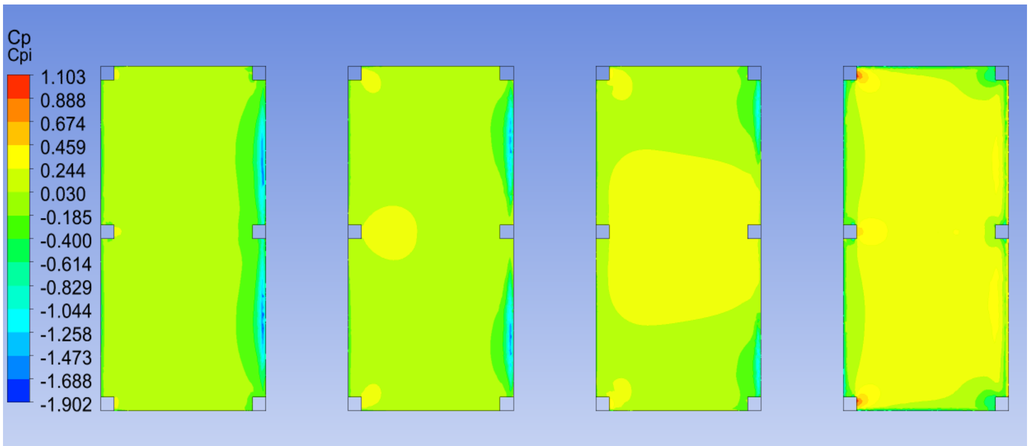

Fig. 3.31 Internal Pressure Coefficient at Wind Direction 180^0

Spacing B = 50

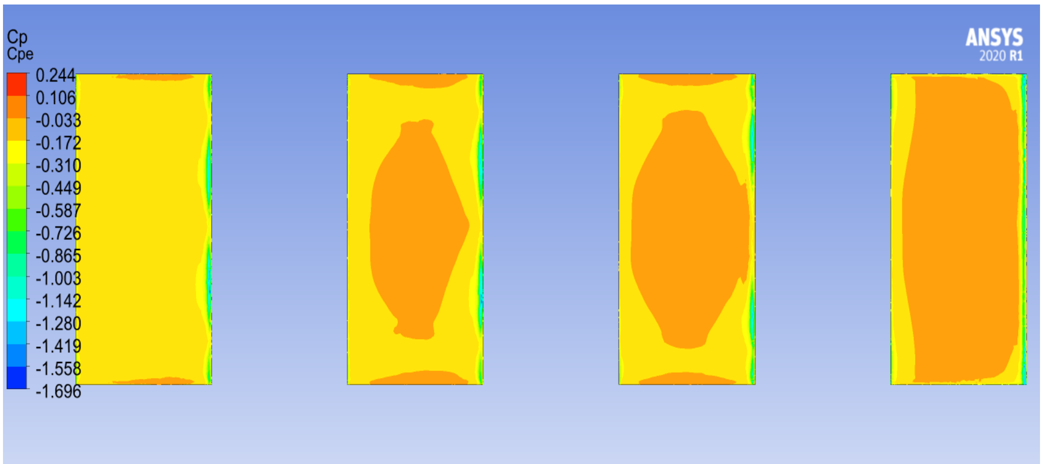

Fig. 3.32 External Pressure Coefficient at Wind Direction 0^0

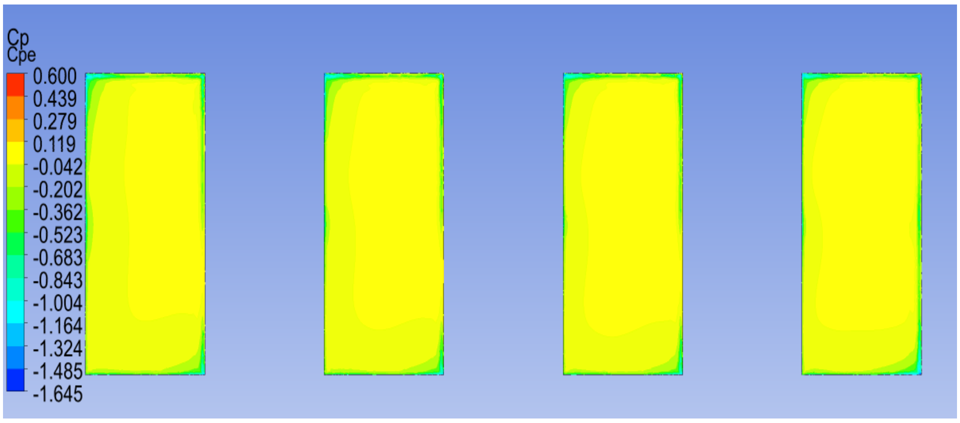

Fig. 3.32 External Pressure Coefficient at Wind Direction 45^0

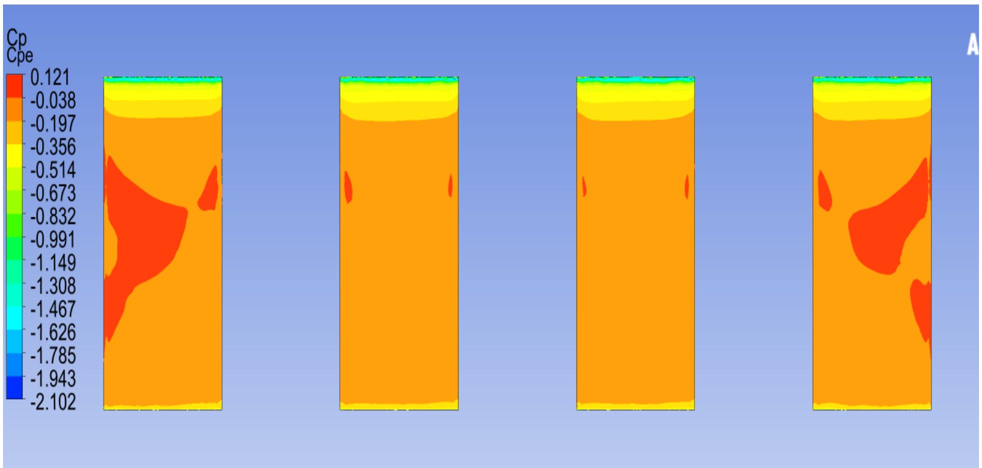

Fig. 3.33 External Pressure Coefficient at Wind Direction 90^0

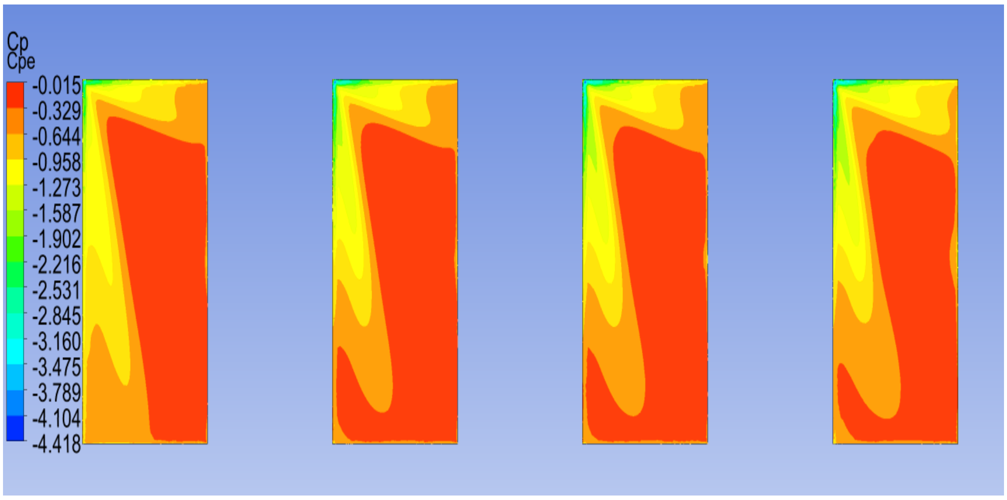

Fig. 3.34 External Pressure Coefficient at Wind Direction 135^0

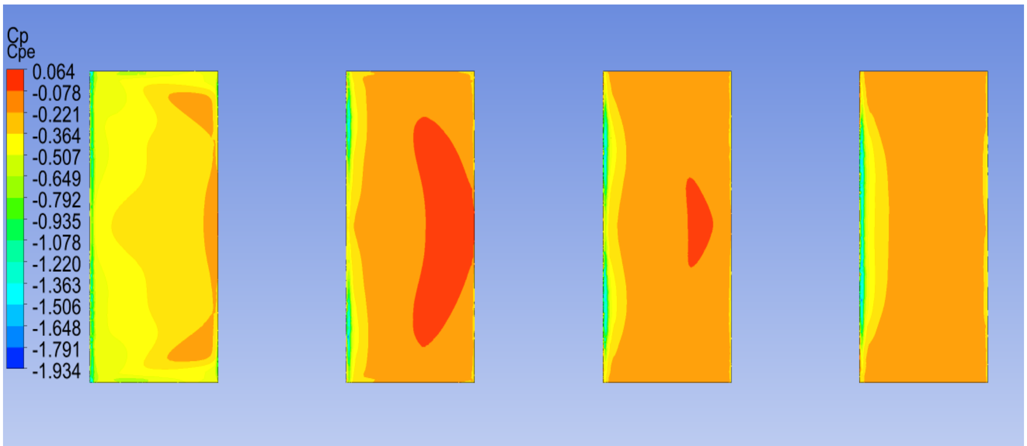

Fig. 3.35 External Pressure Coefficient at Wind Direction 180^0

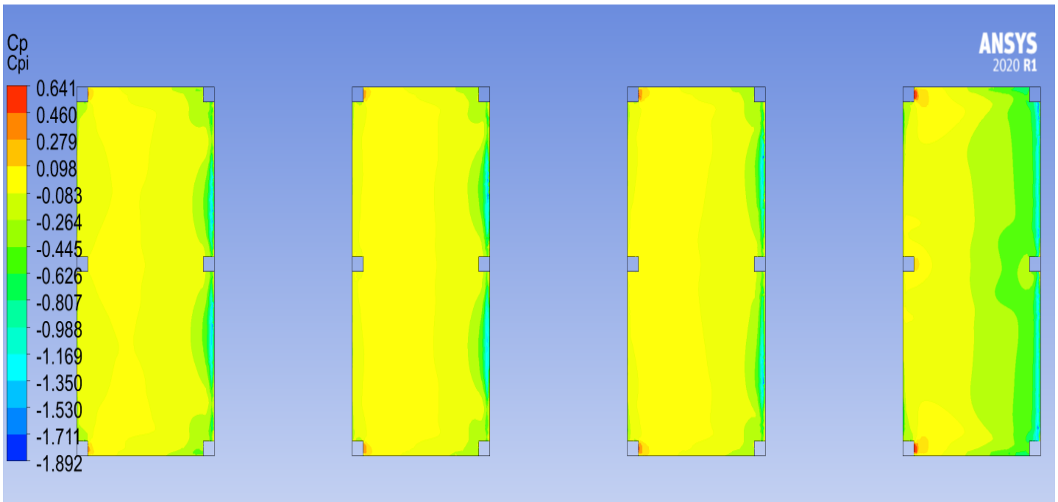

Fig. 3.36 Internal Pressure Coefficient at Wind Direction 0^0

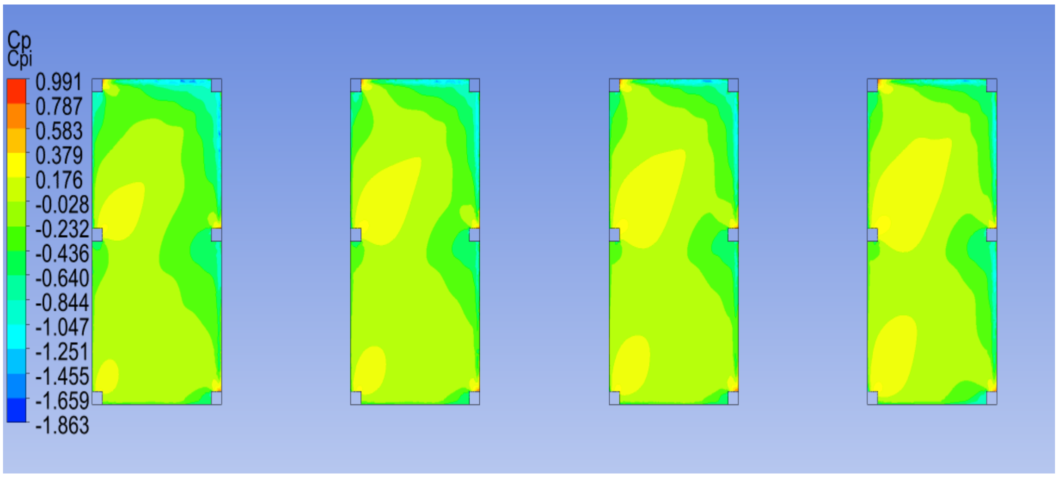

Fig. 3.37 Internal Pressure Coefficient at Wind Direction 45^0

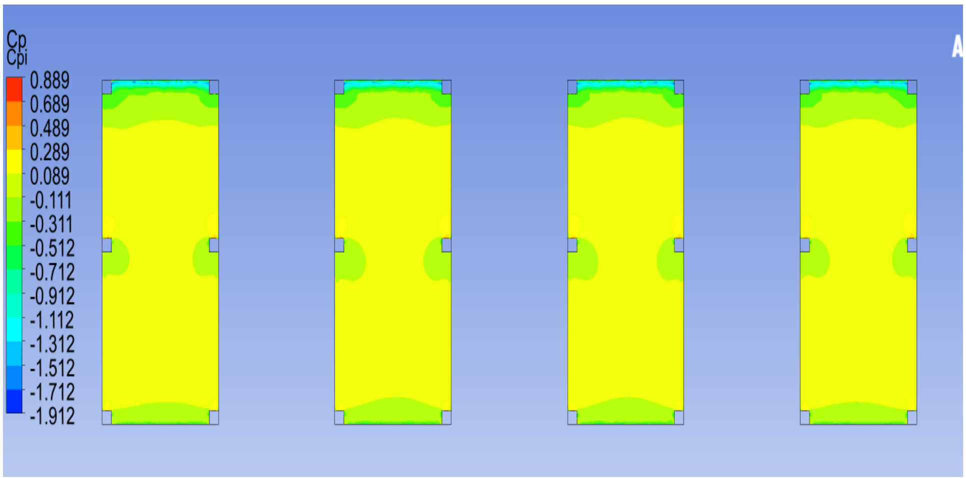

Fig. 3.38 Internal Pressure Coefficient at Wind Direction 90^0

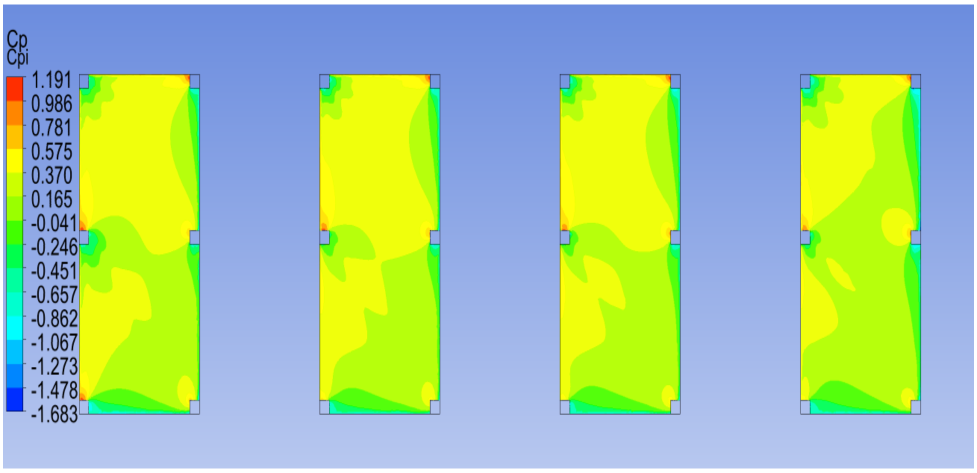

Fig. 3.39 Internal Pressure Coefficient at Wind Direction 135^0

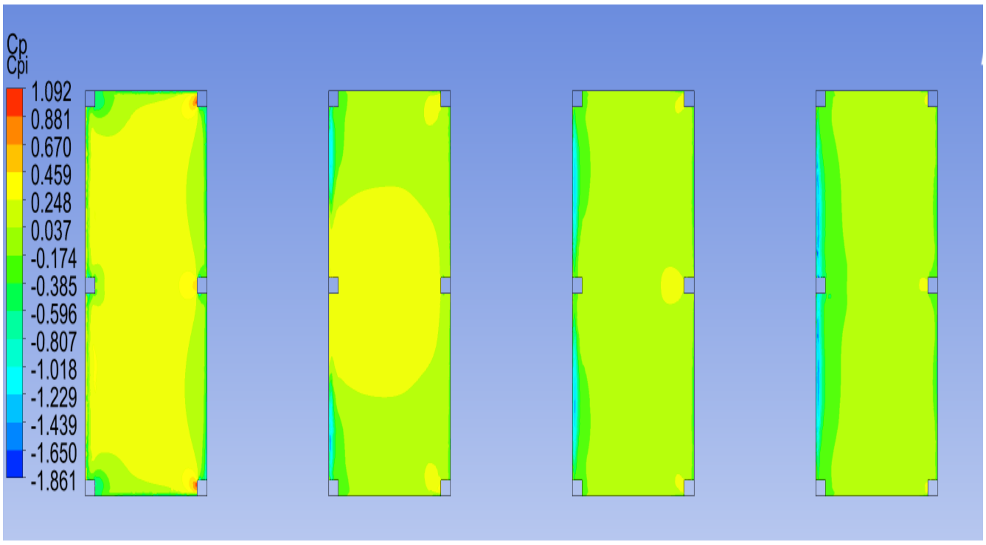

Fig. 3.40 Internal Pressure Coefficient at Wind Direction 180^0

Spacing B = 75

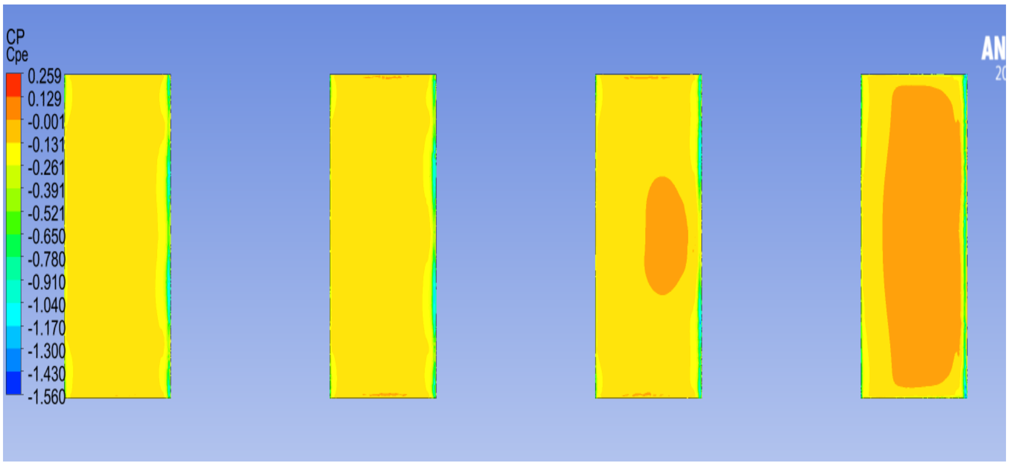

Fig. 3.41 External Pressure Coefficient at Wind Direction 0^0

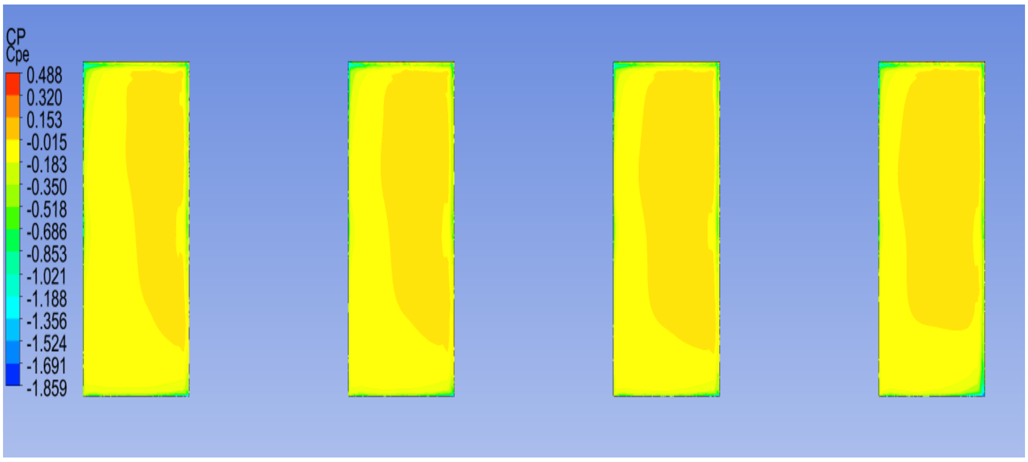

Fig. 3.42 External Pressure Coefficient at Wind Direction 45^0

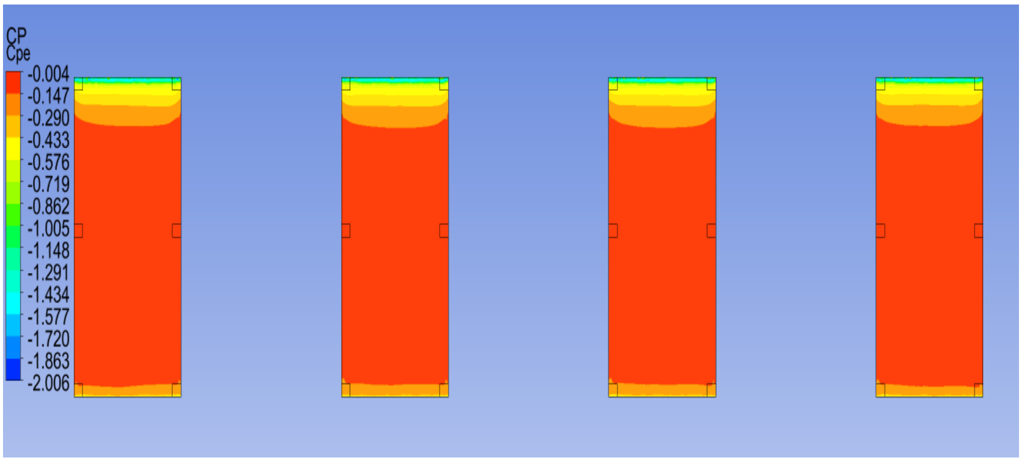

Fig. 3.43 External Pressure Coefficient at Wind Direction 90^0

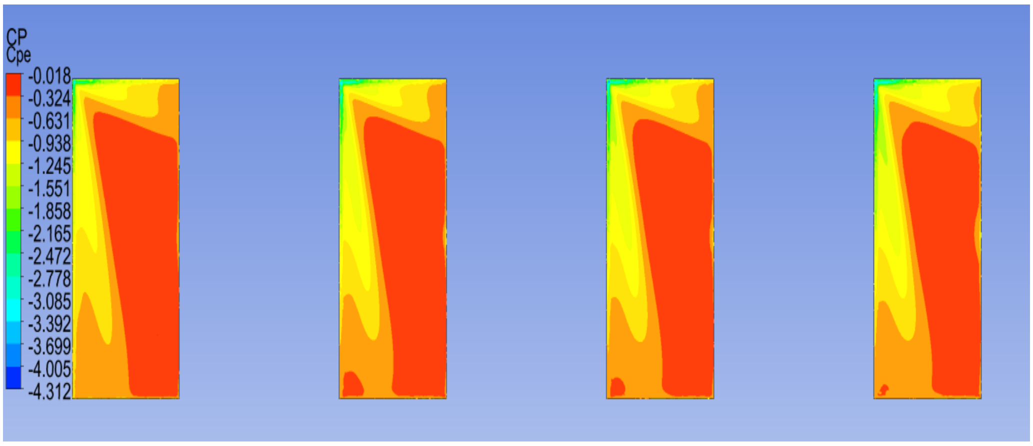

Fig. 3.44 External Pressure Coefficient at Wind Direction 135^0

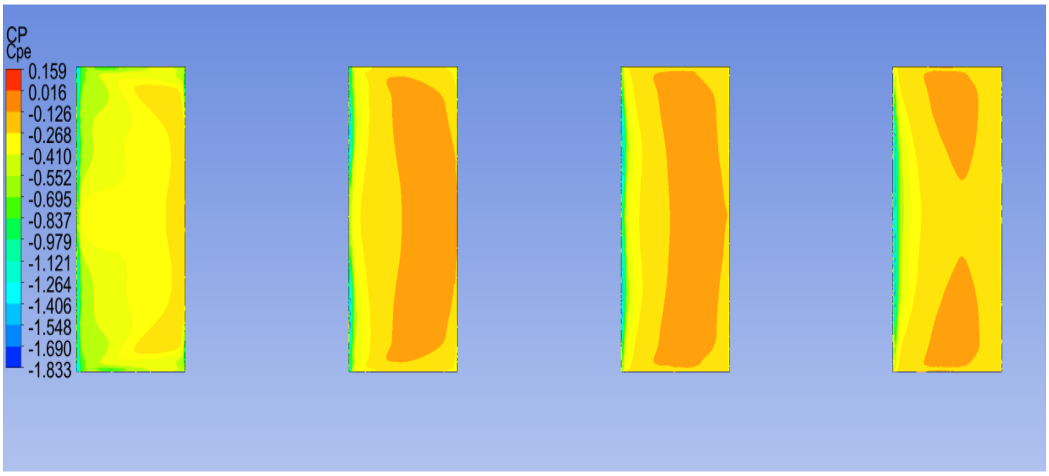

Fig. 3.45 External Pressure Coefficient at Wind Direction 180^0

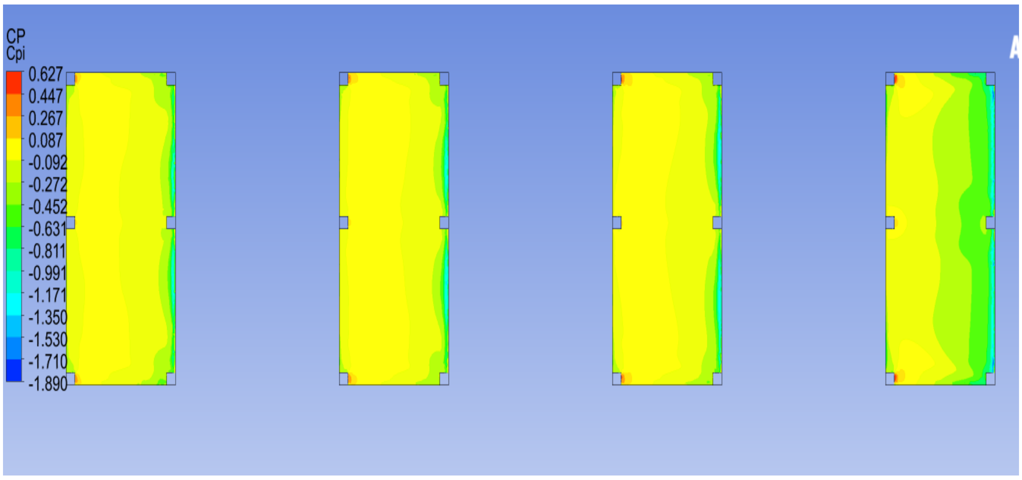

Fig. 3.46 Internal Pressure Coefficient at Wind Direction 0^0

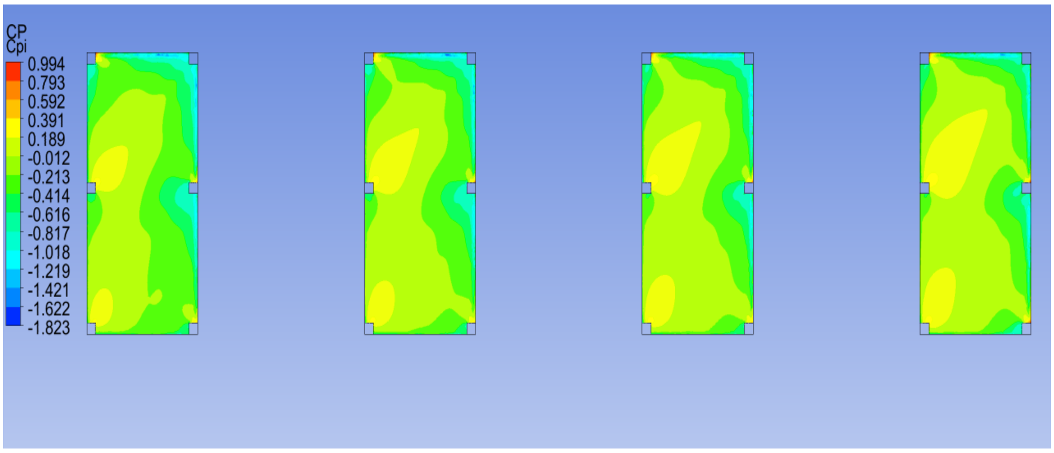

Fig. 3.47 Internal Pressure Coefficient at Wind Direction 45^0

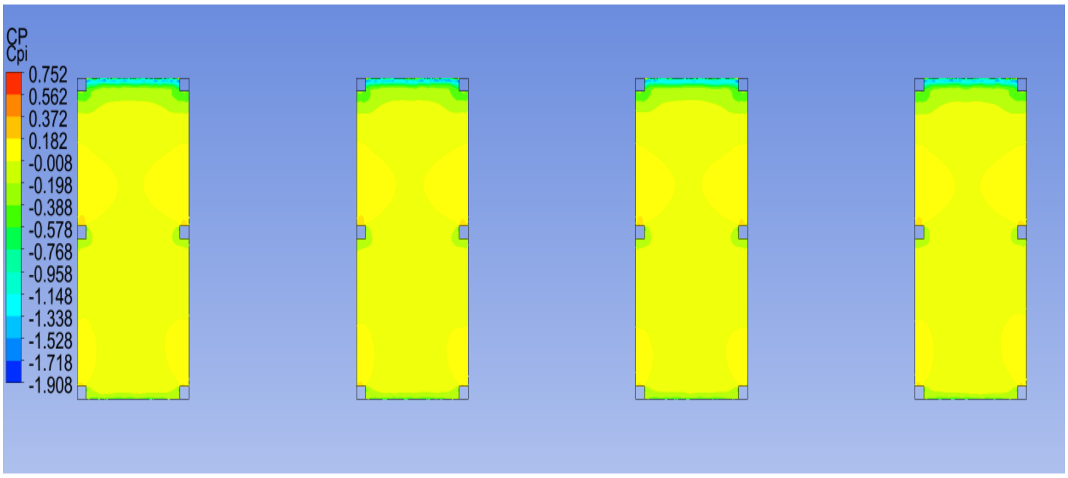

Fig. 3.48 Internal Pressure Coefficient at Wind Direction 90^0

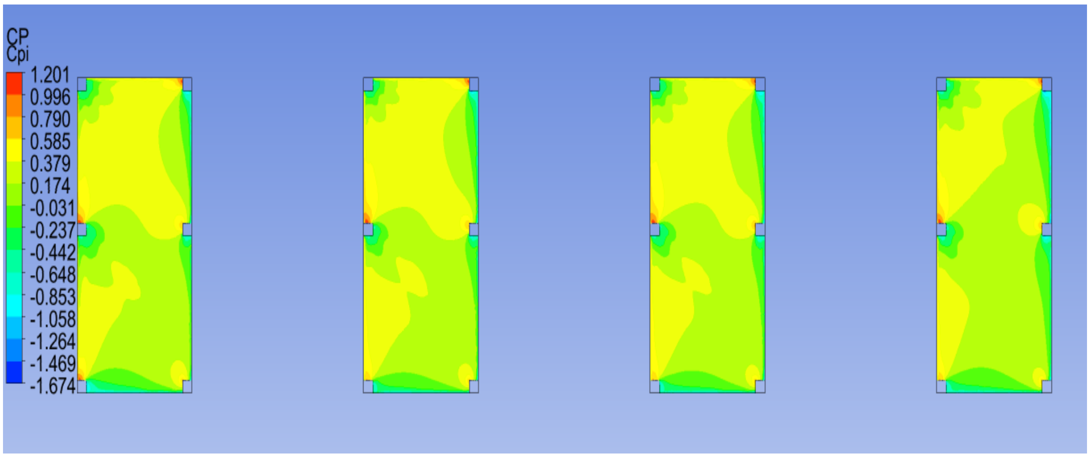

Fig. 3.49 Internal Pressure Coefficient at Wind Direction 135^0

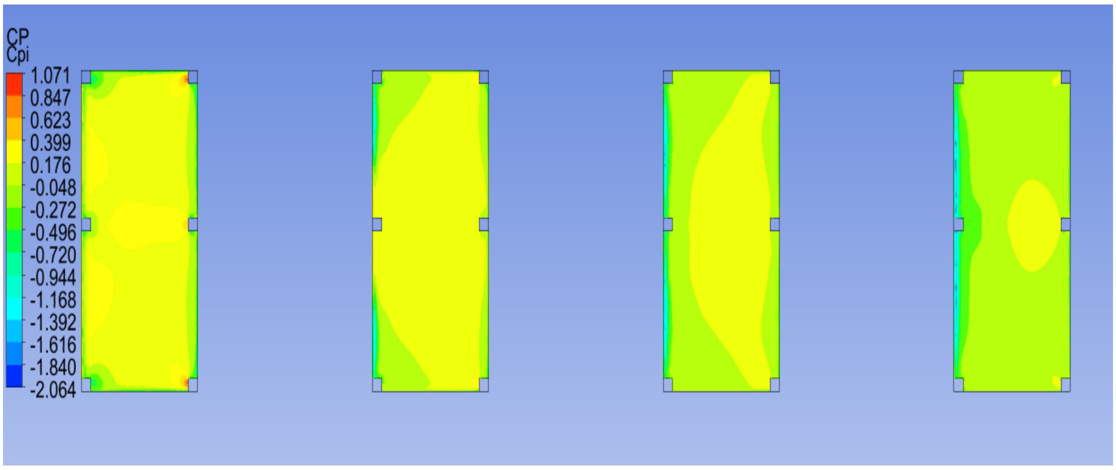

Fig. 3.50 Internal Pressure Coefficient at Wind Direction 180^0

Spacing B = 100

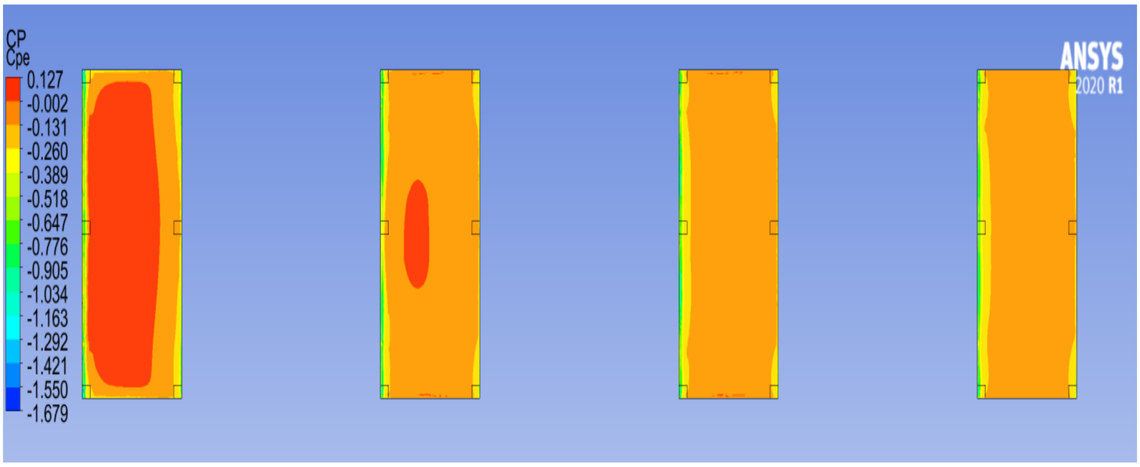

Fig. 3.51 External Pressure Coefficient at Wind Direction 0^0

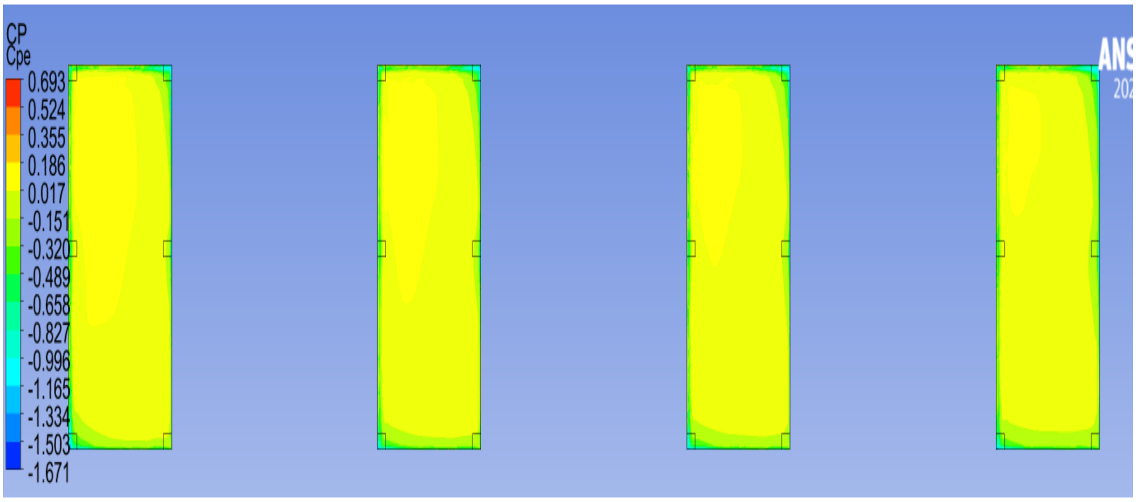

Fig. 3.52 External Pressure Coefficient at Wind Direction 45^0

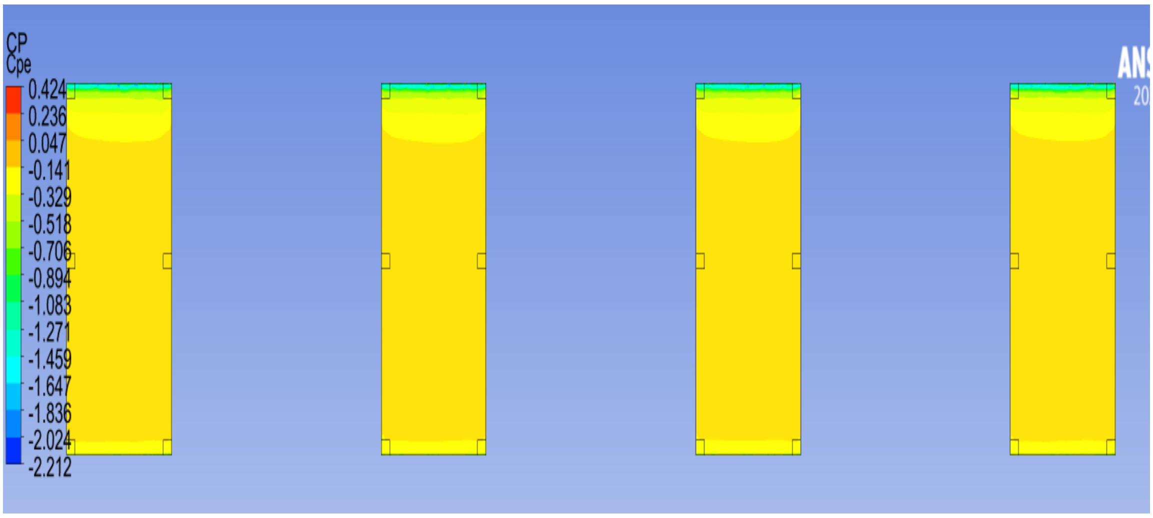

Fig. 3.53 External Pressure Coefficient at Wind Direction 90^0

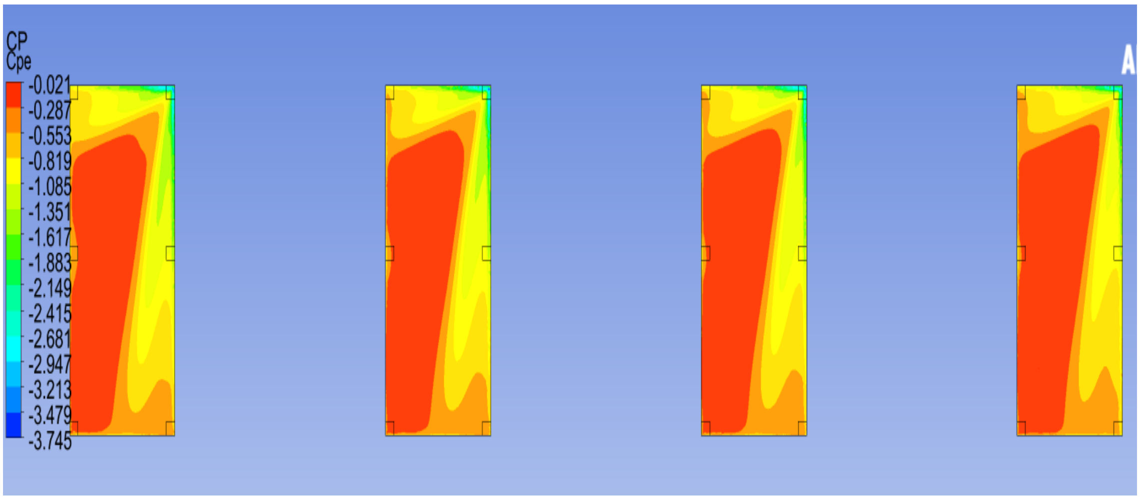

·Fig. 3.54 External Pressure Coefficient at Wind Direction 135^0

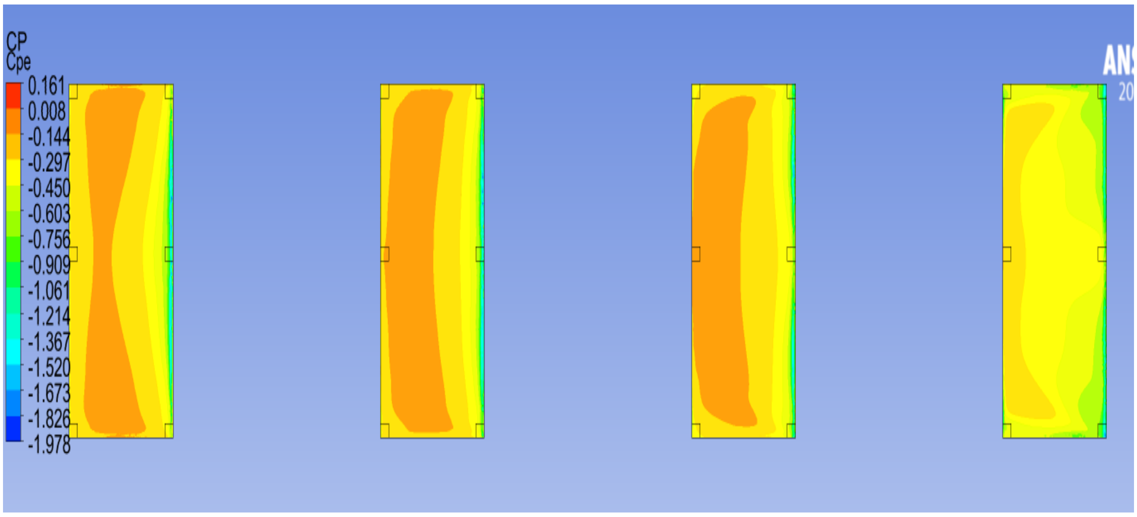

Fig. 3.55 External Pressure Coefficient at Wind Direction 180^0

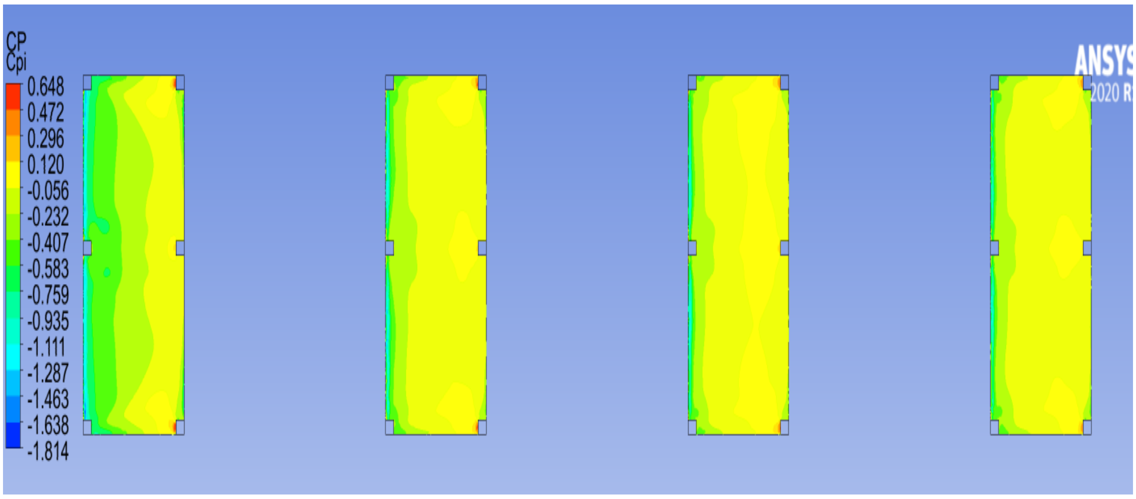

Fig. 3.56 Internal Pressure Coefficient at Wind Direction 0^0

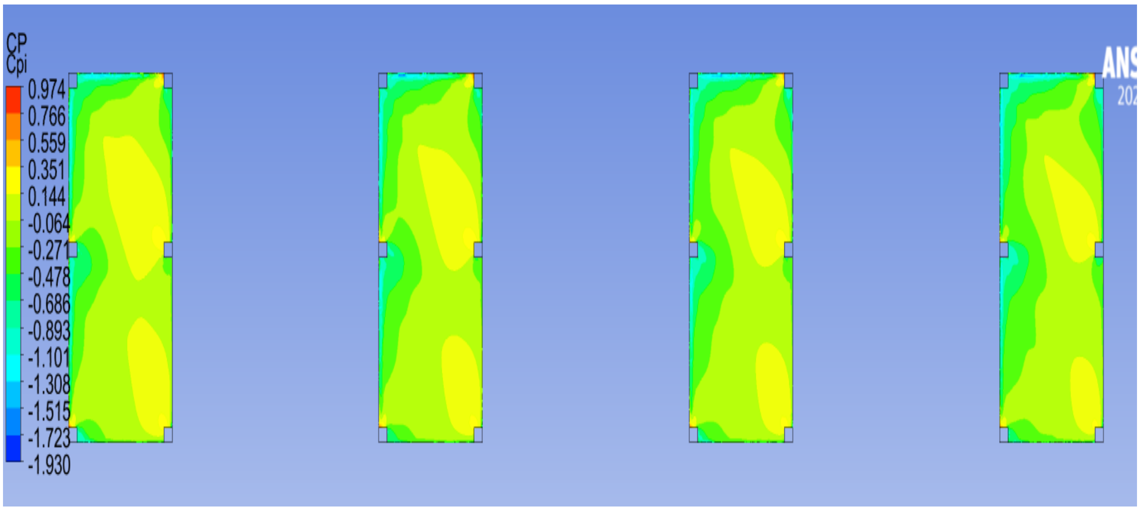

Fig. 3.57 Internal Pressure Coefficient at Wind Direction 45^0

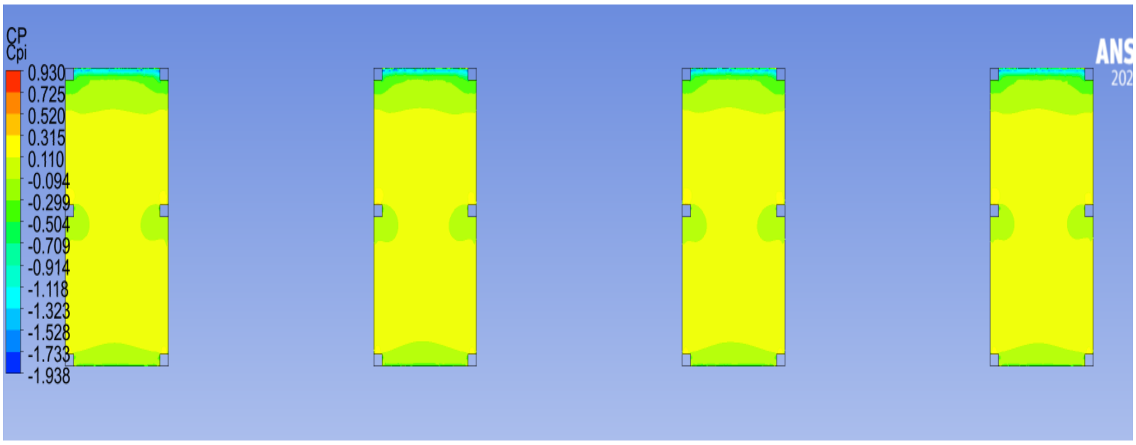

Fig. 3.58 Internal Pressure Coefficient at Wind Direction 90^0

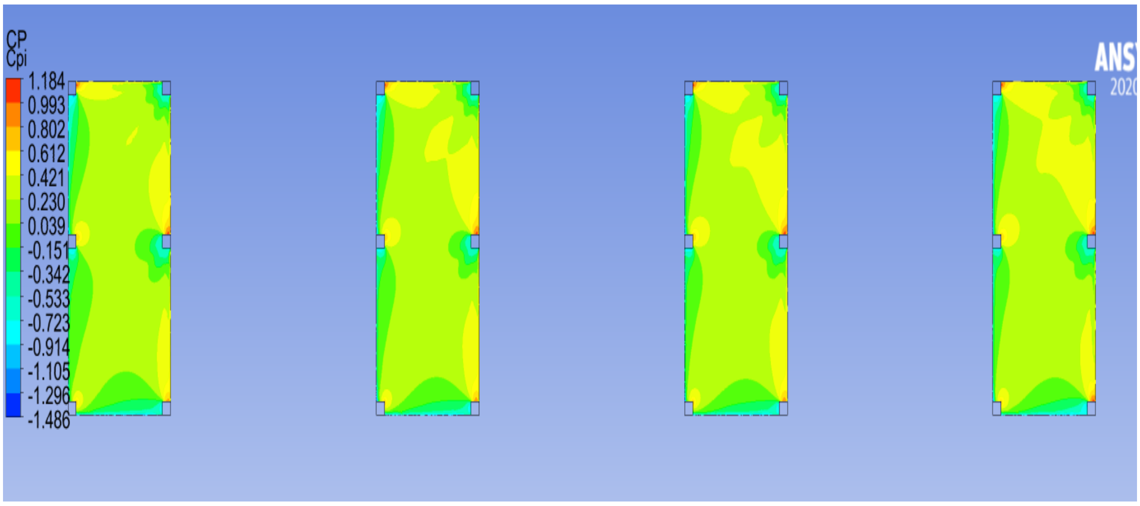

Fig. 3.59 Internal Pressure Coefficient at Wind Direction 135^0

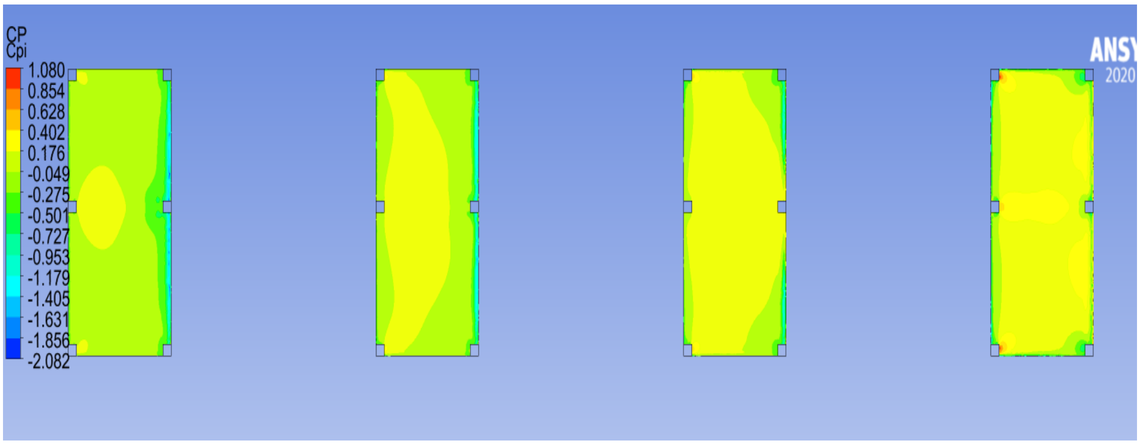

Fig. 3.60 Internal Pressure Coefficient at Wind Direction 180^0

The contours for coeffient of external and internal pressures in Fig. 3.10 to Fig. 60 for the mono slope roof having roof angle 10° by varying wind direction from 0 ° to 180 ° and having different spacing.

The Cpe is observed to be increased from the wind direction 0 ° to 90 ° and significant increment can be seen whereas there was a significant reduction in the value of Cpe in the wind direction ranging from 90 ° to 180 ° . Also, C_{pe} was found to be maximum for the first structure and then goes on decreasing for the other structures.

3.8.6 at Roof Angle 20^0

Spacing B = 0

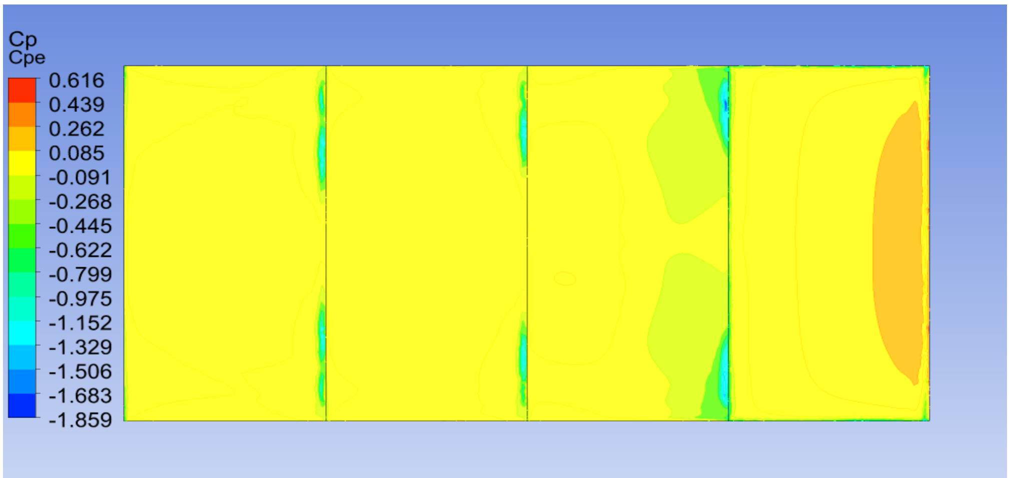

Fig. 3.61 External Pressure Coefficient at Wind Direction 0^0

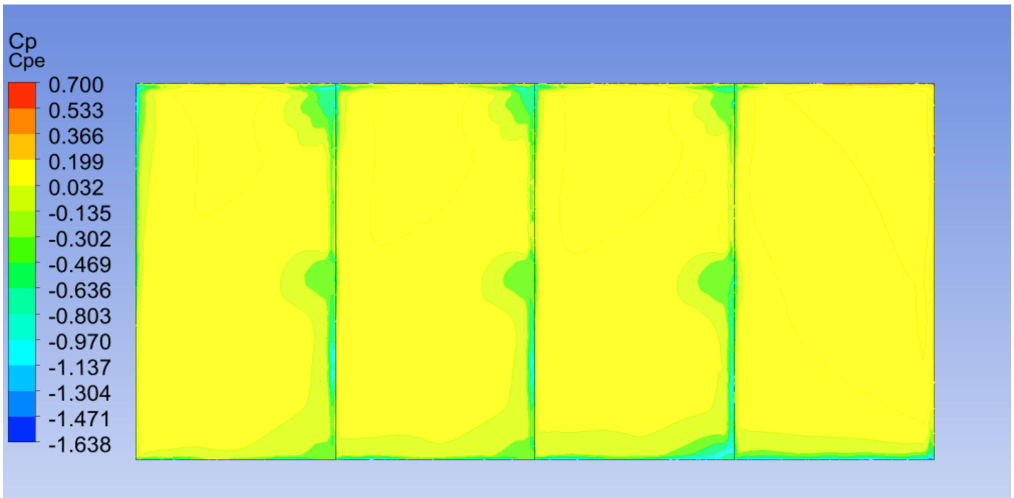

Fig. 3.62 External Pressure Coefficient at Wind Direction 45^0

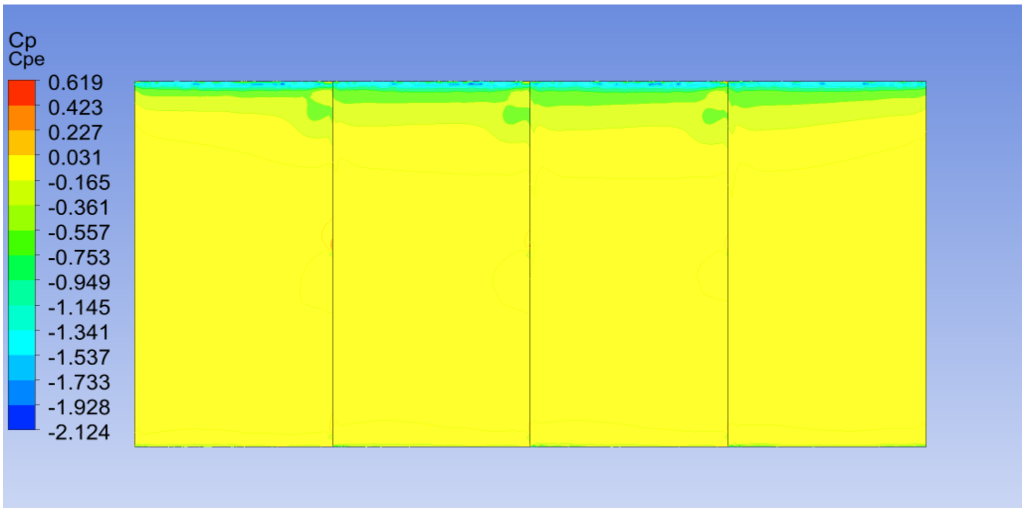

Fig. 3.63 External Pressure Coefficient at Wind Direction 90^0

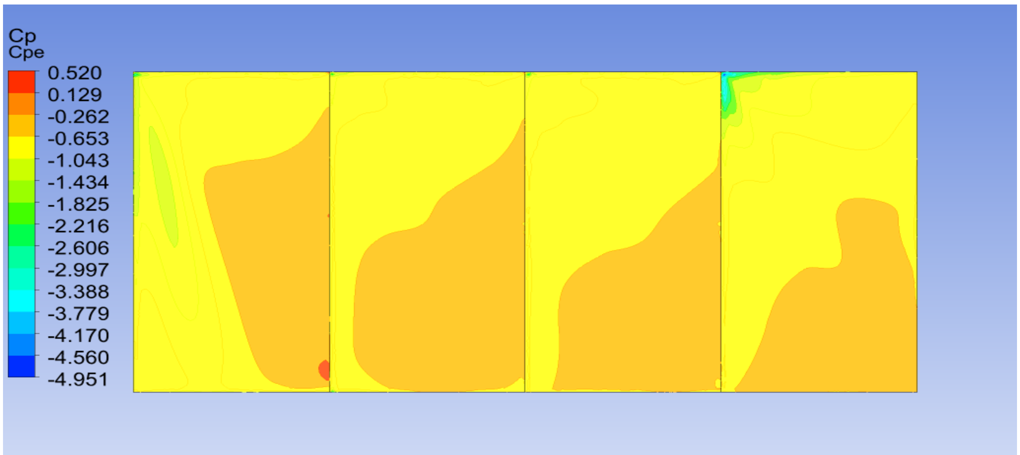

Fig. 3.64 External Pressure Coefficient at Wind Direction 135^0

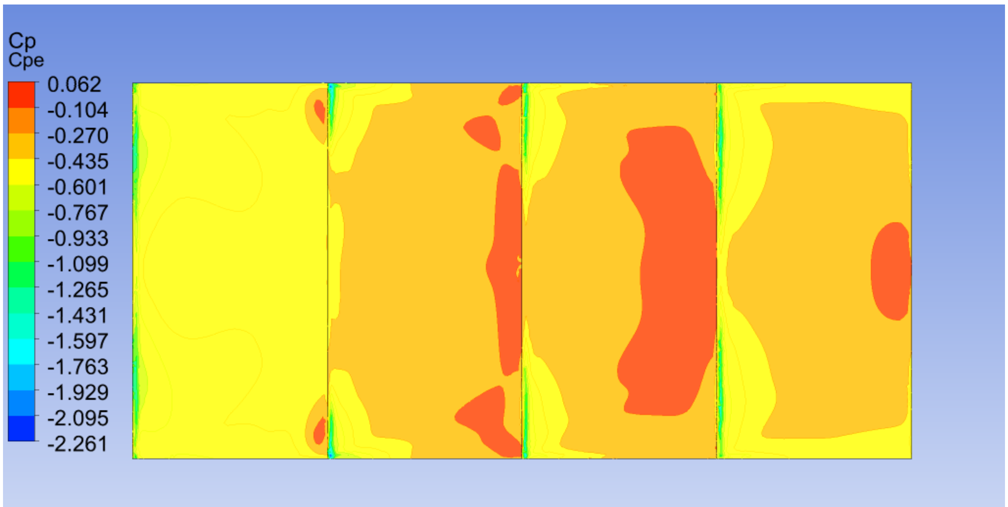

Fig. 3.65 External Pressure Coefficient at Wind Direction 180^0

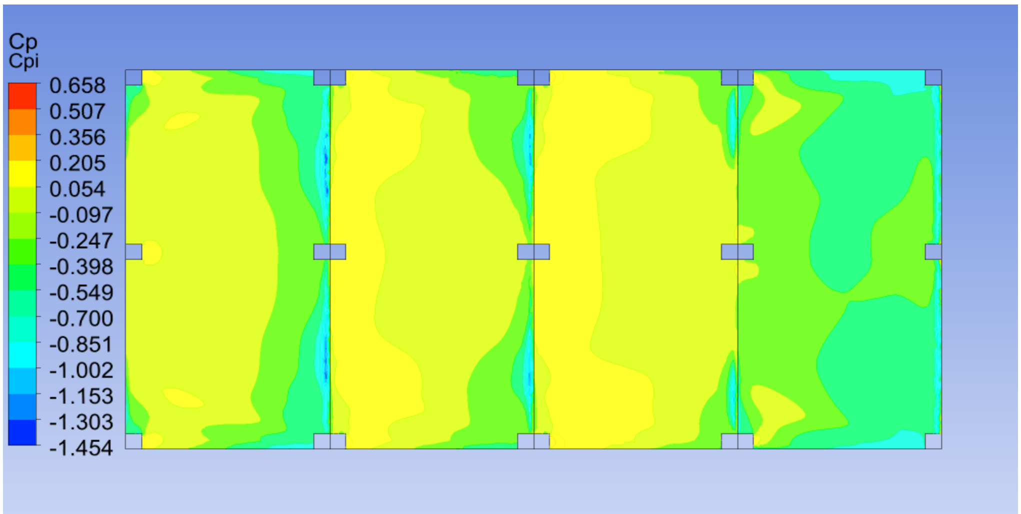

Fig. 3.66 Internal Pressure Coefficient at Wind Direction 0^0

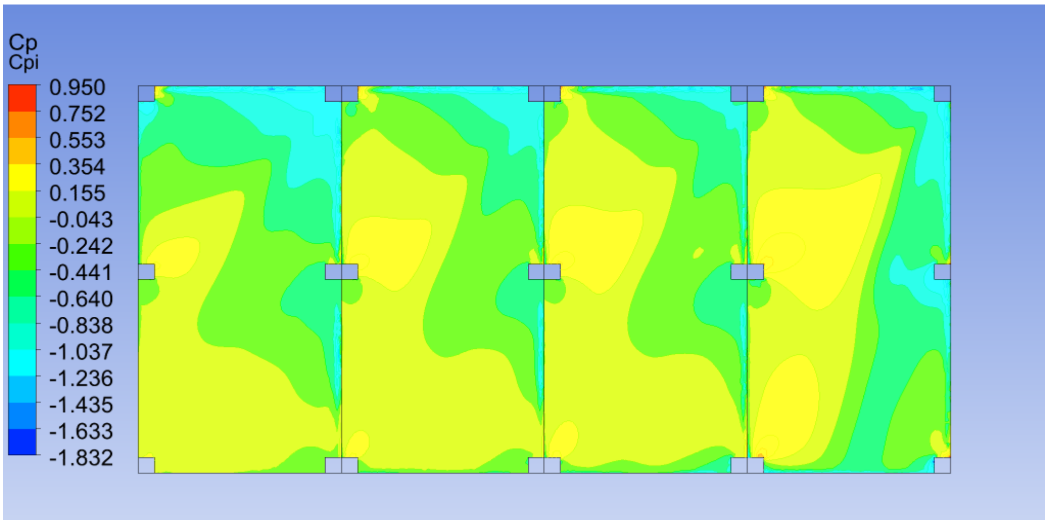

Fig. 3.67 Internal Pressure Coefficient at Wind Direction 45^0

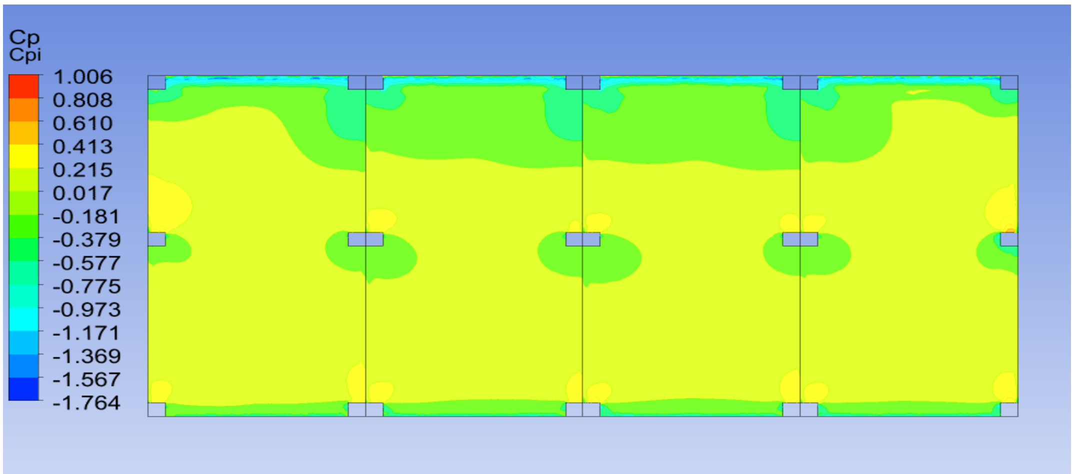

Fig. 3.68 Internal Pressure Coefficient at Wind Direction 90^0

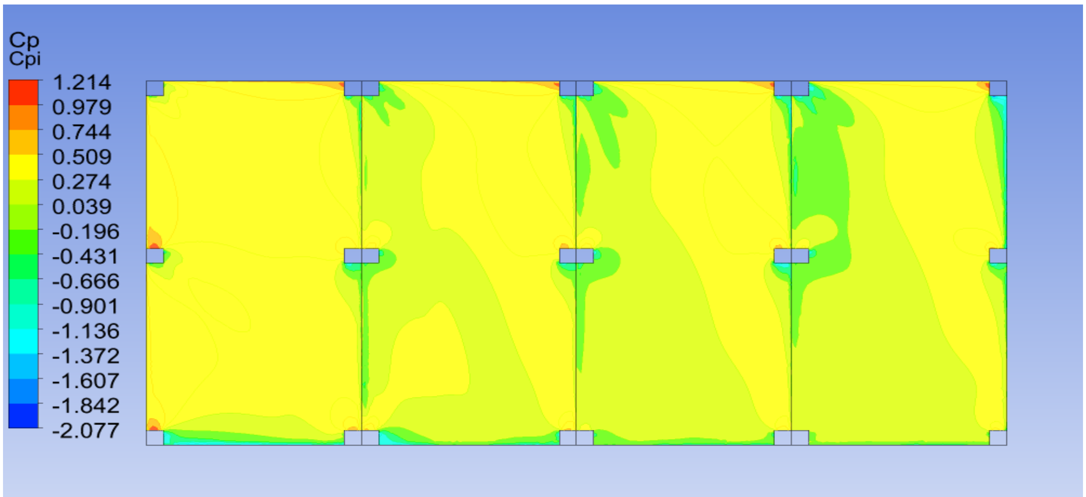

Fig. 3.69 Internal Pressure Coefficient at Wind Direction 135^0

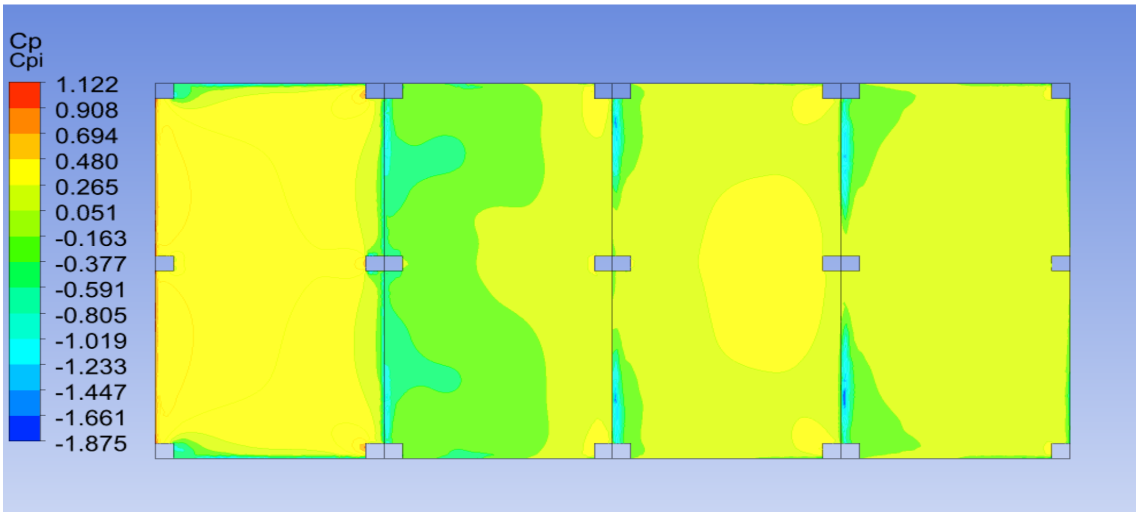

Fig. 3.70 Internal Pressure Coefficient at Wind Direction 180^0

Spacing B = 25

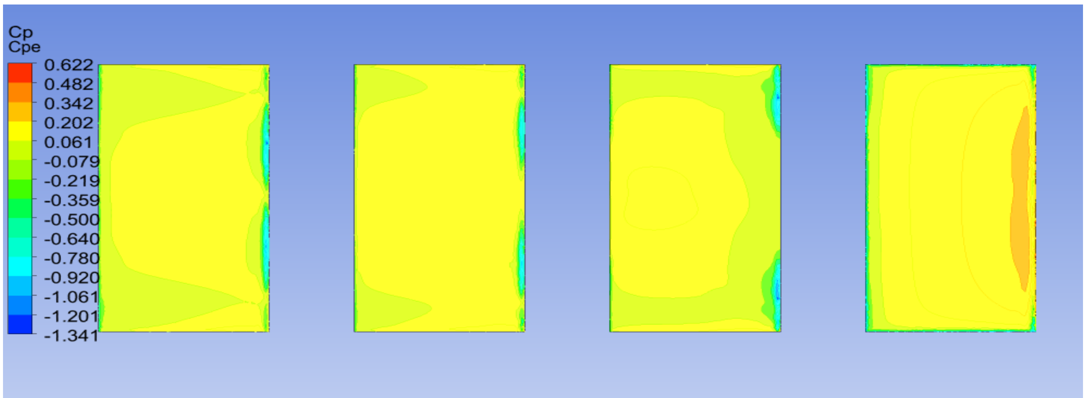

Fig. 3.71 External Pressure Coefficient at Wind Direction 0^0

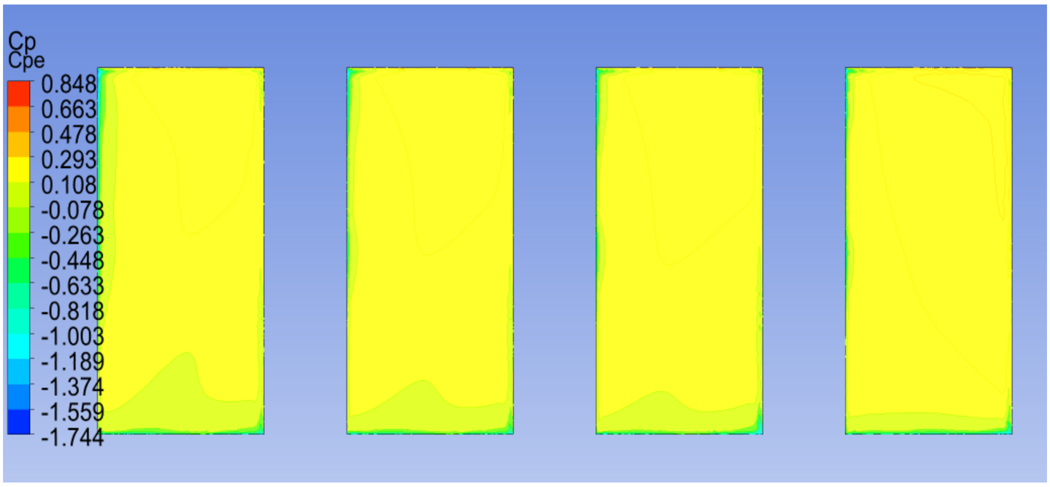

Fig. 3.72 External Pressure Coefficient at Wind Direction 45^0

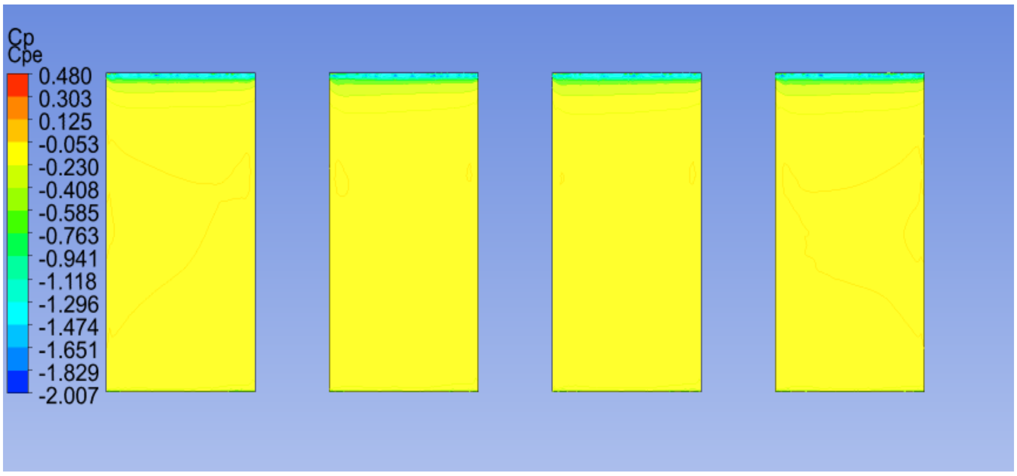

Fig. 3.73 External Pressure Coefficient at Wind Direction 90^0

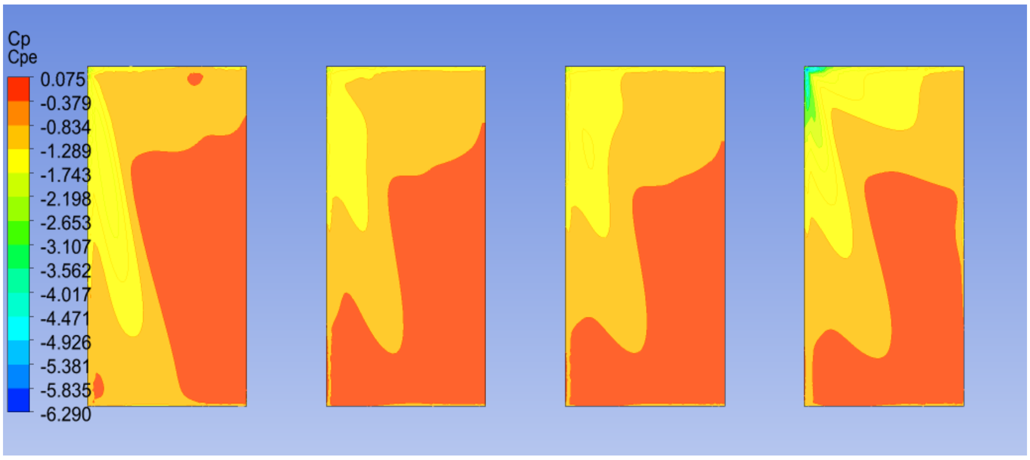

Fig. 3.74 External Pressure Coefficient at Wind Direction 135^0

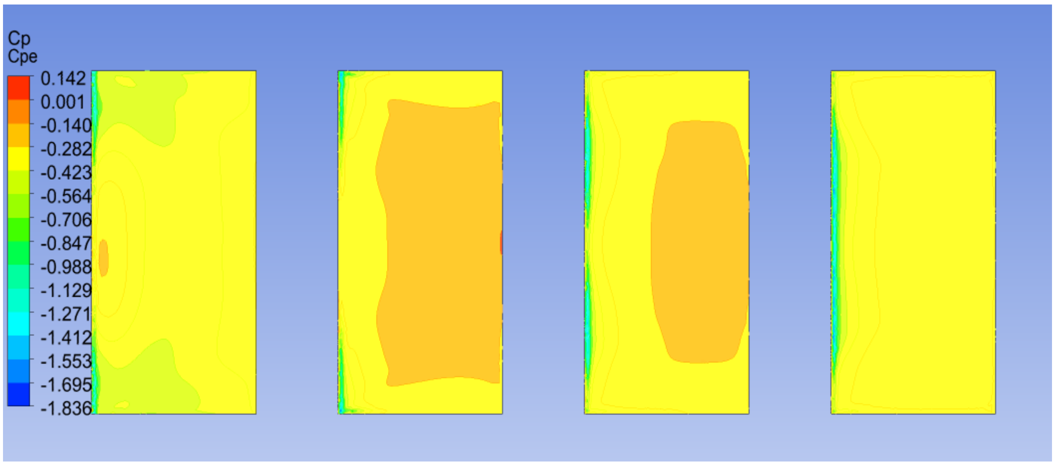

Fig. 3.75 External Pressure Coefficient at Wind Direction 180^0

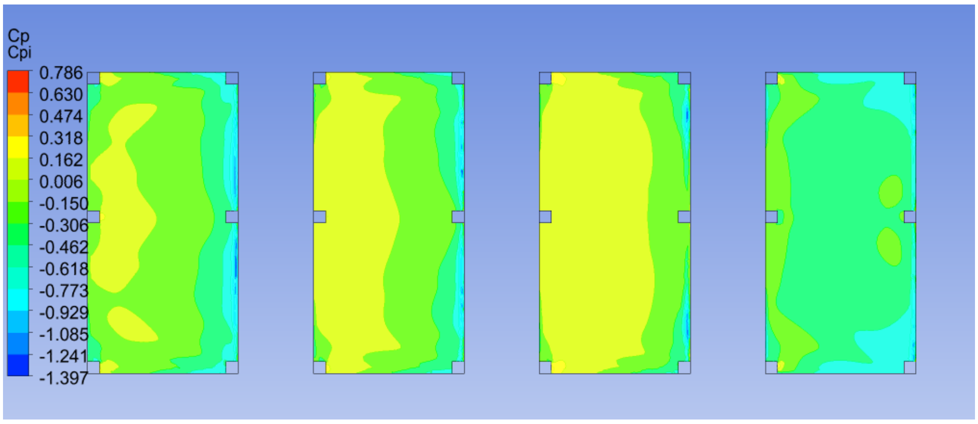

Fig. 3.76 Internal Pressure Coefficient at Wind Direction 0^0

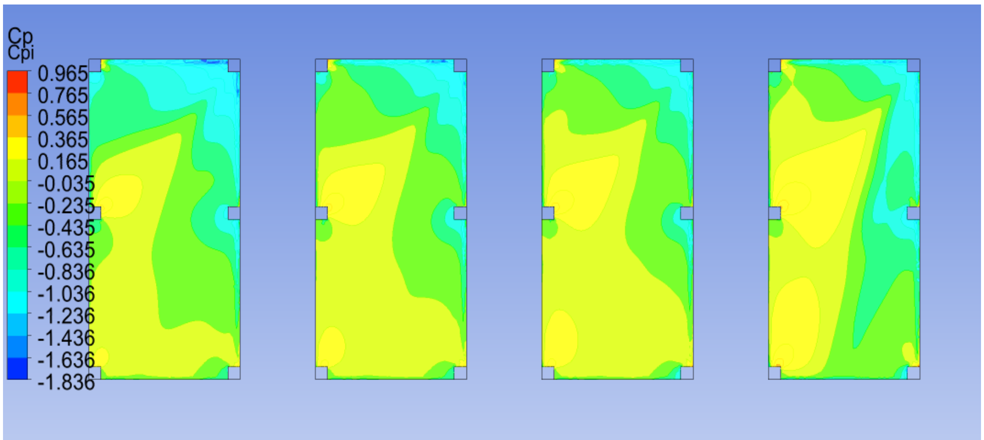

Fig. 3.77 Internal Pressure Coefficient at Wind Direction 45^0

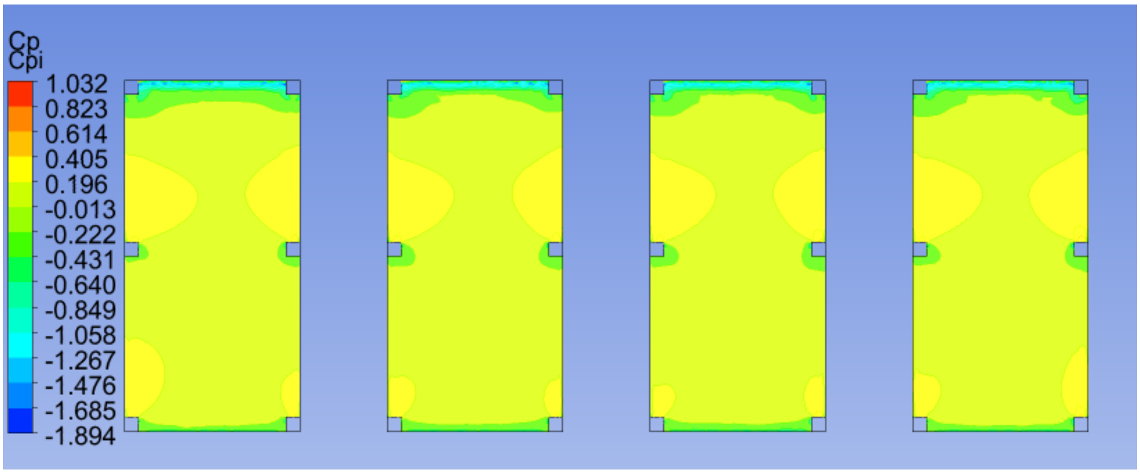

Fig. 3.78 Internal Pressure Coefficient at Wind Direction 90^0

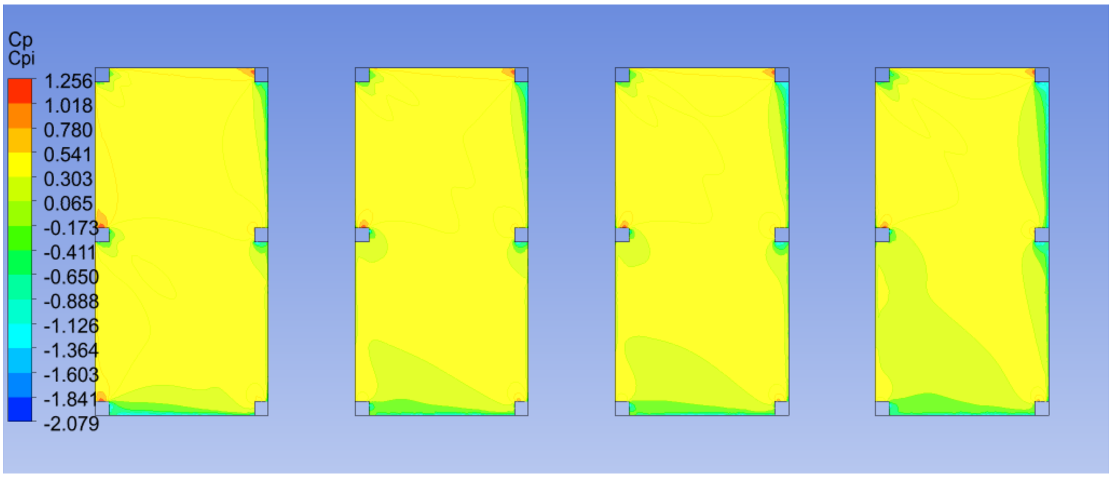

Fig. 3.79 Internal Pressure Coefficient at Wind Direction 135^0

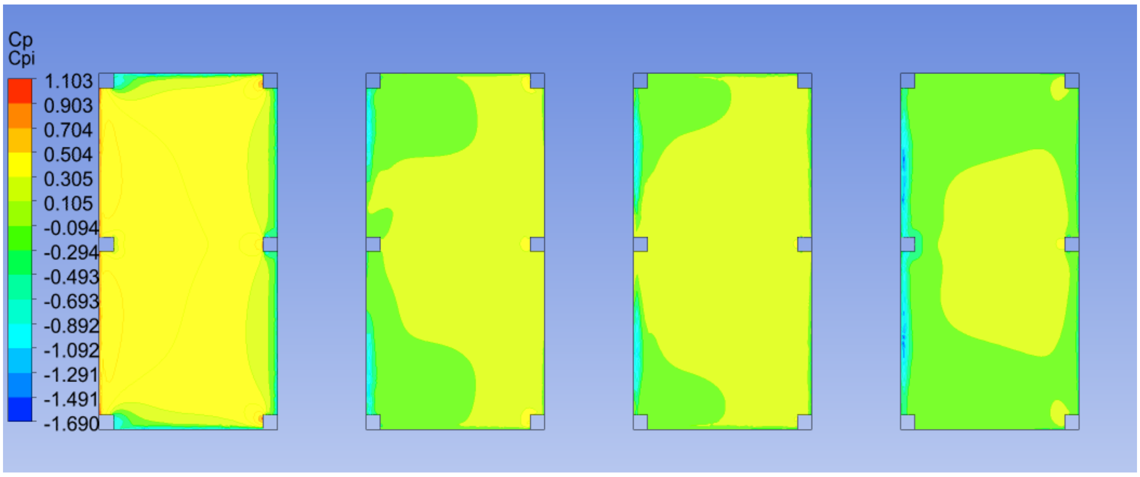

Fig. 3.80 Internal Pressure Coefficient at Wind Direction 180^0

Spacing B = 50

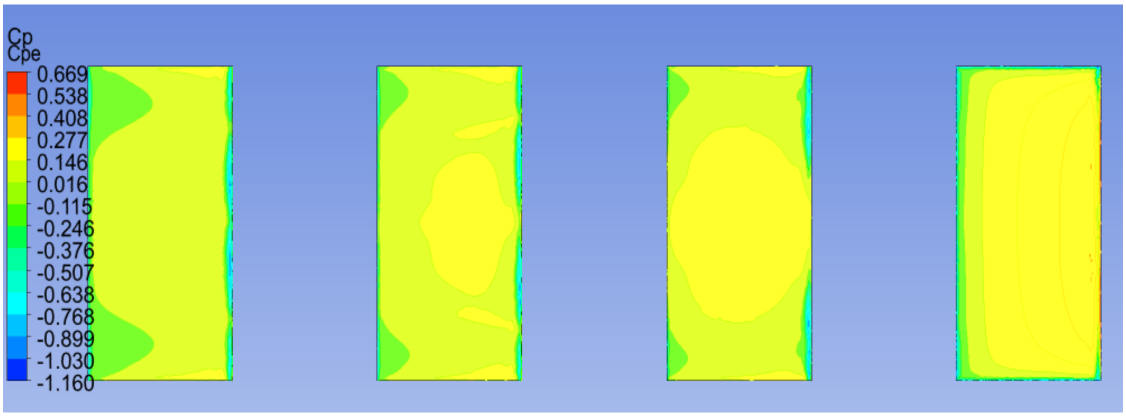

Fig. 3.81 External Pressure Coefficient at Wind Direction 0^0

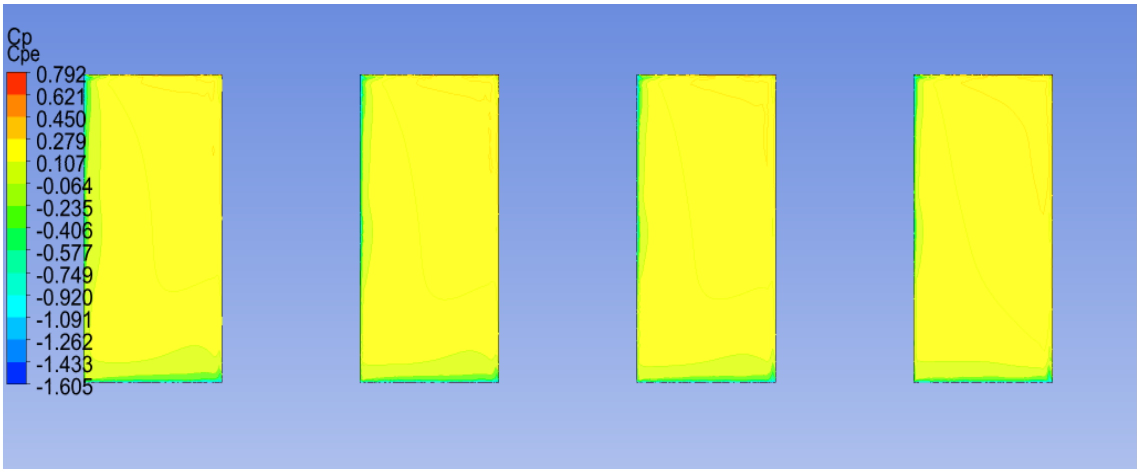

Fig. 3.82 External Pressure Coefficient at Wind Direction 45^0

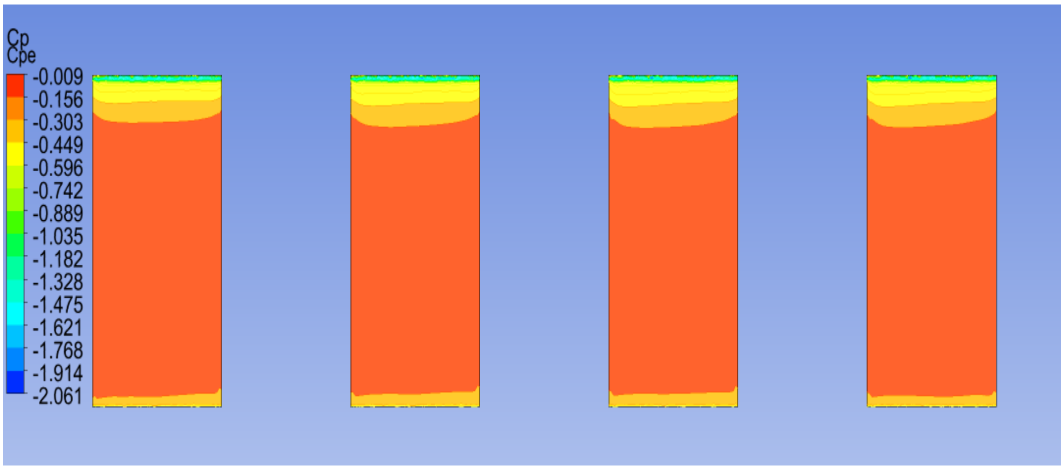

Fig. 3.83 External Pressure Coefficient at Wind Direction 90^0

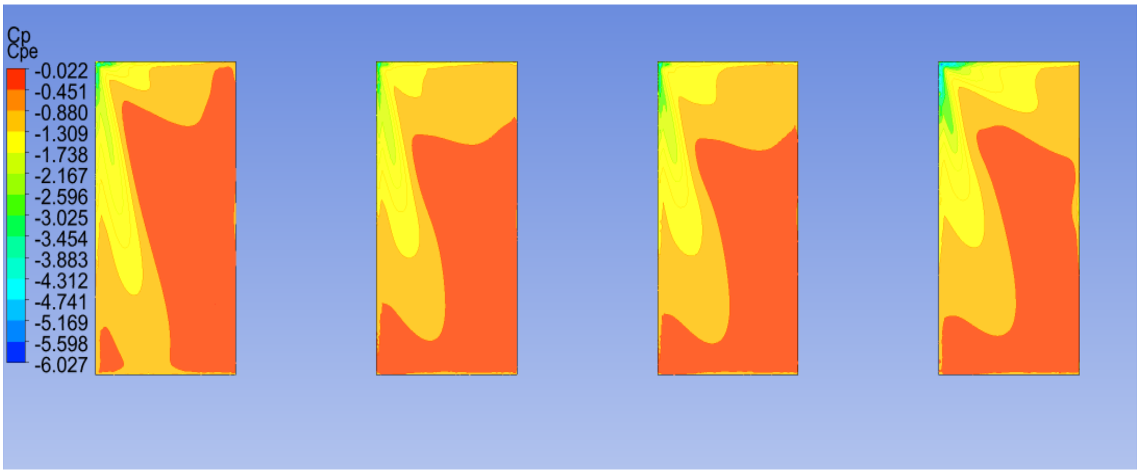

Fig. 3.84 External Pressure Coefficient at Wind Direction 135^0

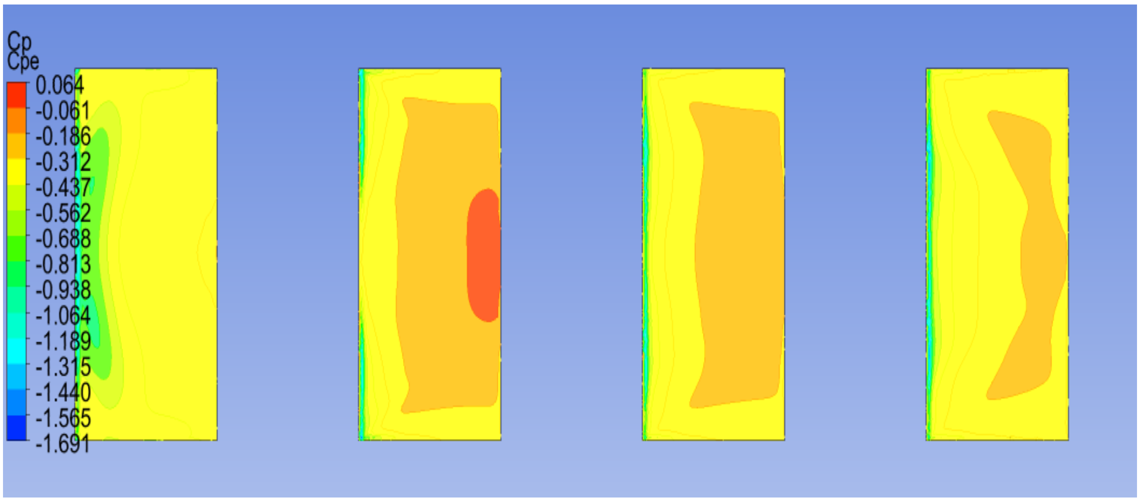

Fig. 3.85 External Pressure Coefficient at Wind Direction 180^0

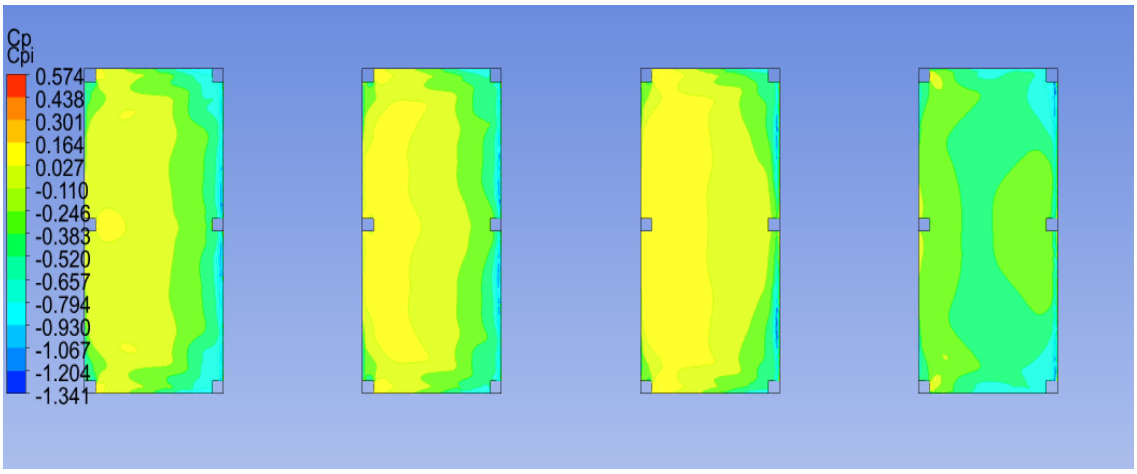

Fig. 3.86 Internal Pressure Coefficient at Wind Direction 0^0

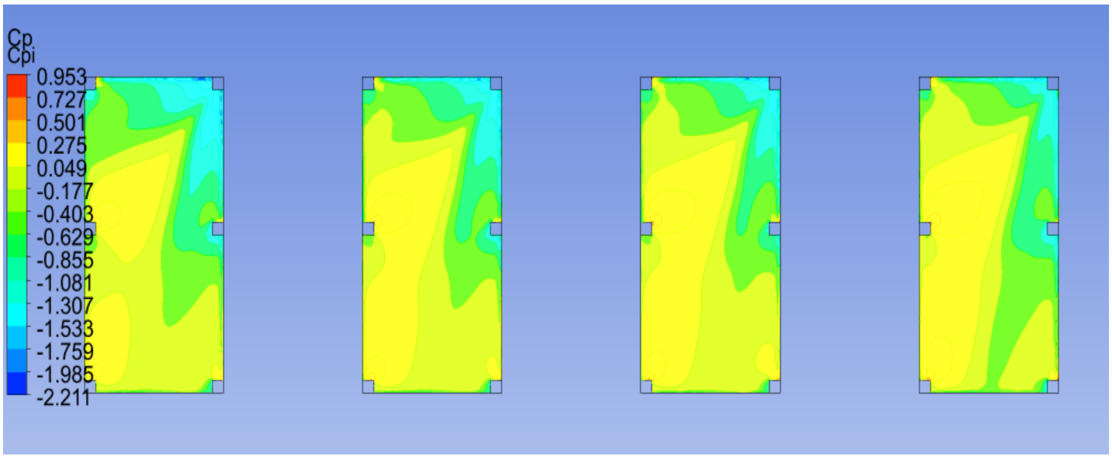

Fig. 3.87 Internal Pressure Coefficient at Wind Direction 45^0

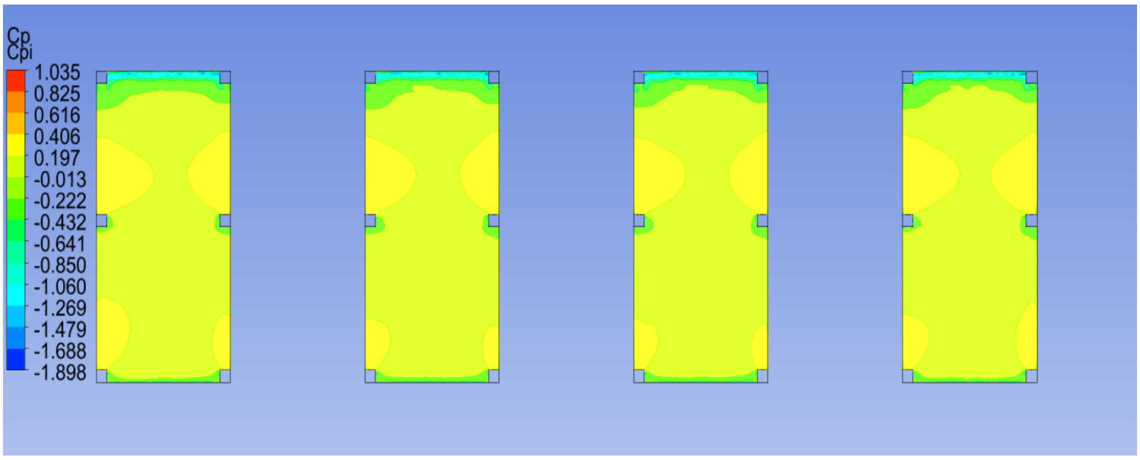

Fig. 3.88 Internal Pressure Coefficient at Wind Direction 90^0

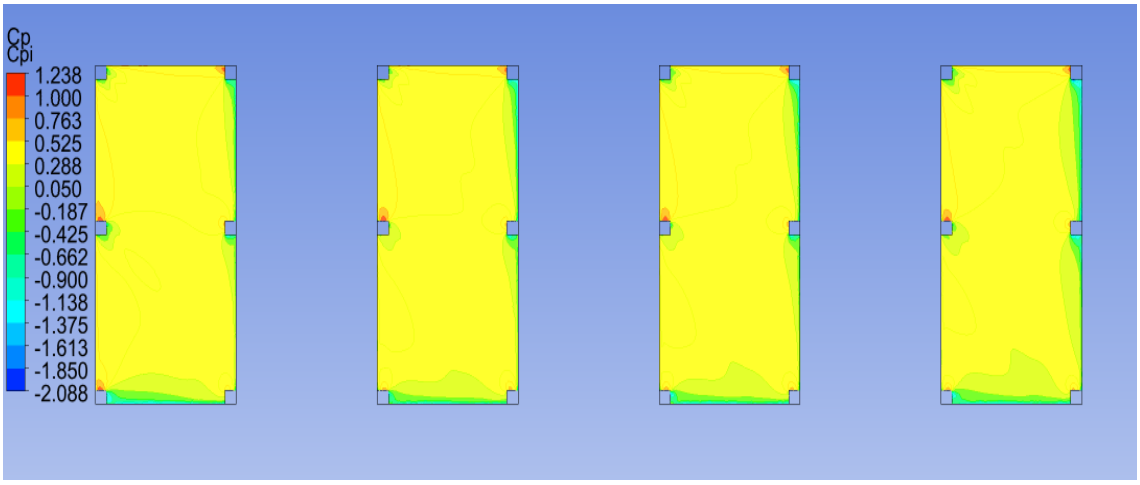

Fig. 3.89 Internal Pressure Coefficient at Wind Direction 135^0

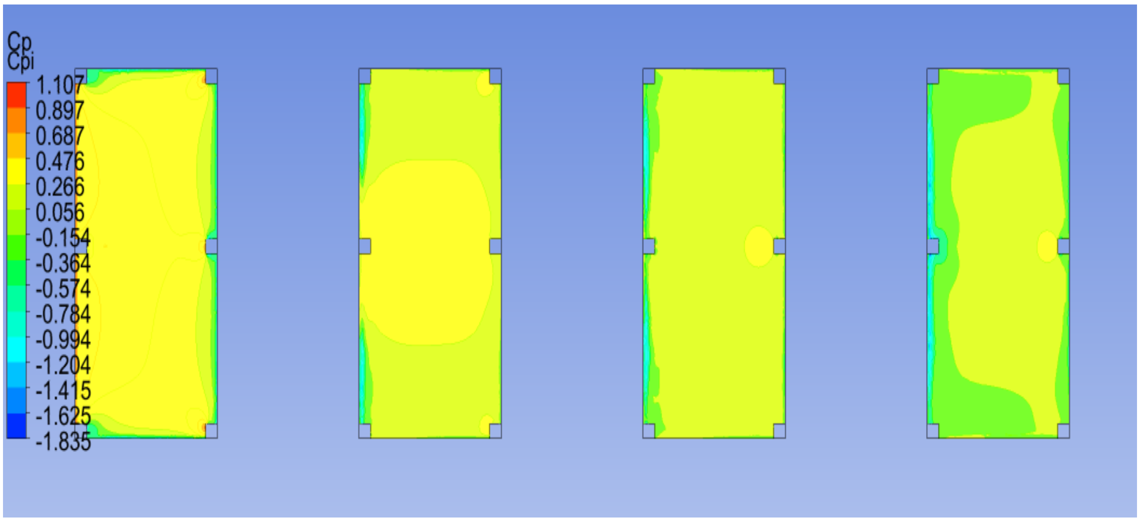

Fig. 3.90 Internal Pressure Coefficient at Wind Direction 180^0

Spacing B = 75

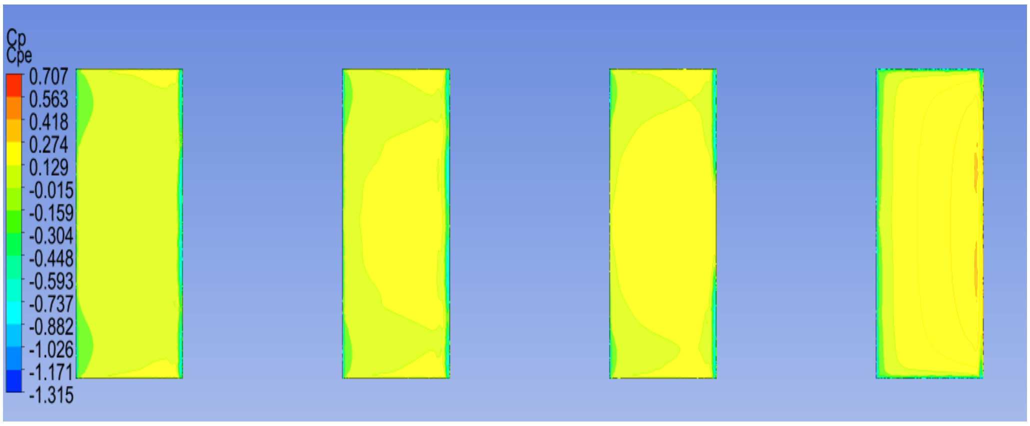

Fig. 3.91 External Pressure Coefficient at Wind Direction 0^0

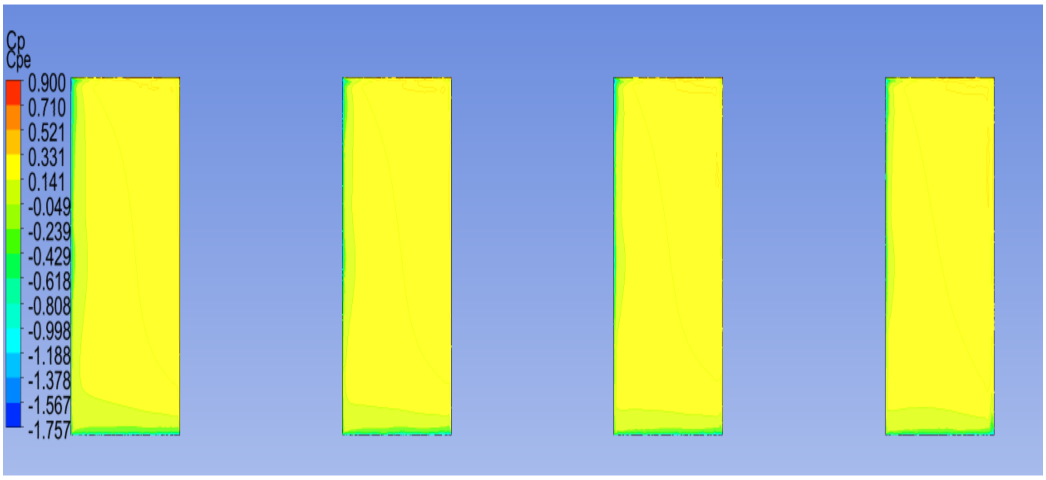

Fig.3.92 External Pressure Coefficient at Wind Direction 45^0

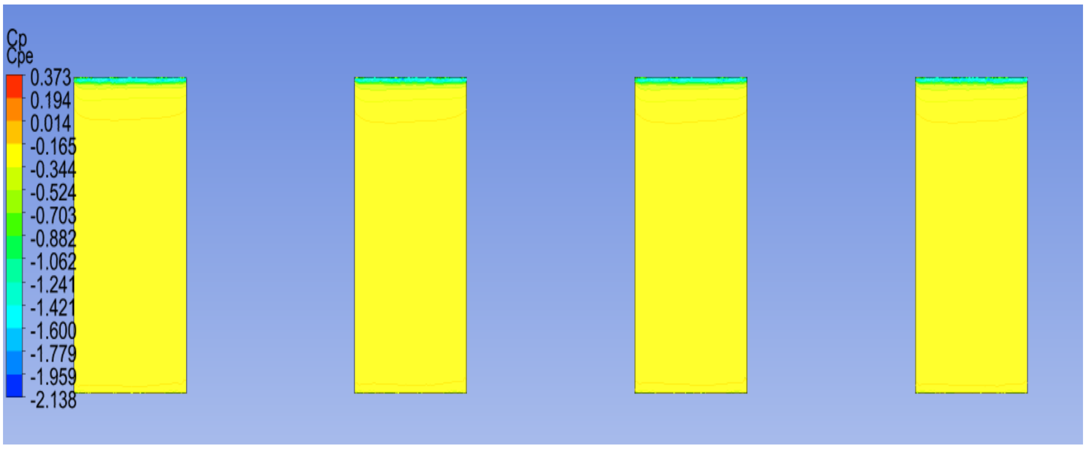

Fig. 3.93 External Pressure Coefficient at Wind Direction 90^0

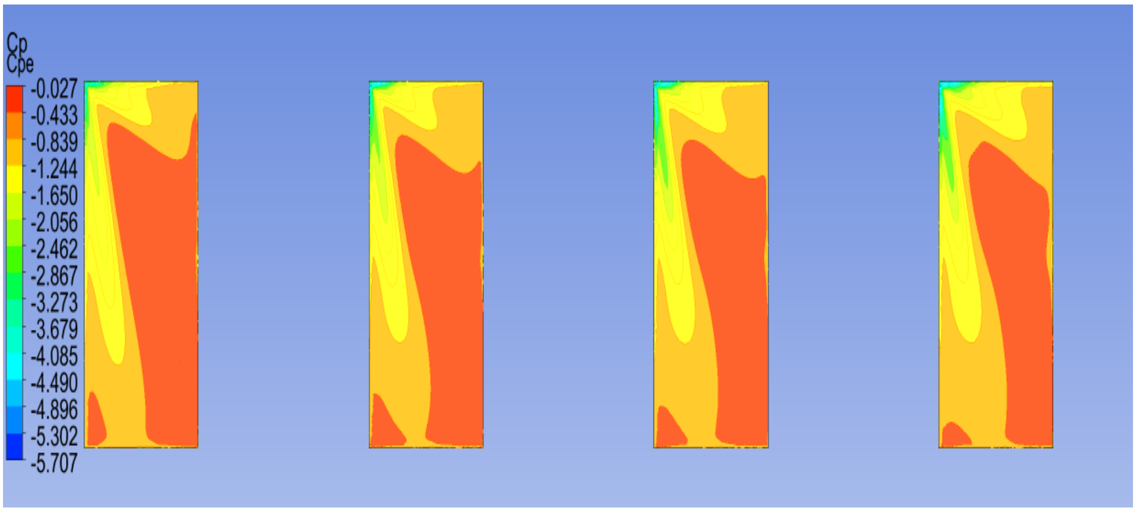

Fig. 3.94 External Pressure Coefficient at Wind Direction 135^0

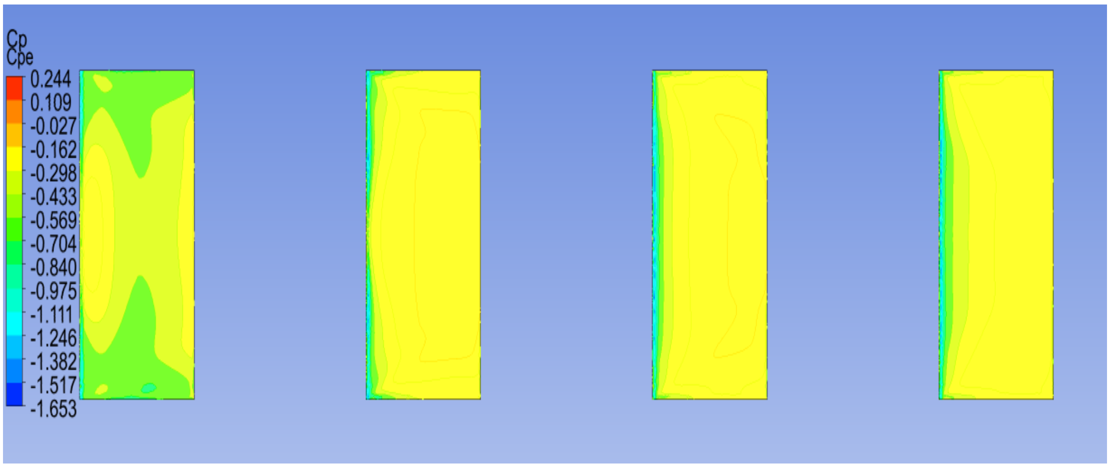

Fig. 3.95 External Pressure Coefficient at Wind Direction 180^0

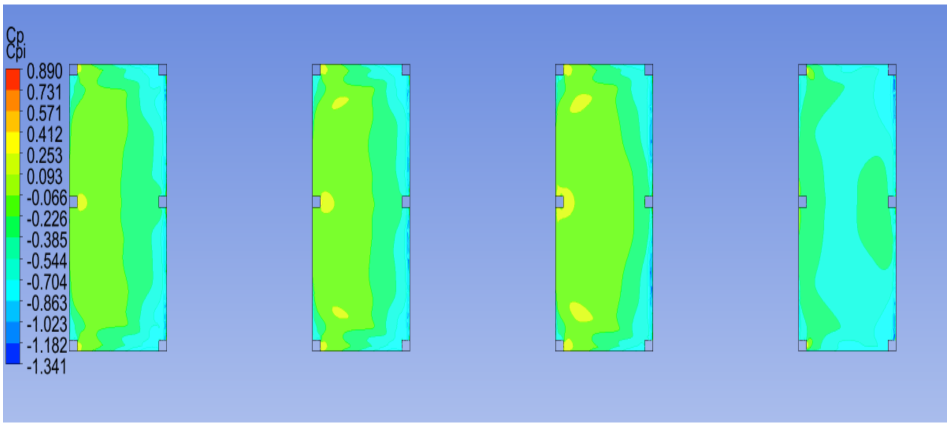

Fig. 3.96 Internal Pressure Coefficient at Wind Direction 0

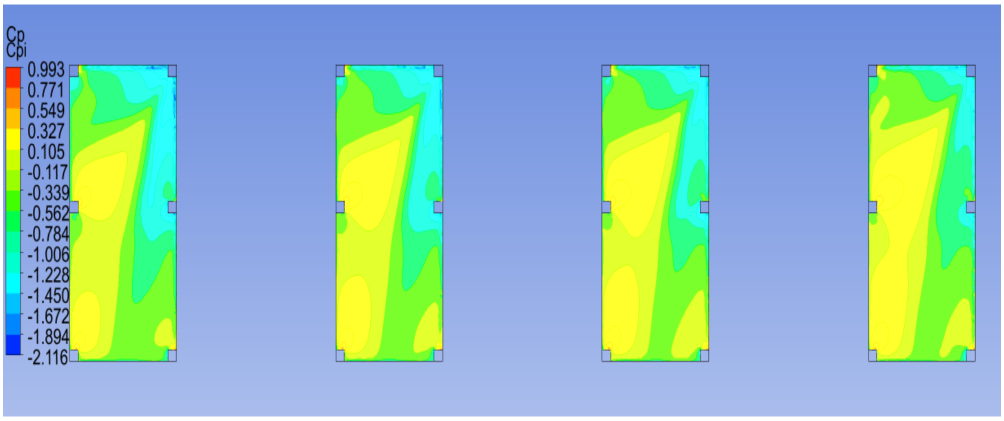

Fig. 3.97 Internal Pressure Coefficient at Wind Direction 45^0

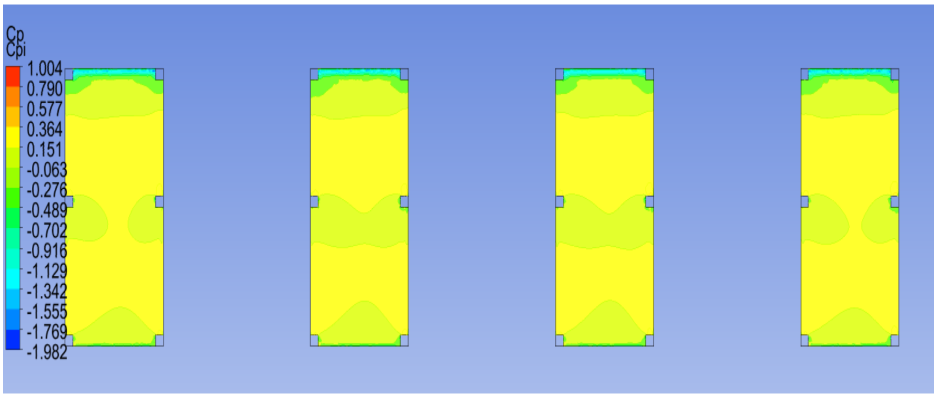

Fig. 3.98 Internal Pressure Coefficient at Wind Direction 90^0

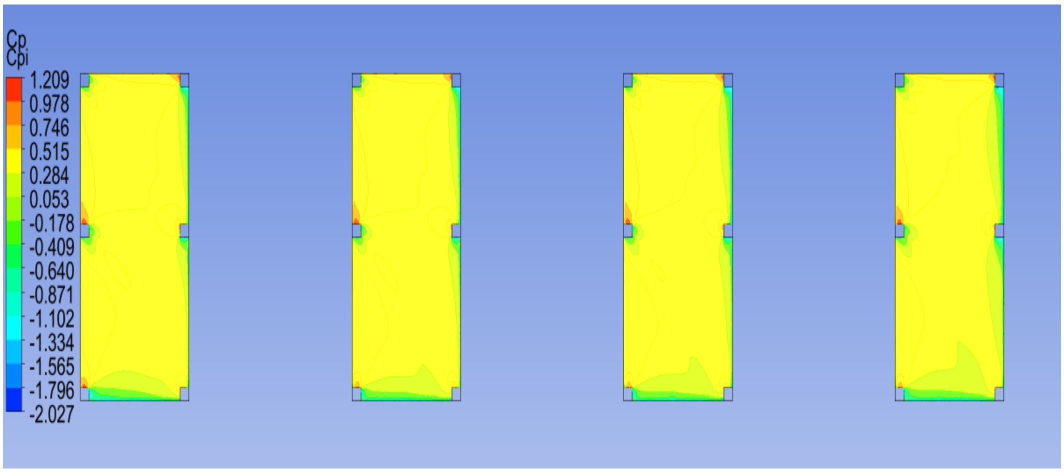

Fig. 3.99 Internal Pressure Coefficient at Wind Direction 135^0

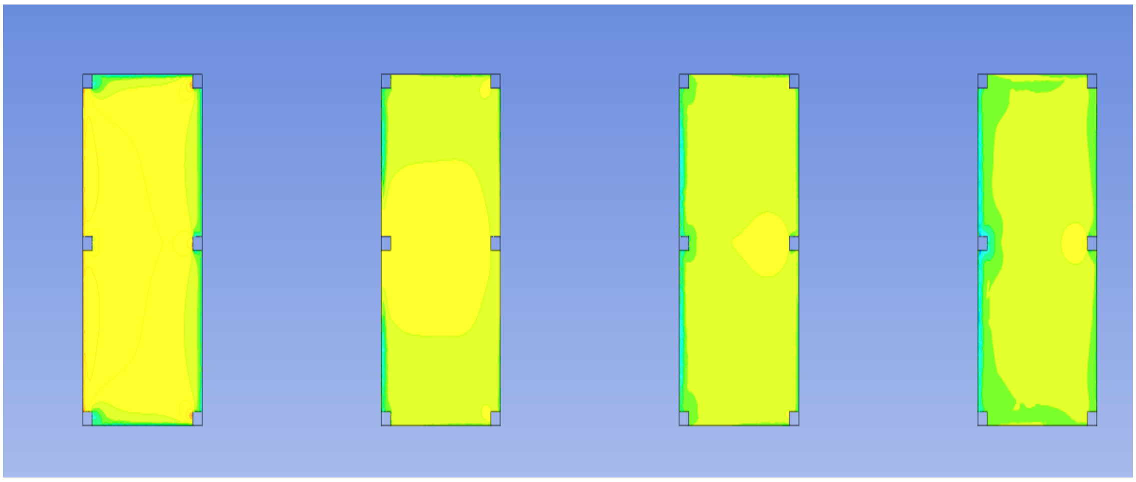

Fig. 3.100 Internal Pressure Coefficient at Wind Direction 180^0

Spacing B = 100

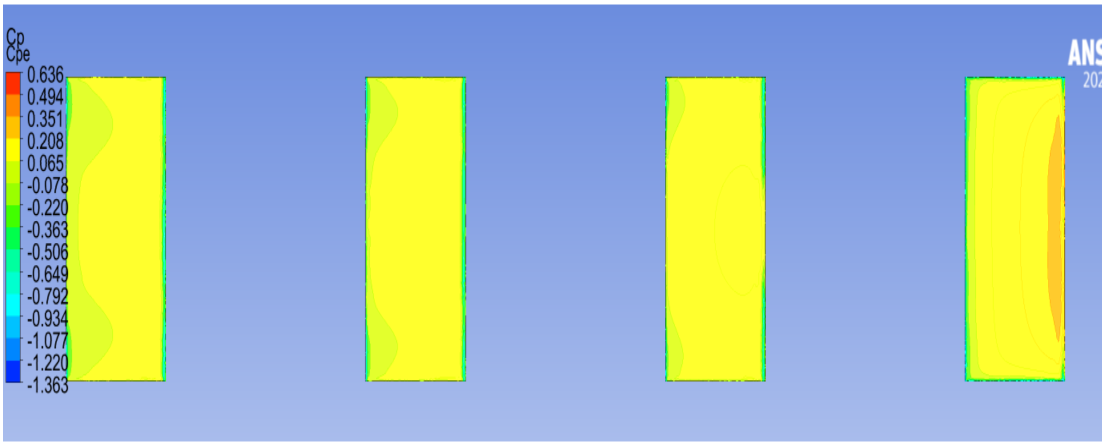

Fig. 3.101 External Pressure Coefficient at Wind Direction 0^0

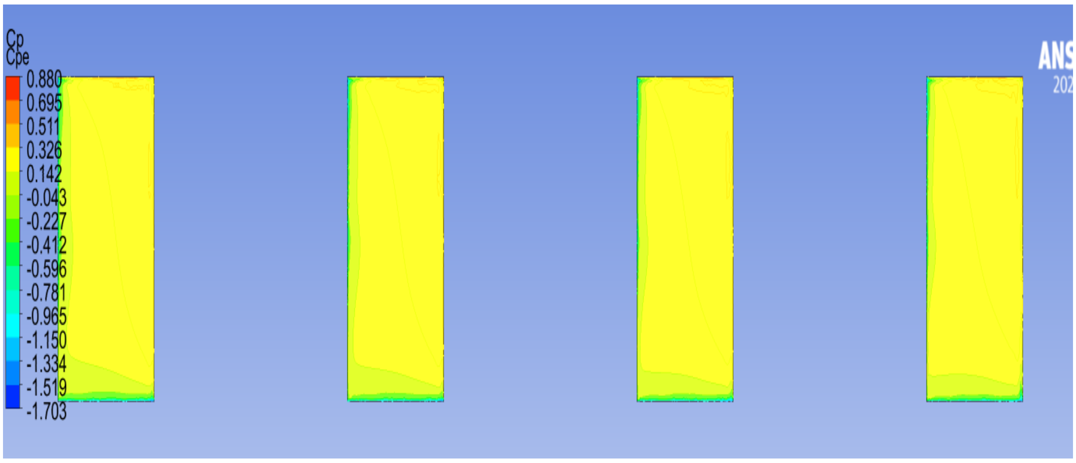

Fig. 3.102 External Pressure Coefficient at Wind Direction 45^0

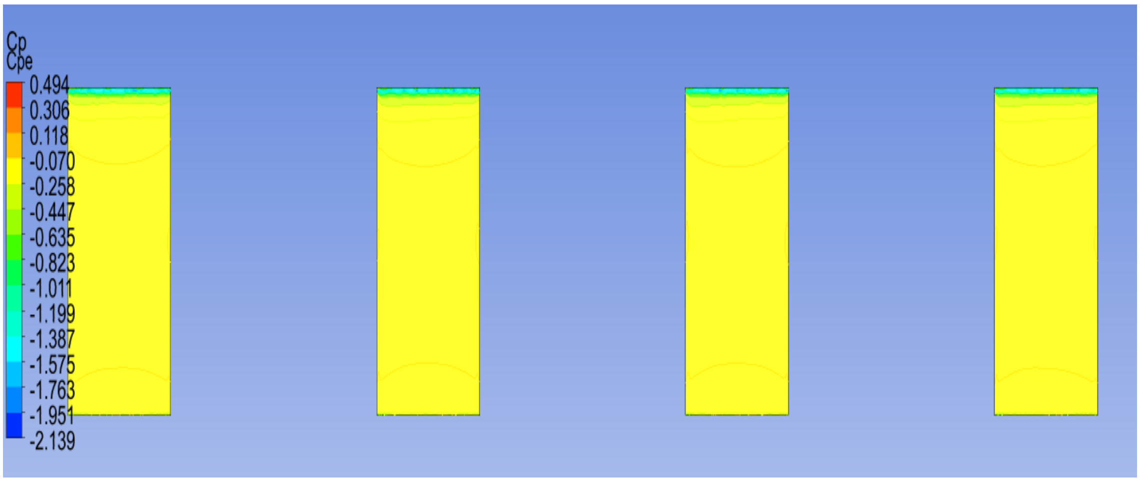

Fig. 3.103 External Pressure Coefficient at Wind Direction 90^0

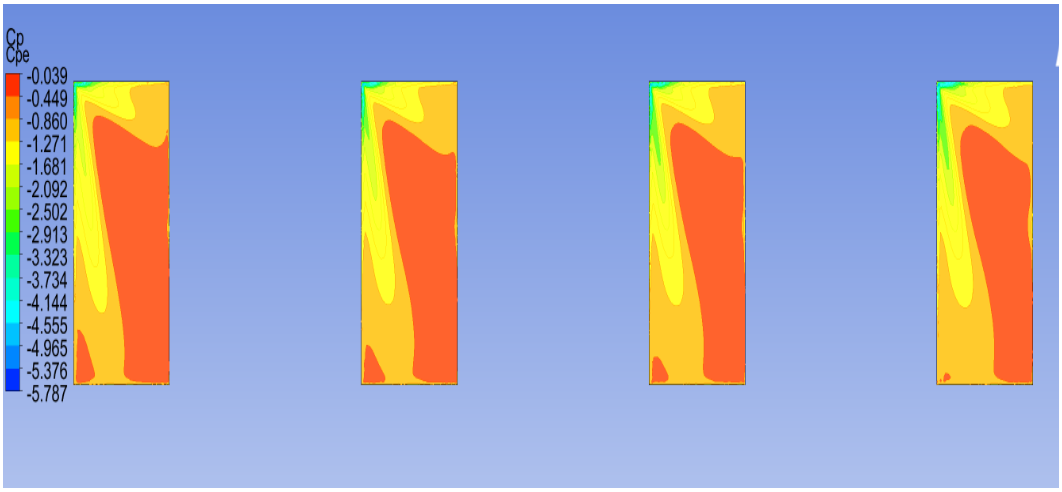

Fig. 3.104 External Pressure Coefficient at Wind Direction 135^0

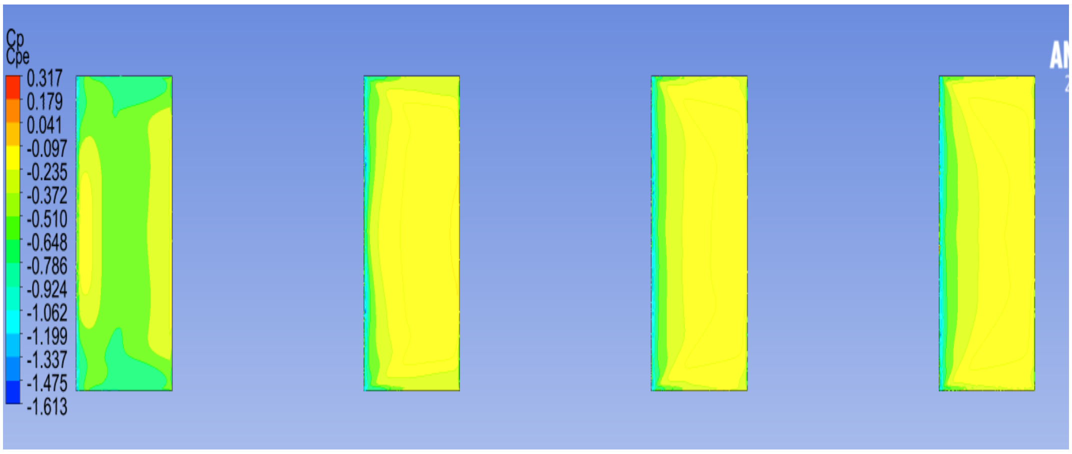

Fig. 3.105 External Pressure Coefficient at Wind Direction 180^0

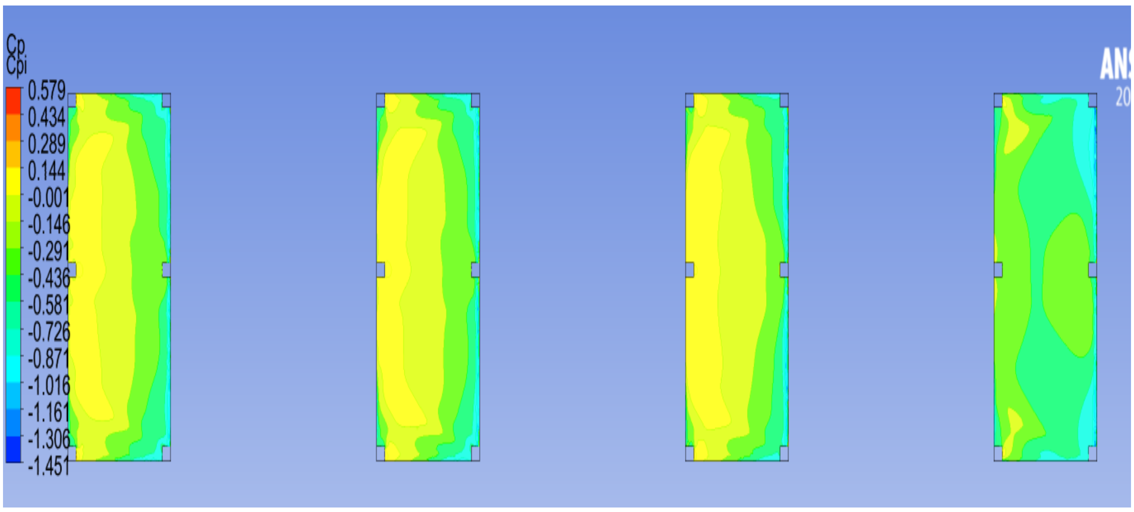

Fig. 3.106 Internal Pressure Coefficient at Wind Direction 0^0

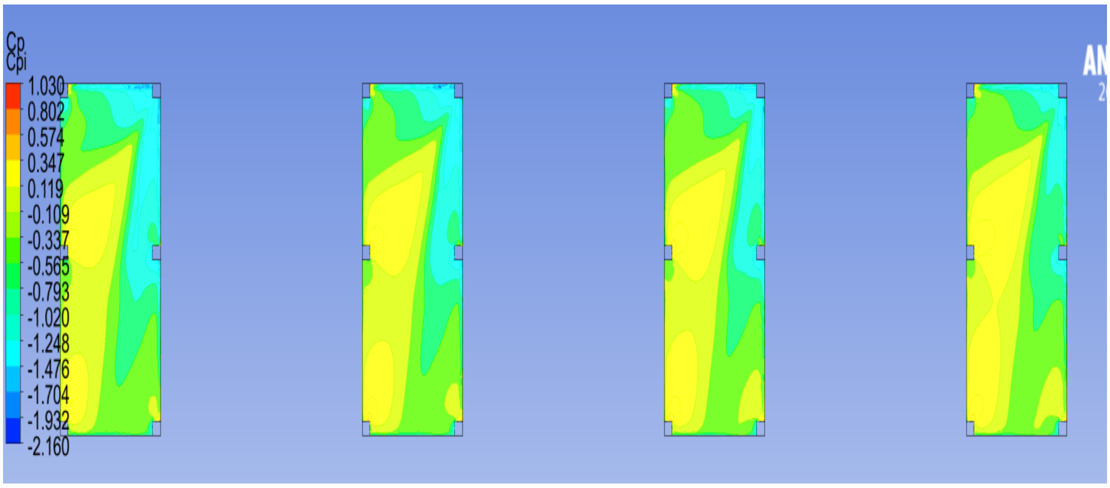

Fig. 3.107 Internal Pressure Coefficient at Wind Direction 45^0

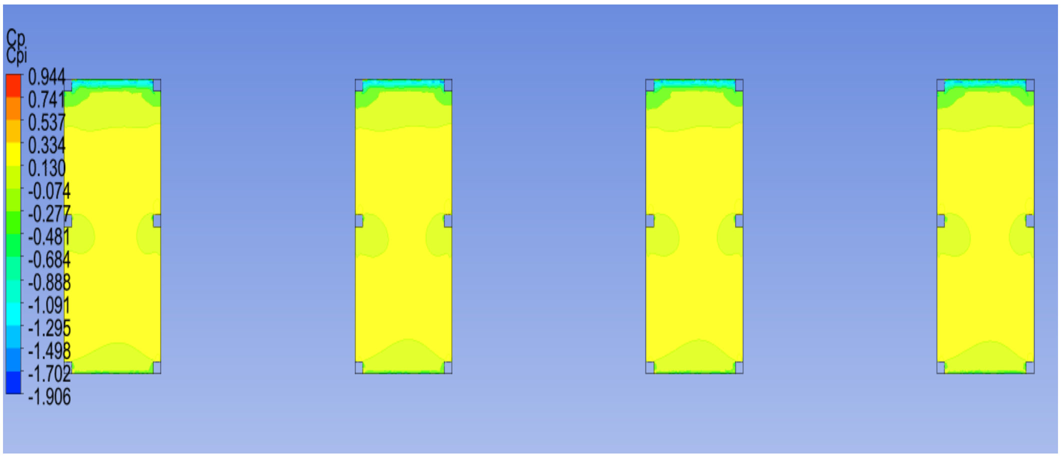

Fig. 3.108 Internal Pressure Coefficient at Wind Direction 90^0

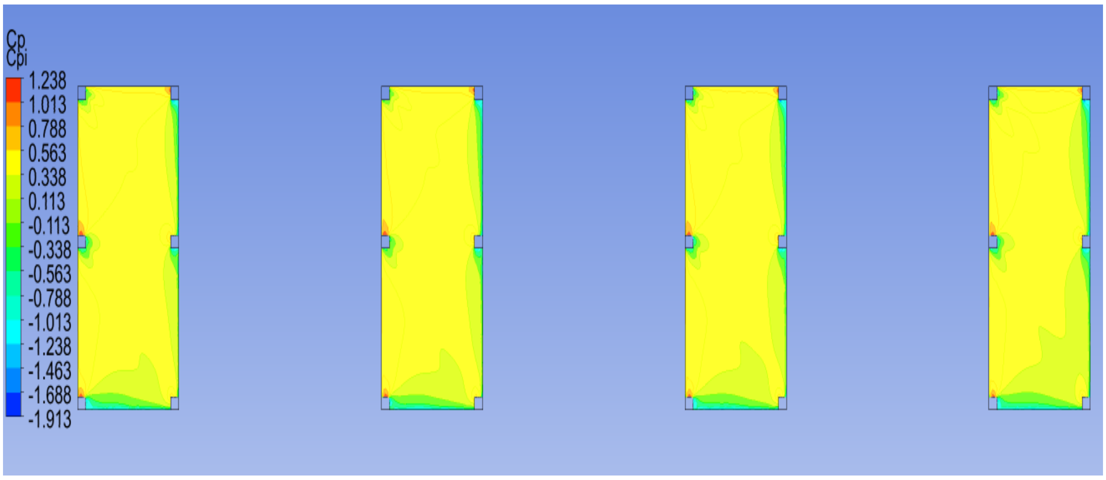

Fig. 3.109 Internal Pressure Coefficient at Wind Direction 135^0

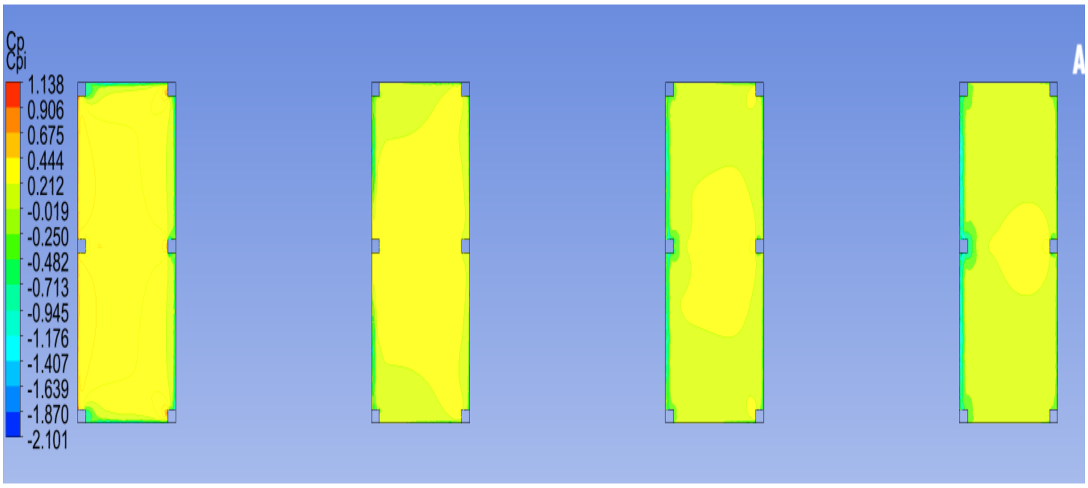

Fig. 3.110 Internal Pressure Coefficient at Wind Direction 180^0

The Fig.61 to Fig 110 shows the contours for external and internal pressure for roof slope 20 ° having various spacing and change in the values of Cpe was obserbved to the change in incidence wind direction from 0 ° to 180°. It was seen that values of respective Cpe was higher as we increase roof slope from 10 ° to 20° .The same pattern was obersved as seen in roof angle 10 °

3.8.11 at Roof Angle 30^0

Spacing B = 0

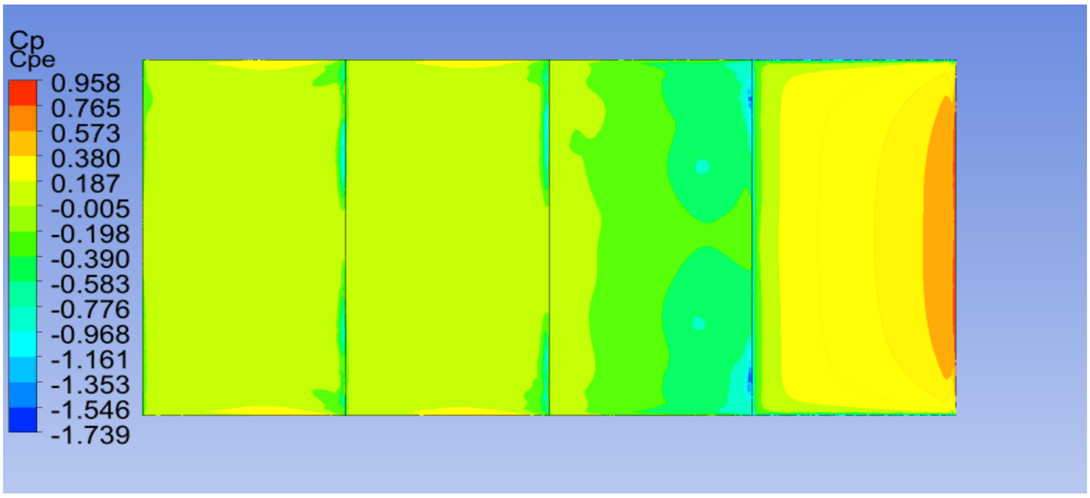

Fig. 3.111 External Pressure Coefficient at Wind Direction 0^0

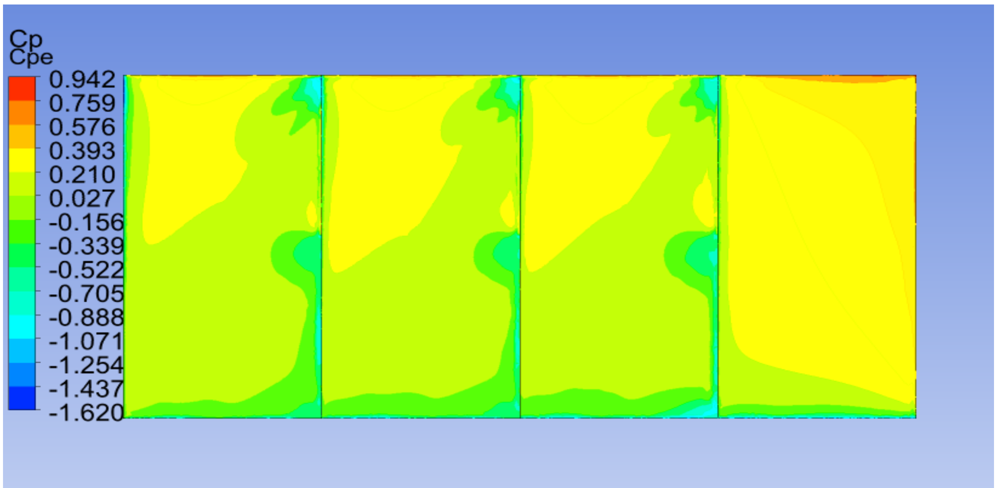

Fig. 3.112 External Pressure Coefficient at Wind Direction 45^0

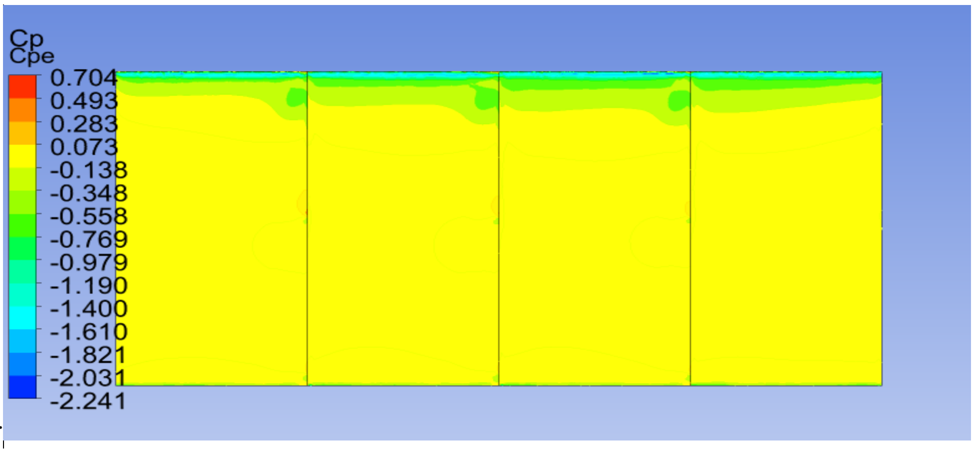

Fig. 3.113 External Pressure Coefficient at Wind Direction 90^0

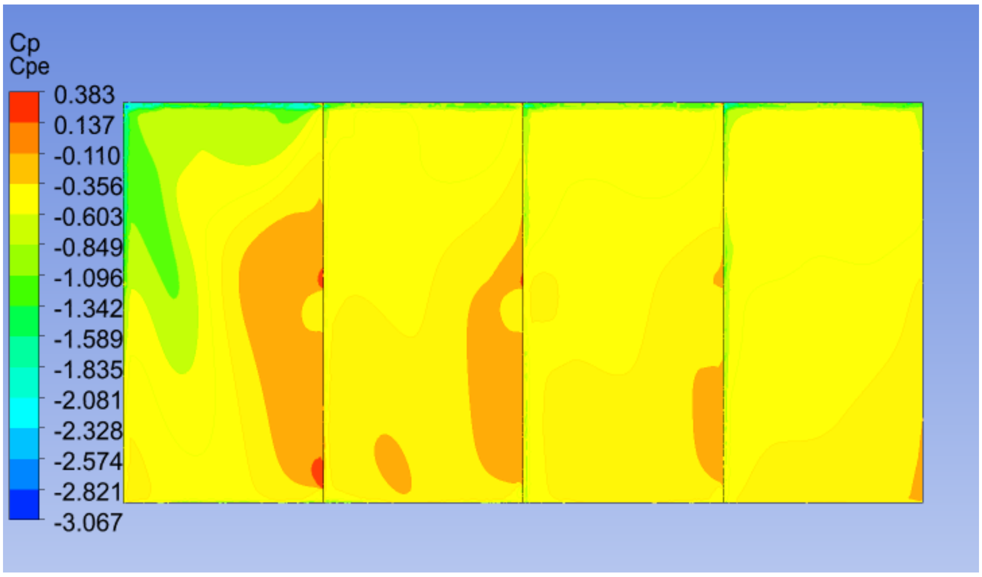

Fig. 3.114 External Pressure Coefficient at Wind Direction 135^0

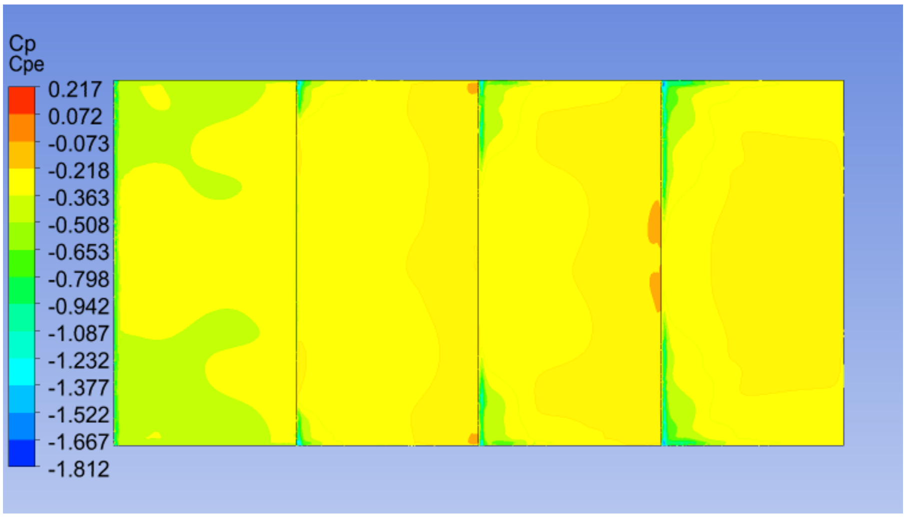

Fig.

3.115 External Pressure Coefficient at Wind Direction 180^0

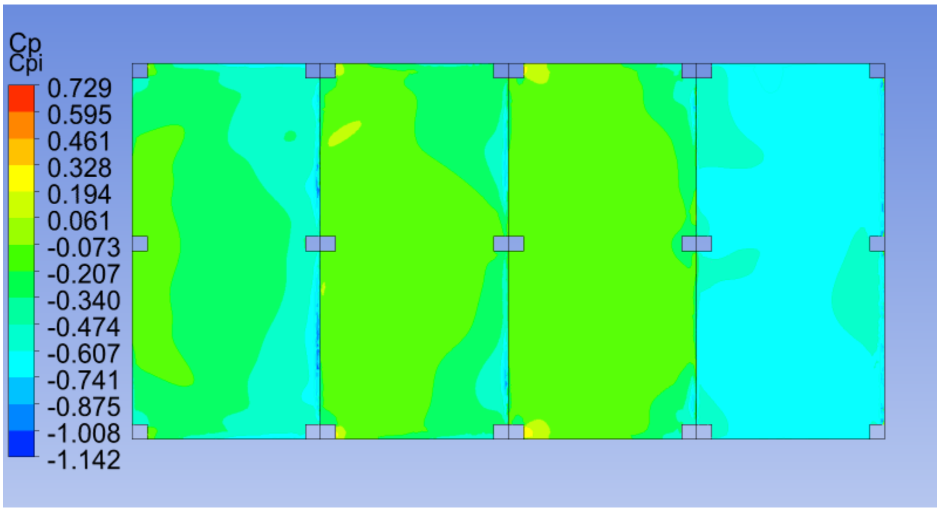

Fig.

3.116 Internal Pressure Coefficient at Wind Direction 0^0

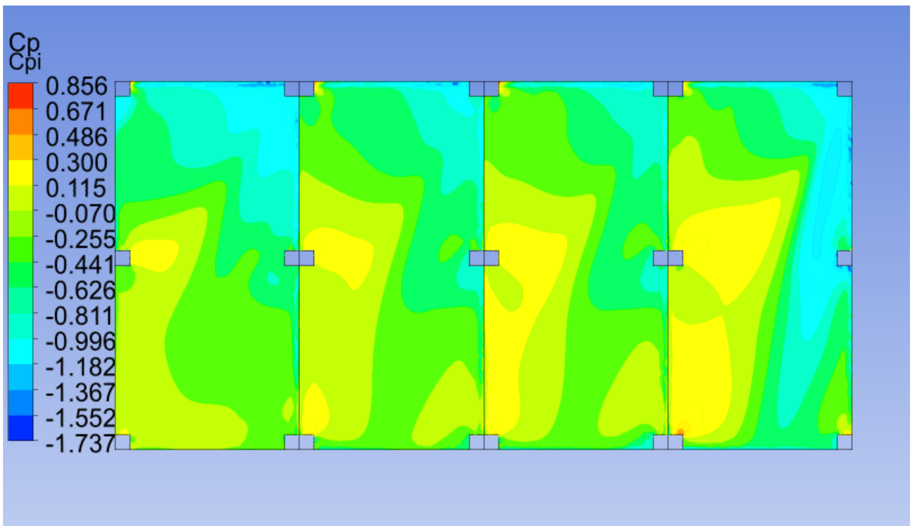

Fig.

3.117 Internal Pressure Coefficient at Wind Direction 45^0

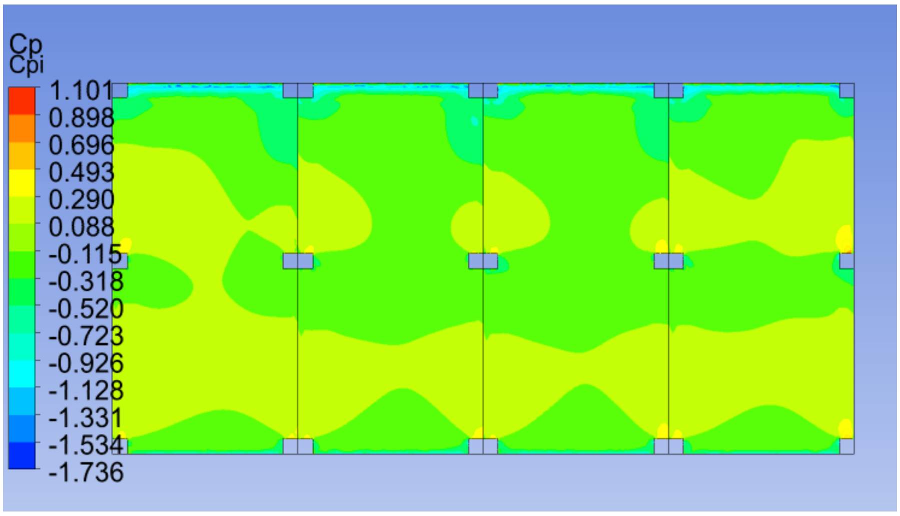

Fig. 3.118 Internal Pressure Coefficient at Wind Direction 90^0

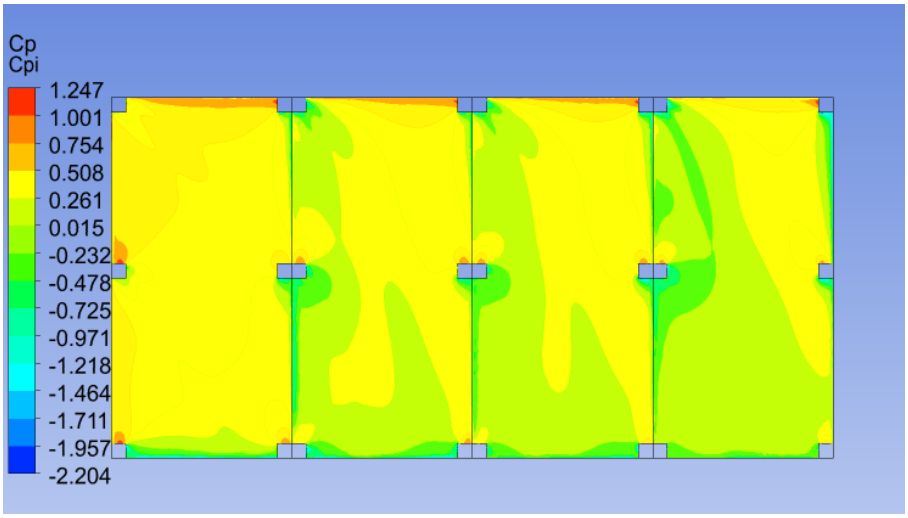

Fig. 3.119 Internal Pressure Coefficient at Wind Direction 135^0

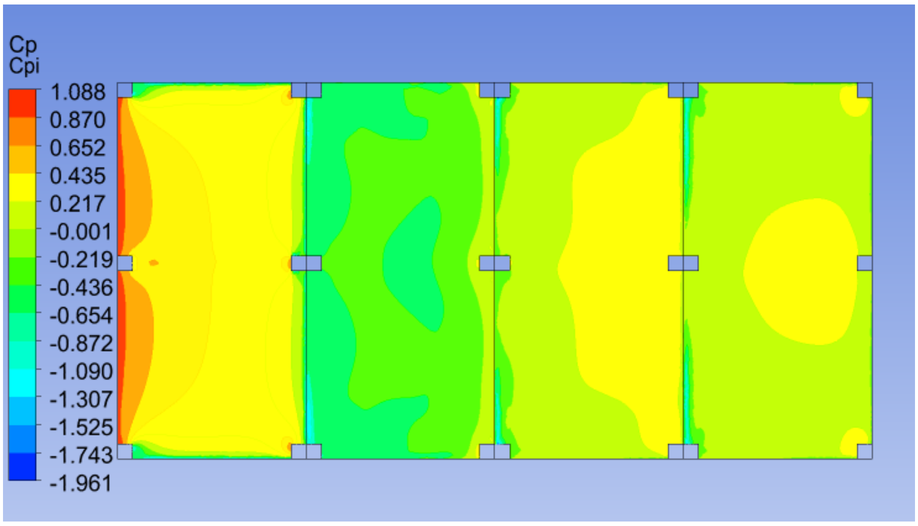

Fig. 3.120 Internal Pressure Coefficient at Wind Direction 180^0

Spacing B = 25

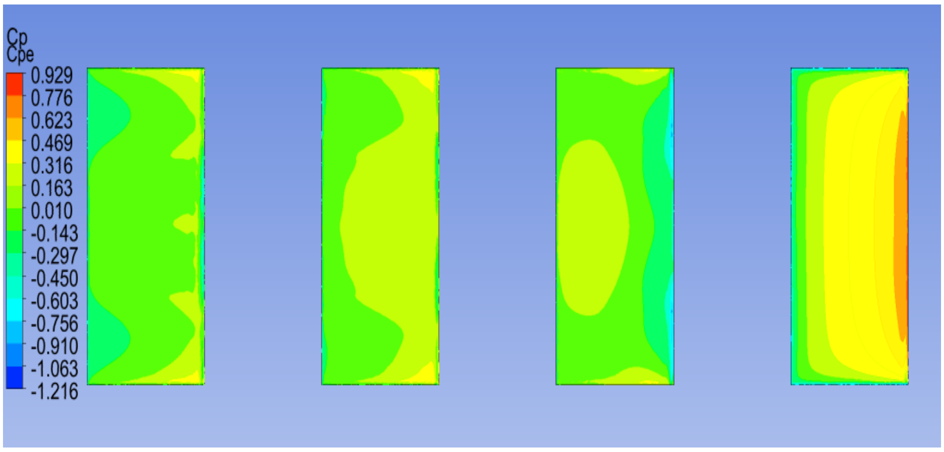

Fig. 3.121 External Pressure Coefficient at Wind Direction 0^0

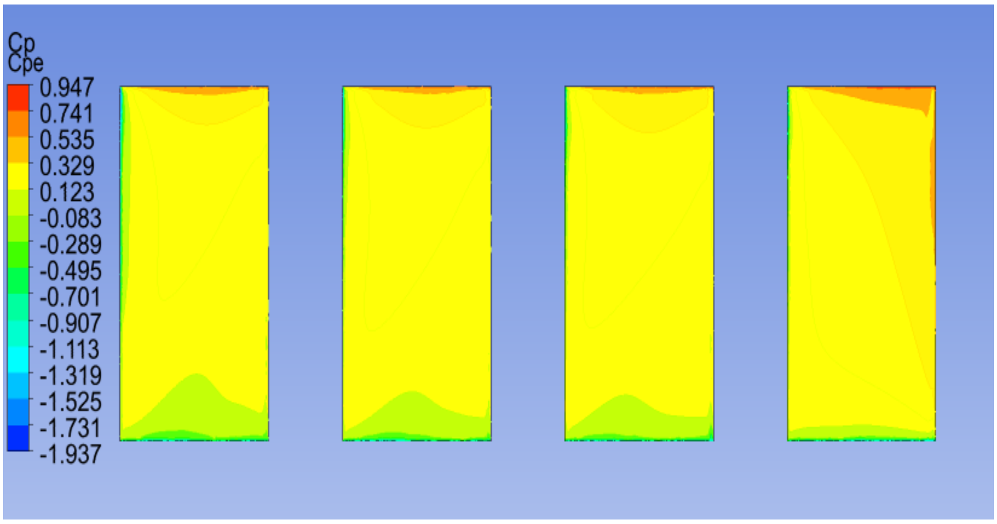

Fig. 3.122 External Pressure Coefficient at Wind Direction 45^0

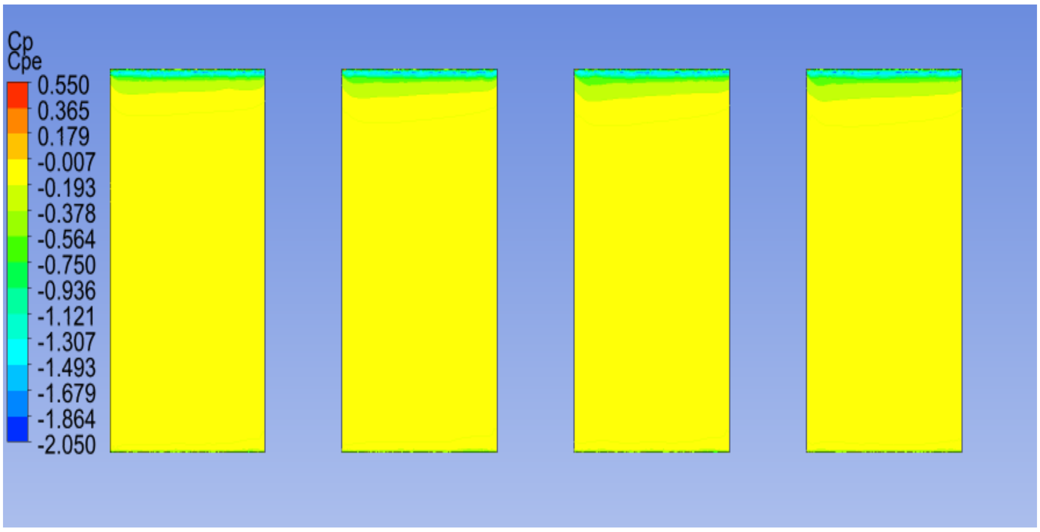

Fig. 3.123 External Pressure Coefficient at Wind Direction 90^0

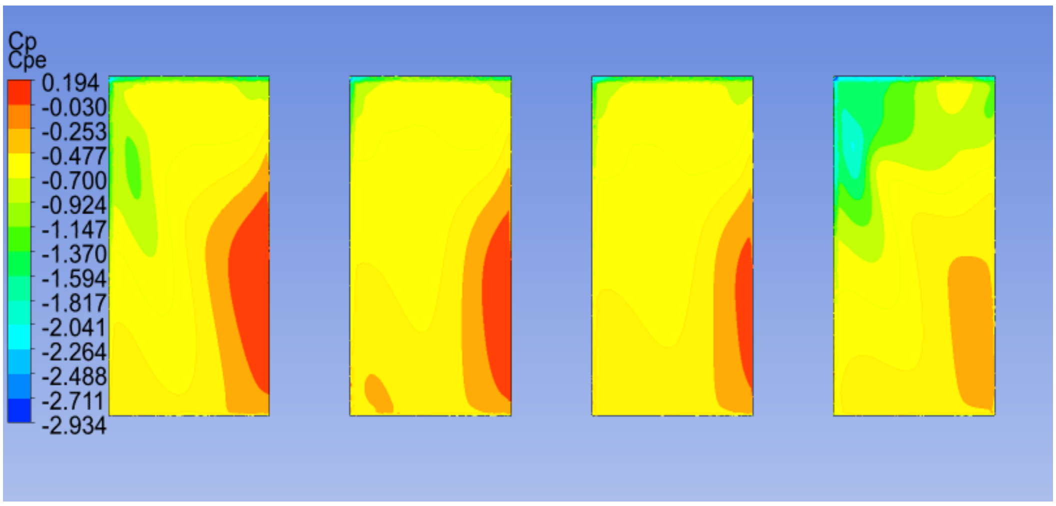

Fig. 3.124 External Pressure Coefficient at Wind Direction 135^0

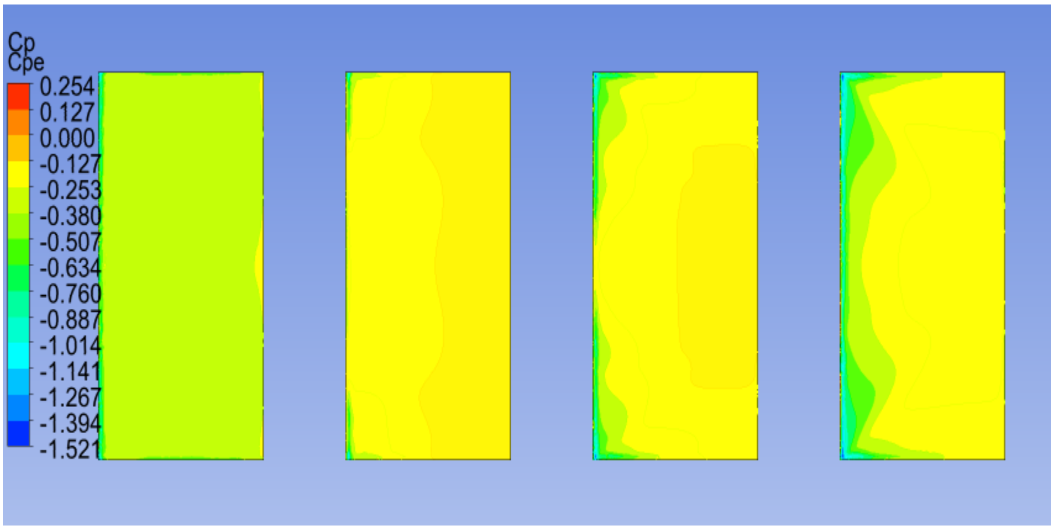

Fig. 3.125 External Pressure Coefficient at Wind Direction 180^0

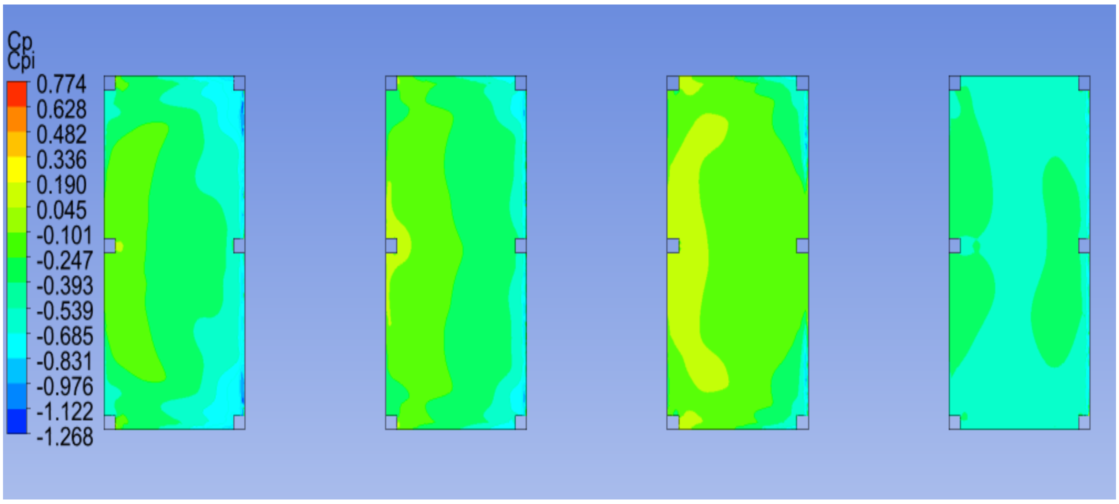

Fig. 3.126 Internal Pressure Coefficient at Wind Direction 0^0

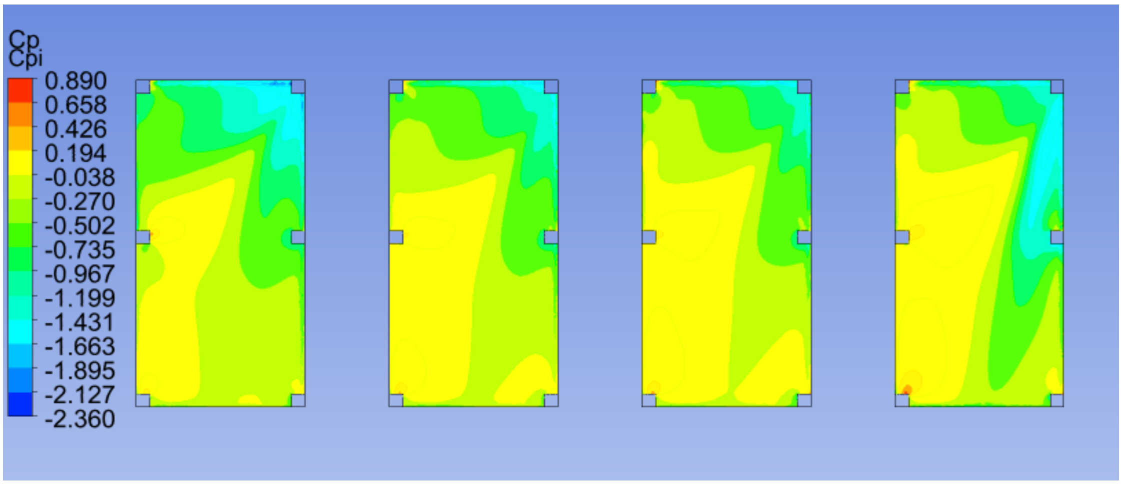

Fig. 3.127 Internal Pressure Coefficient at Wind Direction 45^0

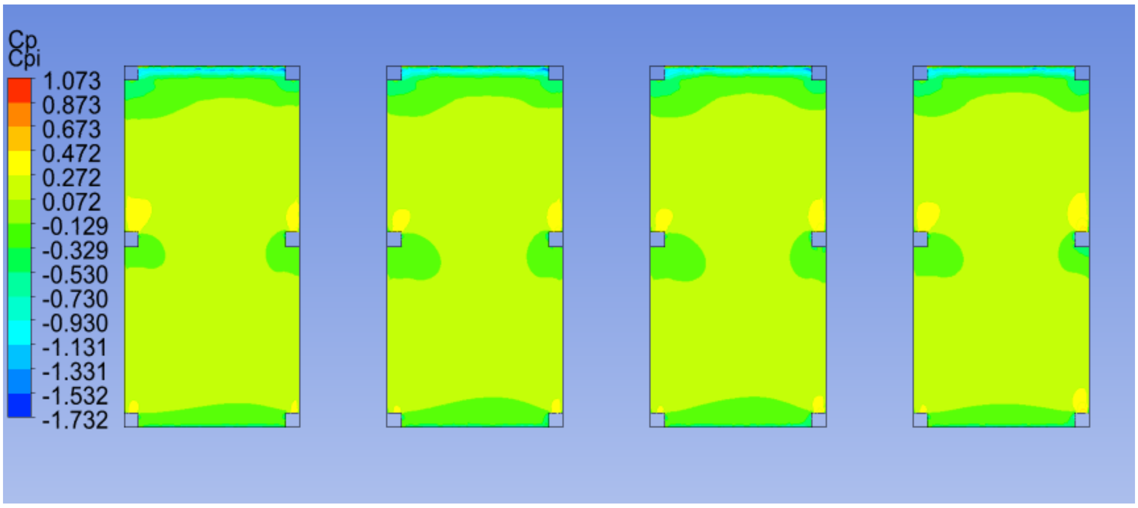

Fig. 3.128 Internal Pressure Coefficient at Wind Direction 90^0

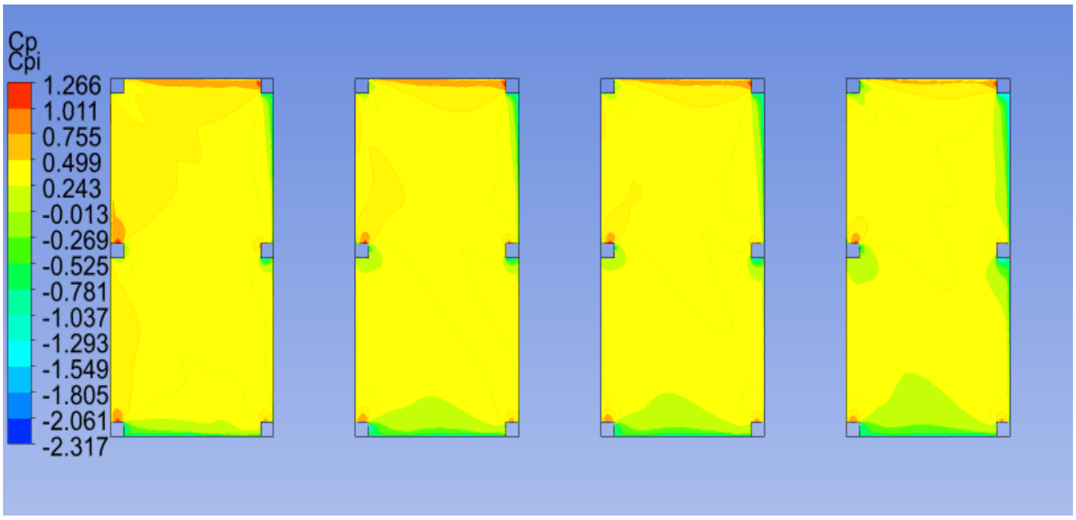

Fig. 3.129 Internal Pressure Coefficient at Wind Direction 135^0

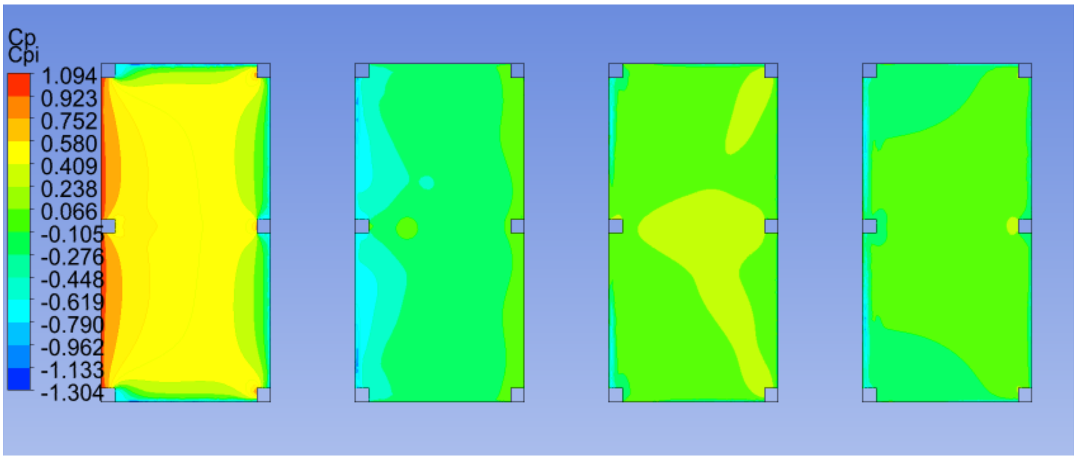

Fig. 3.130 Internal Pressure Coefficient at Wind Direction 180^0

Spacing B = 50

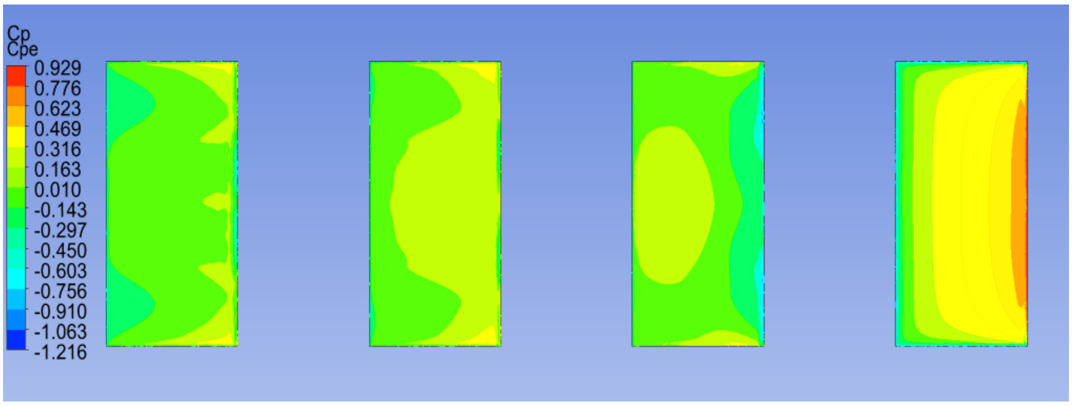

Fig. 3.131 External Pressure Coefficient at Wind Direction 0^0

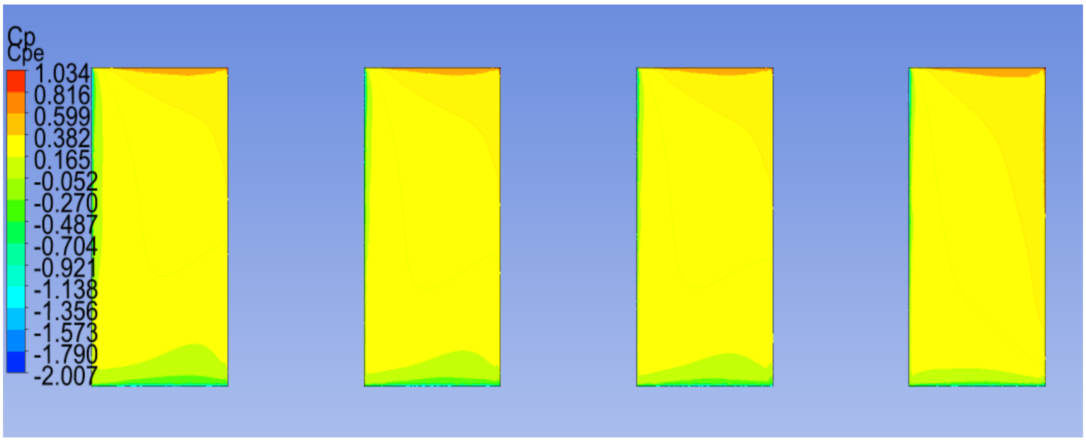

Fig. 3.132 External Pressure Coefficient at Wind Direction 45^0

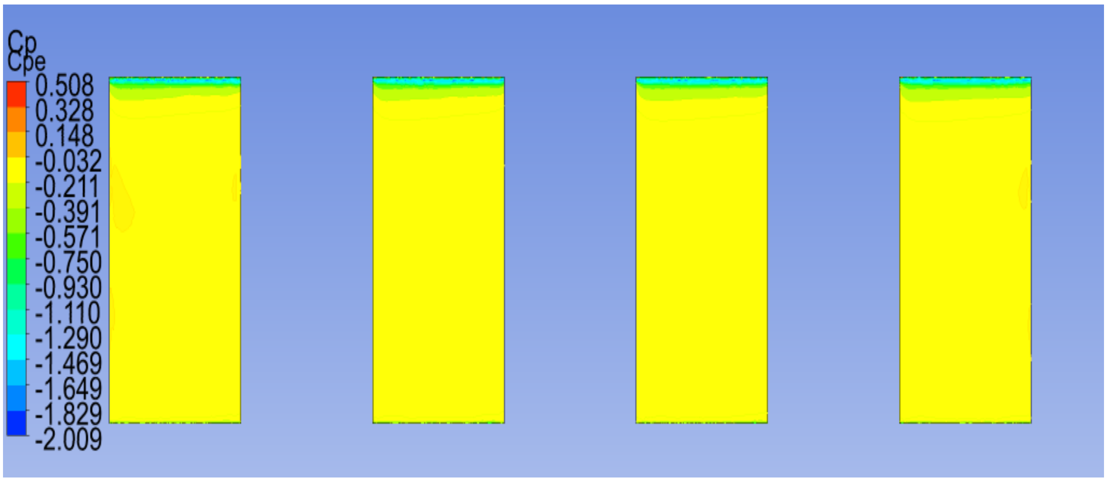

Fig. 3.133 External Pressure Coefficient at Wind Direction 90^0

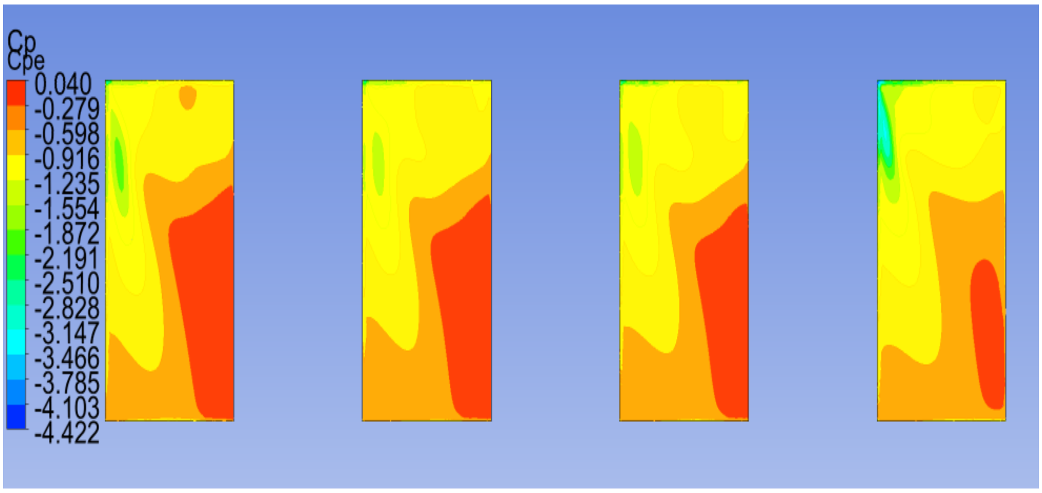

Fig. 3.134 External Pressure Coefficient at Wind Direction 135^0

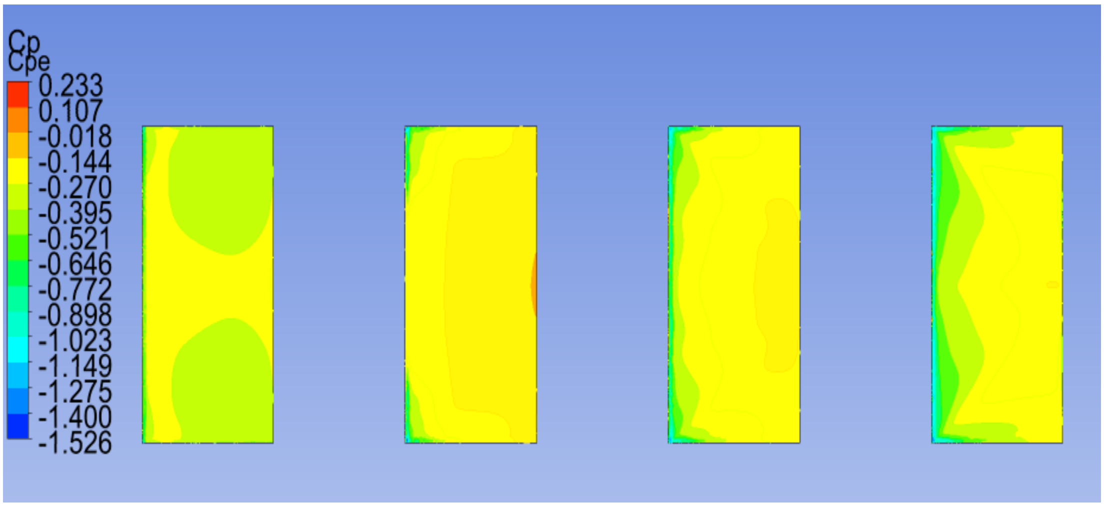

Fig. 3.135 External Pressure Coefficient at Wind Direction 180^0

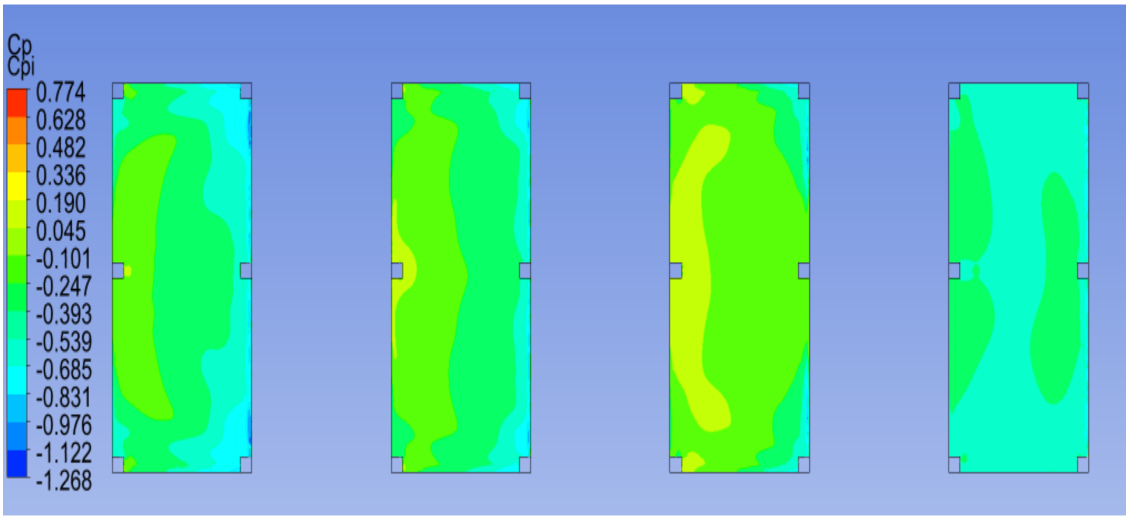

Fig. 3.136 Internal Pressure Coefficient at Wind Direction 0^0

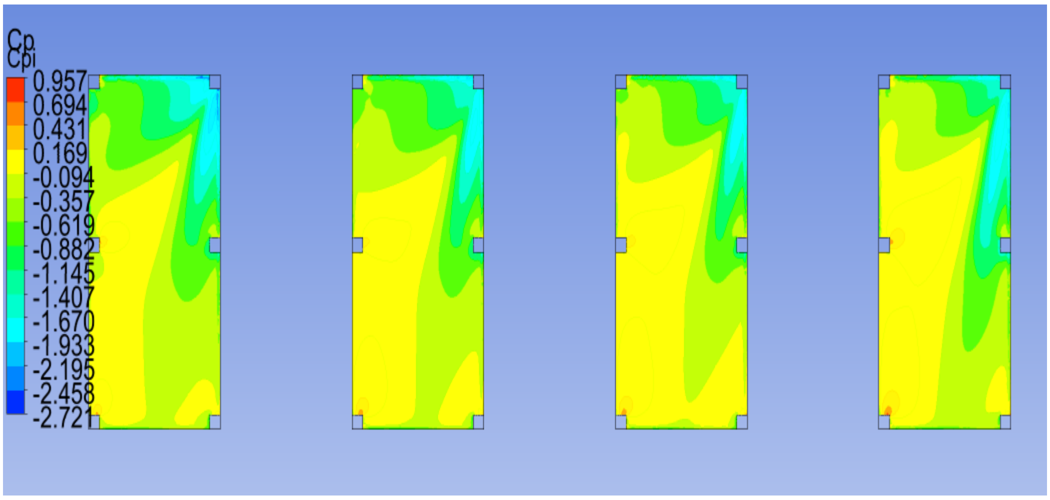

Fig. 3.137 Internal Pressure Coefficient at Wind Direction 45^0

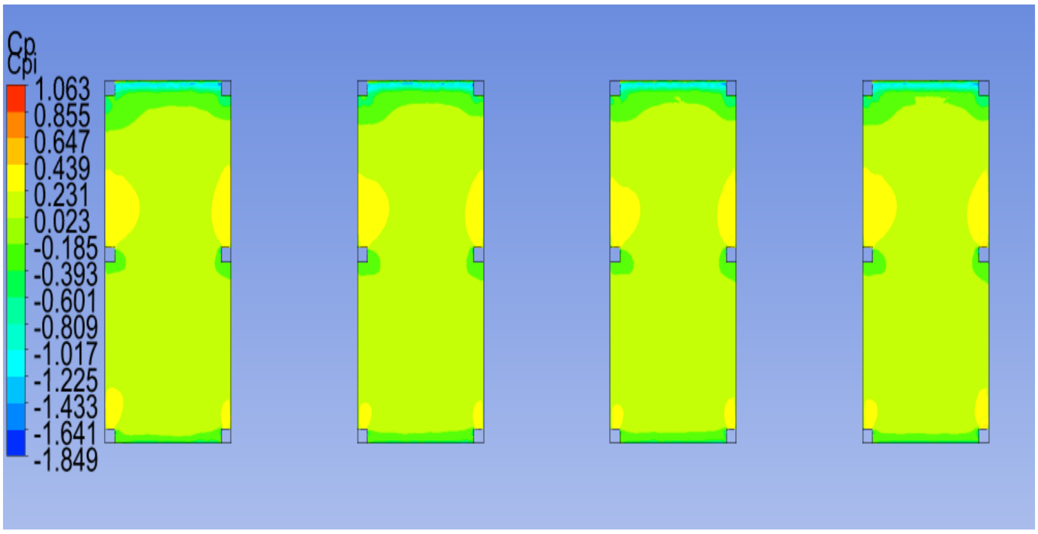

Fig. 3.138 Internal Pressure Coefficient at Wind Direction 90^0

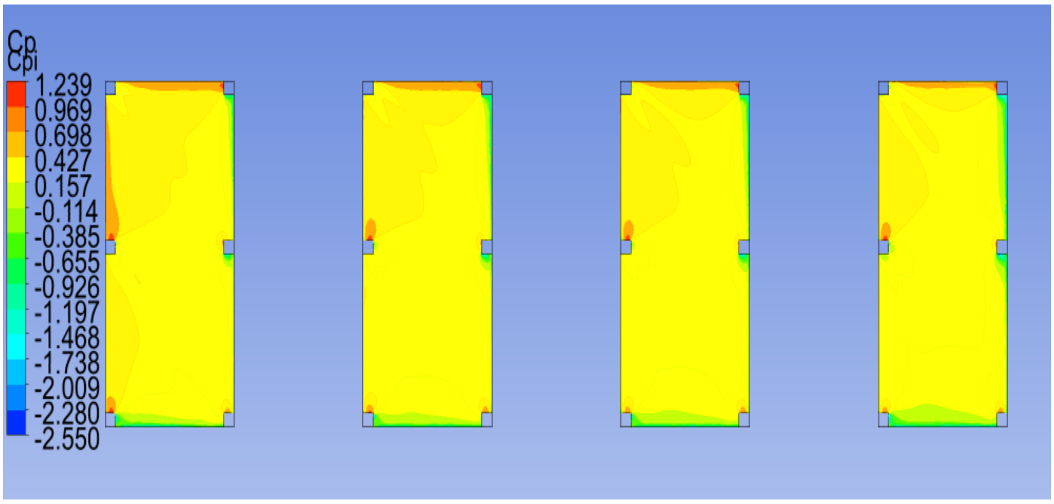

Fig. 3.139 Internal Pressure Coefficient at Wind Direction 135^0

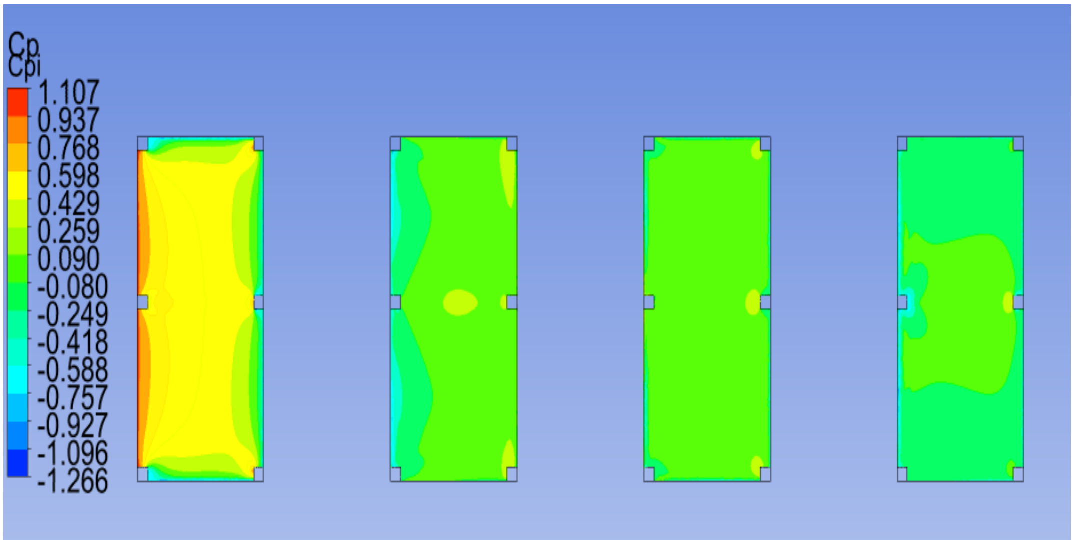

Fig. 3.139 Internal Pressure Coefficient at Wind Direction 180^0

Spacing B = 75

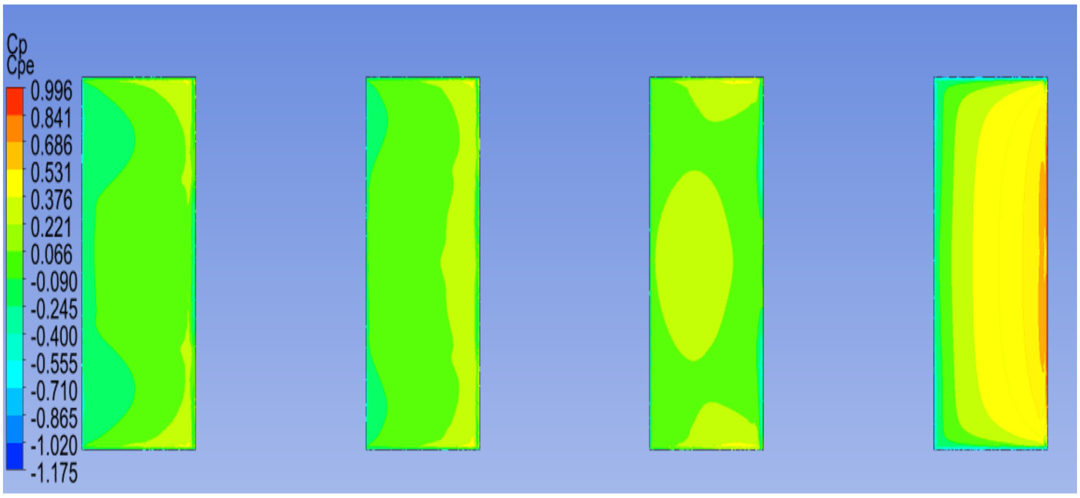

Fig. 3.140 External Pressure Coefficient at Wind Direction 0^0

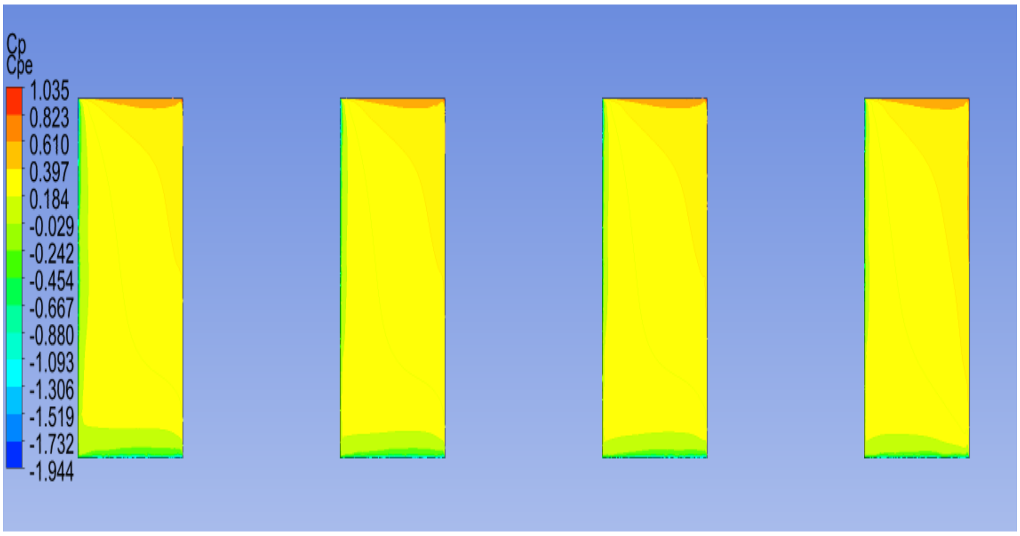

Fig. 3.141 External Pressure Coefficient at Wind Direction 45^0

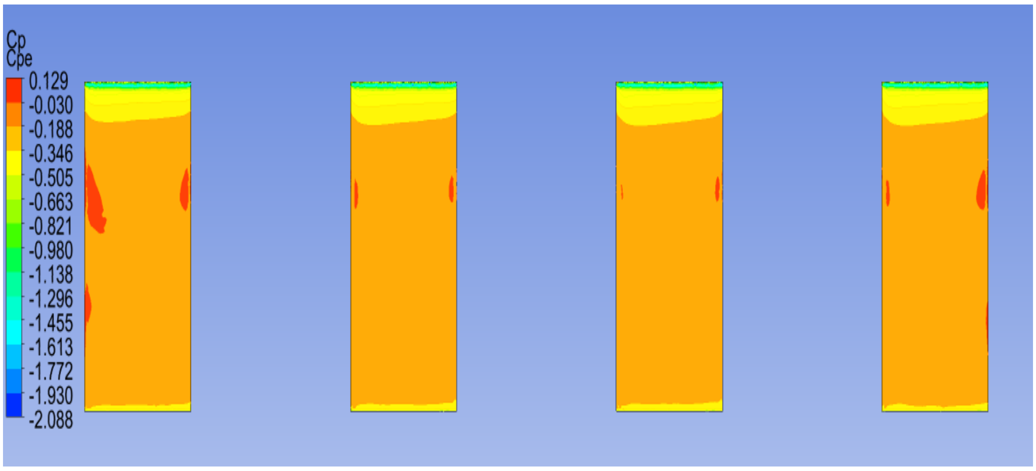

Fig. 3.142 External Pressure Coefficient at Wind Direction 90^0

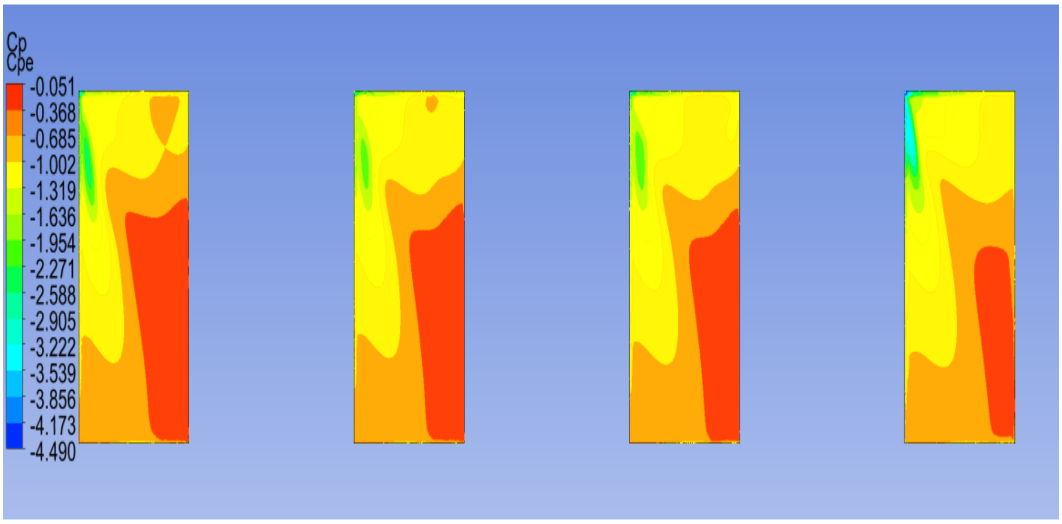

Fig. 3.143 External Pressure Coefficient at Wind Direction 135^0

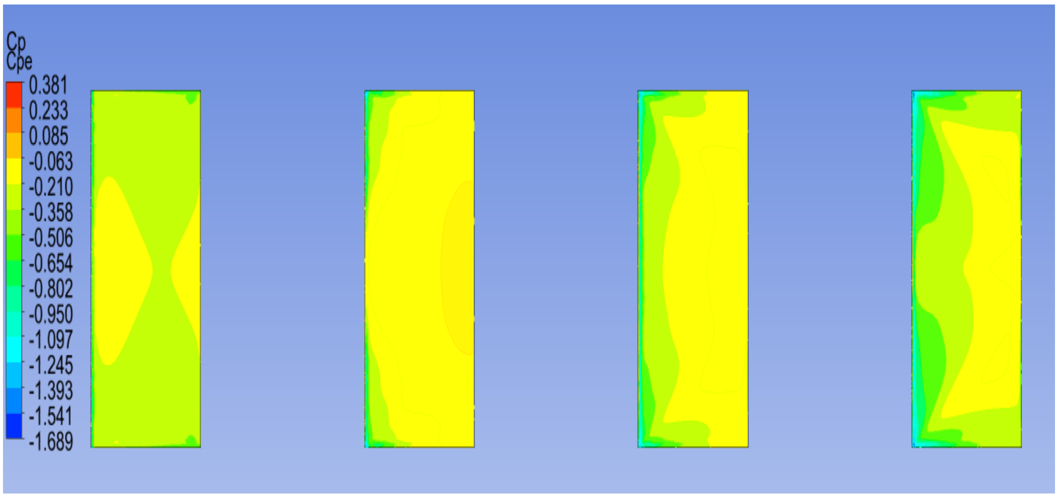

Fig. 3.144 External Pressure Coefficient at Wind Direction 180^0

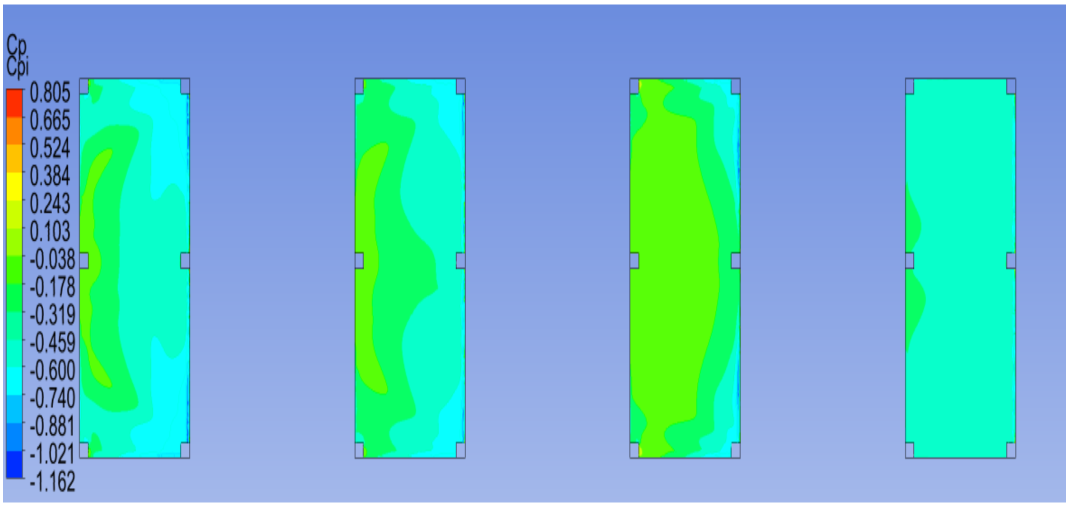

Fig. 3.145 Internal Pressure Coefficient at Wind Direction 0^0

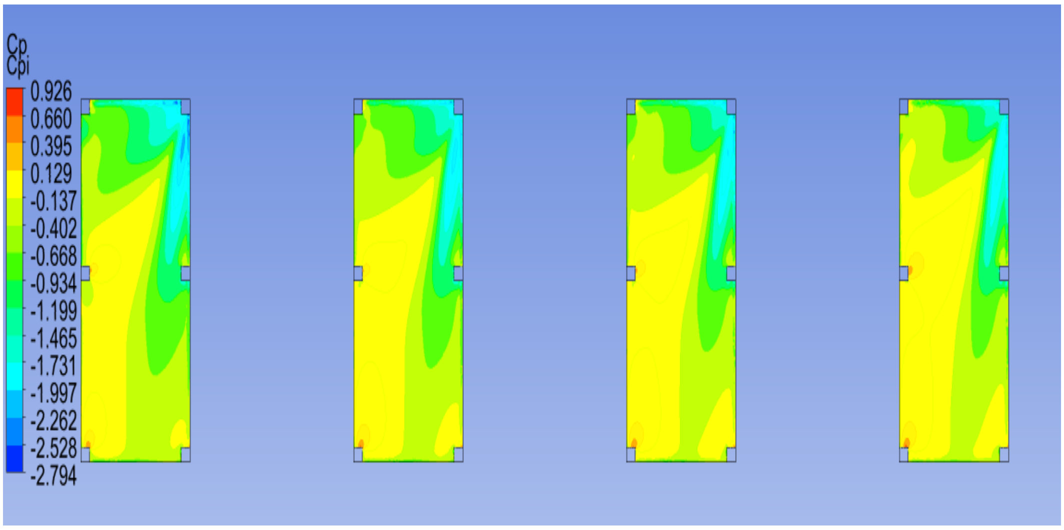

Fig. 3.146 Internal Pressure Coefficient at Wind Direction 45^0

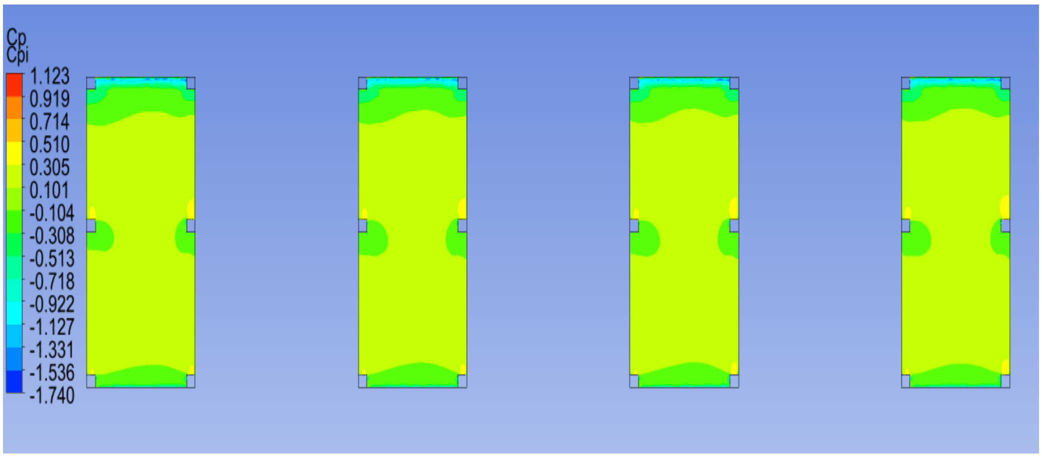

Fig. 3.147 Internal Pressure Coefficient at Wind Direction 90^0

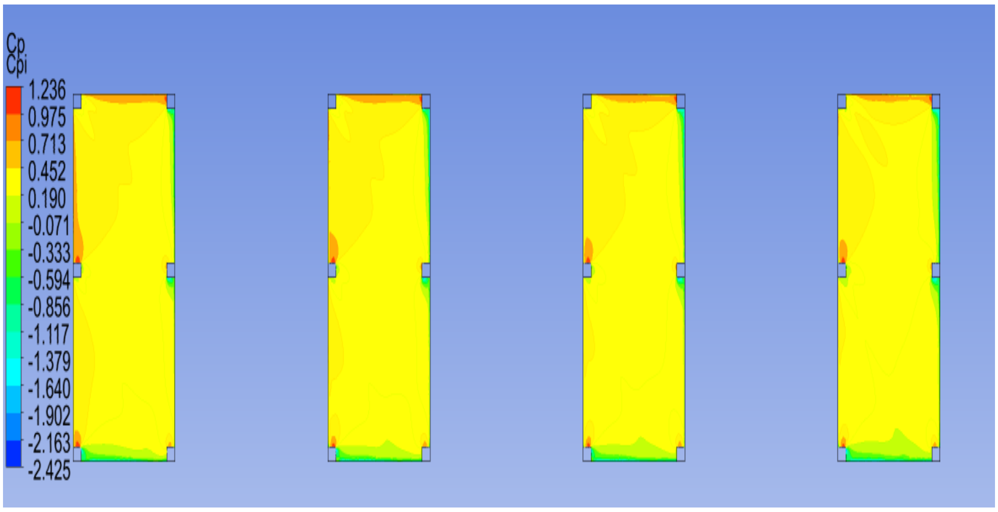

Fig. 3.148 Internal Pressure Coefficient at Wind Direction 135^0

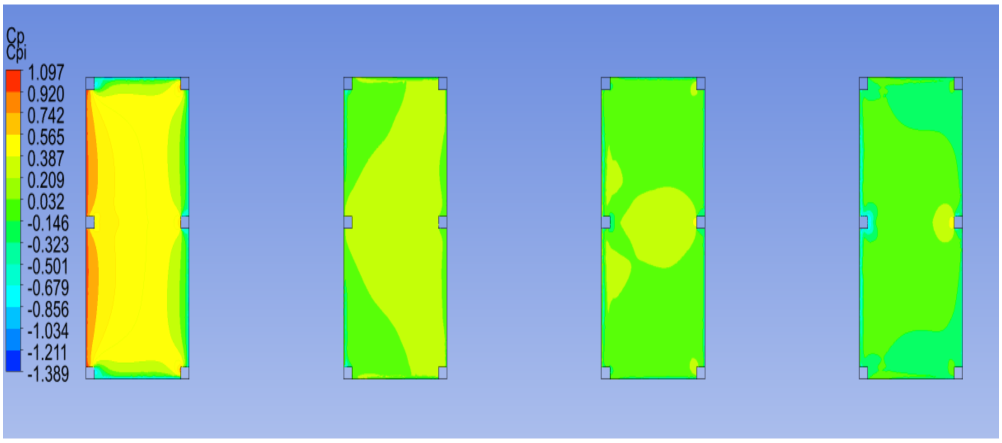

Fig. 3.149 Internal Pressure Coefficient at Wind Direction 180^0

Spacing B = 100

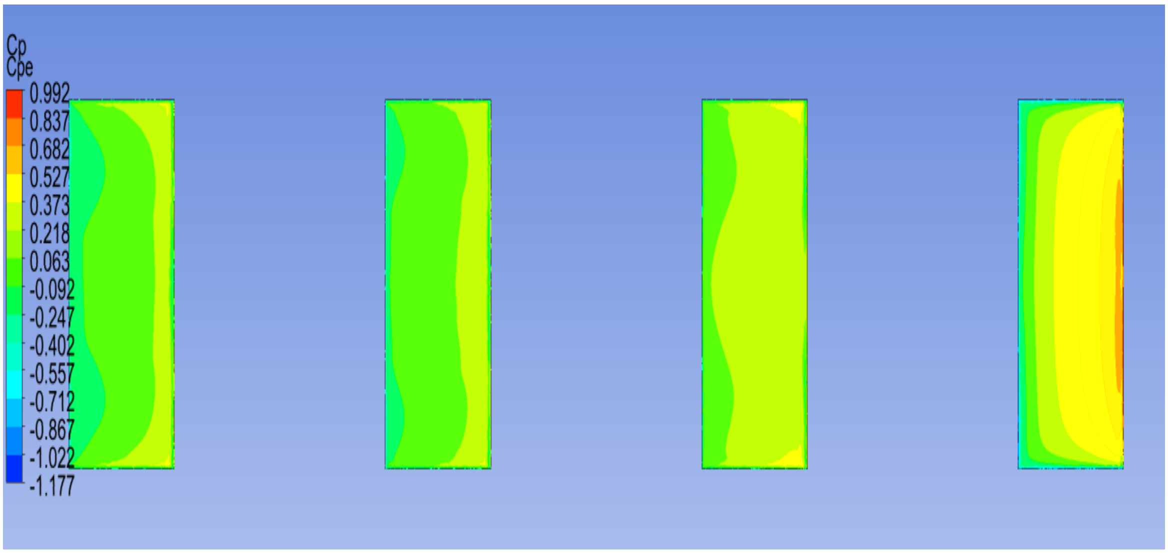

Fig. 3.150 External Pressure Coefficient at Wind Direction 0^0

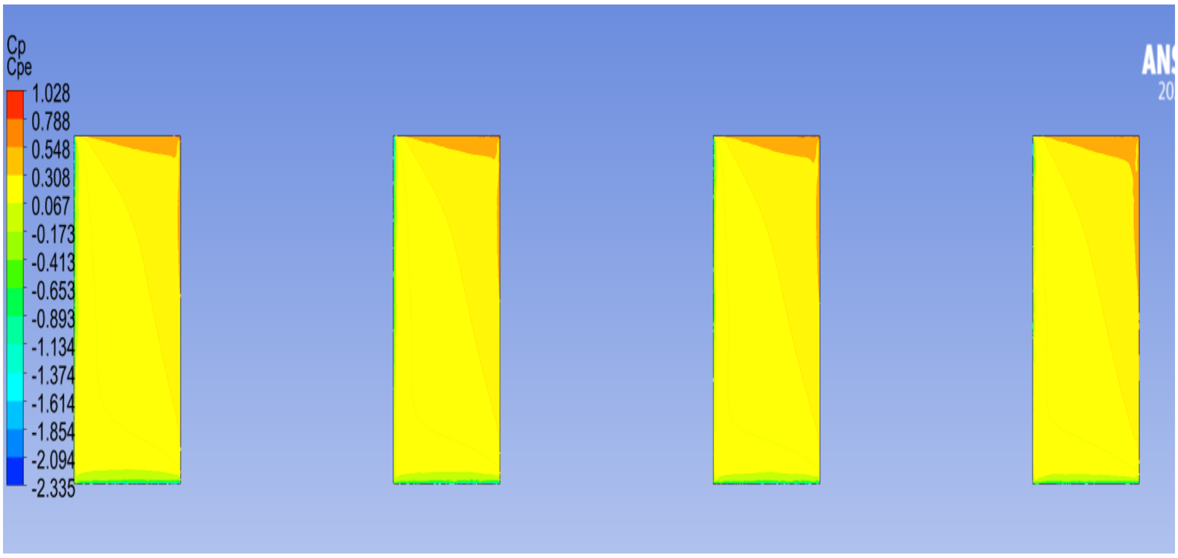

Fig. 3.151 External Pressure Coefficient at Wind Direction 45^0

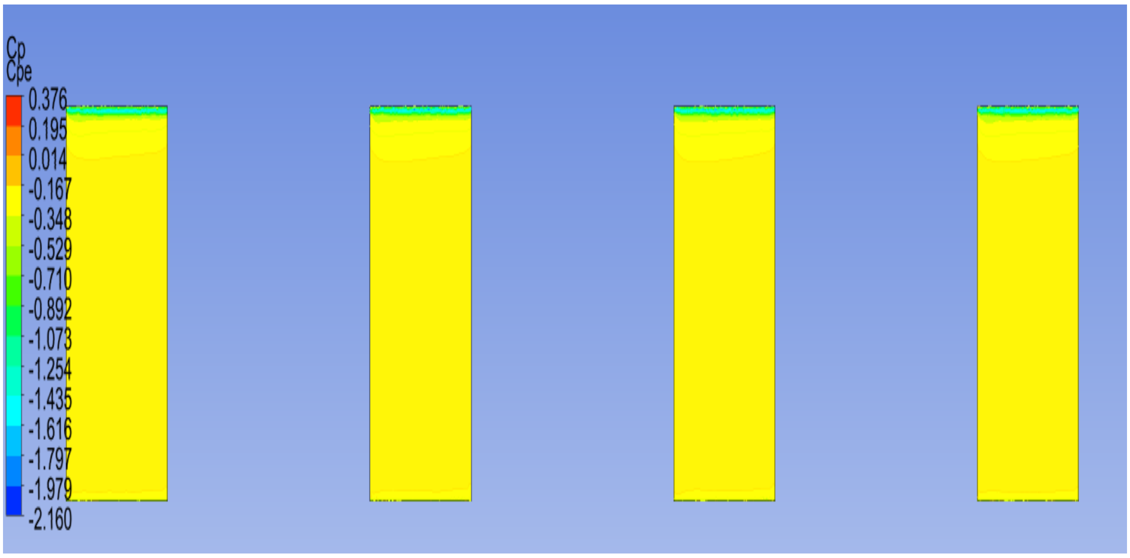

Fig. 3.152 External Pressure Coefficient at Wind Direction 90^0

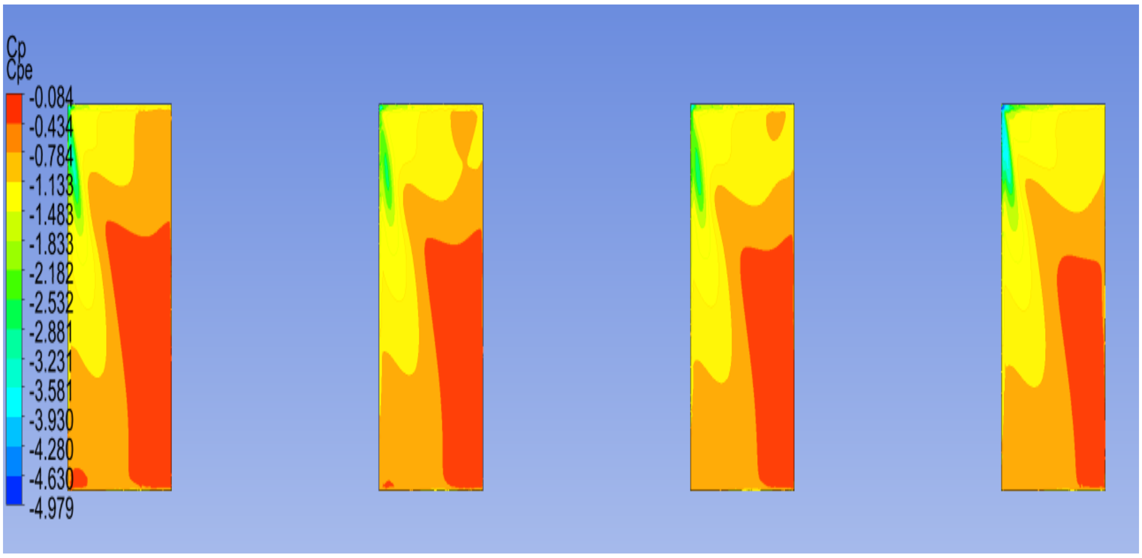

Fig. 3.153 External Pressure Coefficient at Wind Direction 135^0

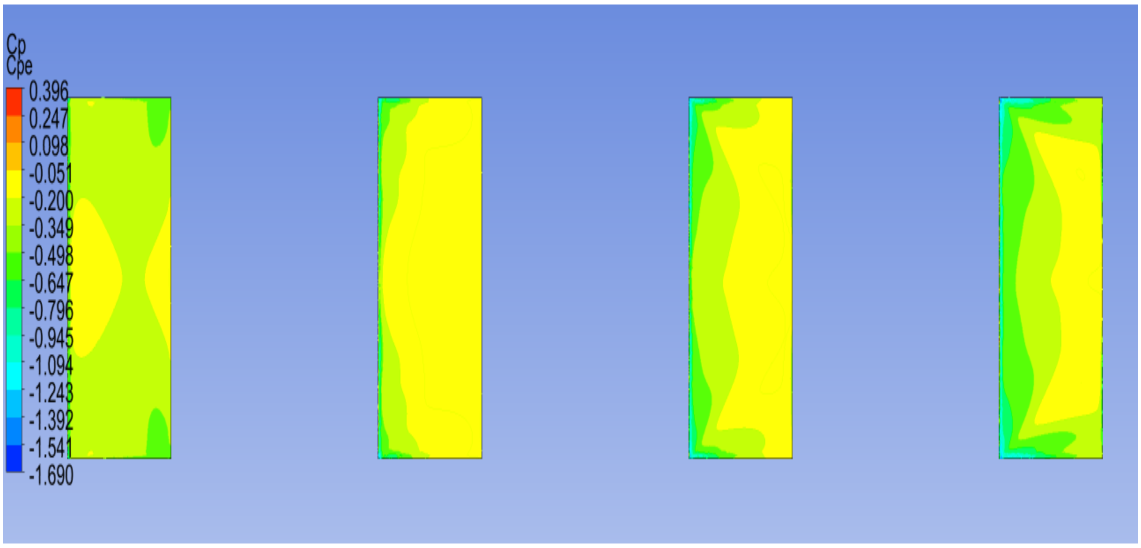

Fig. 3.154 External Pressure Coefficient at Wind Direction 180^0

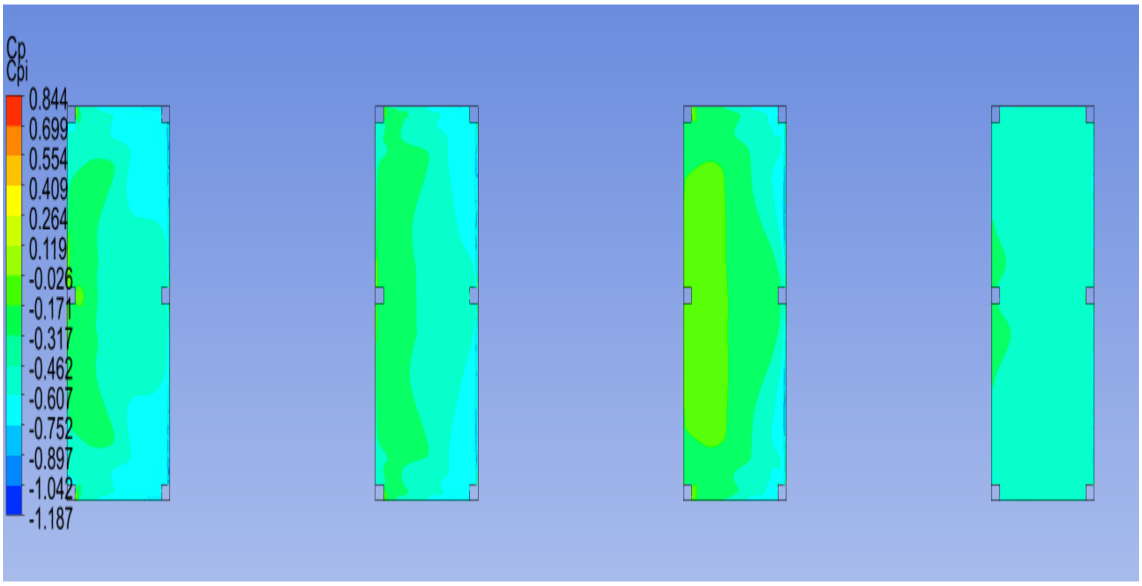

Fig. 3.155 Internal Pressure Coefficient at Wind Direction 0^0

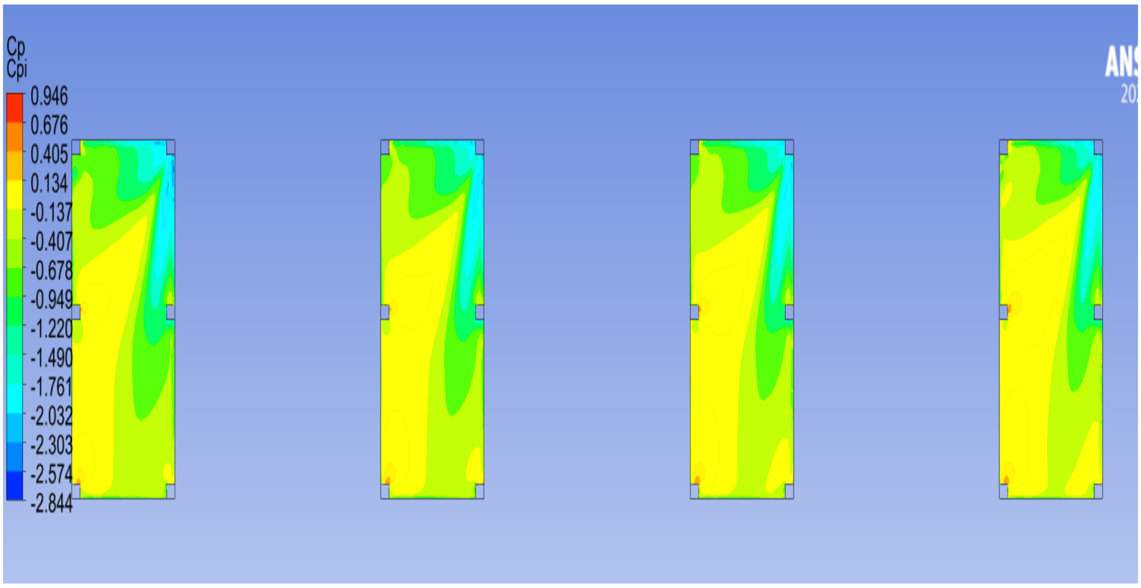

Fig. 3.156 Internal Pressure Coefficient at Wind Direction 45^0

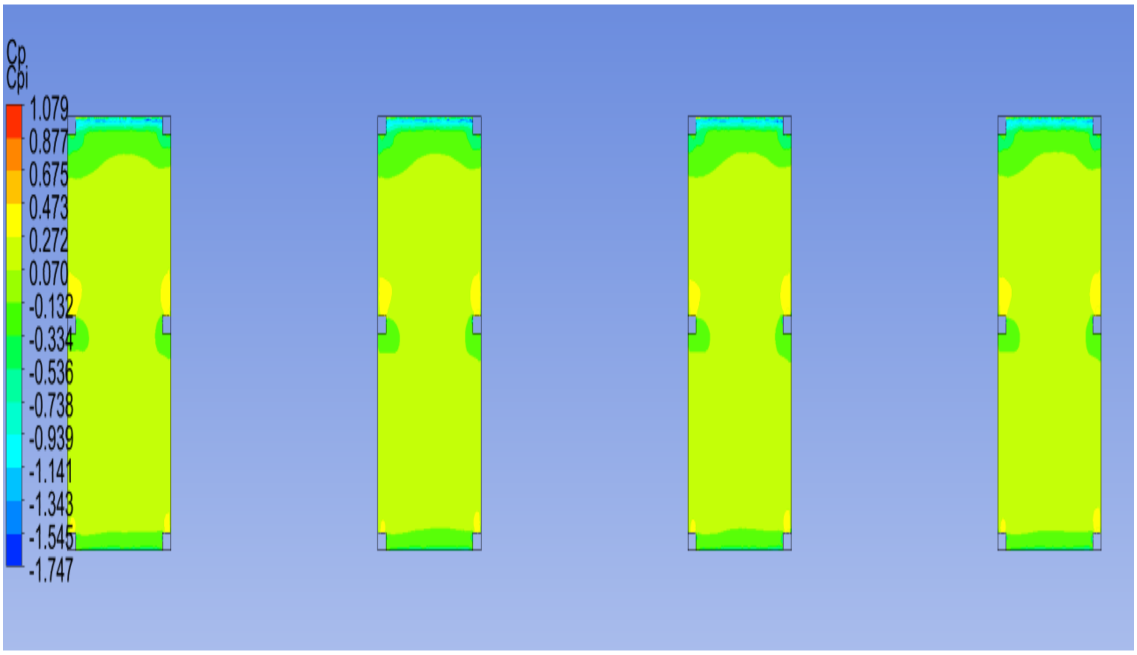

Fig. 3.157 Internal Pressure Coefficient at Wind Direction 90^0

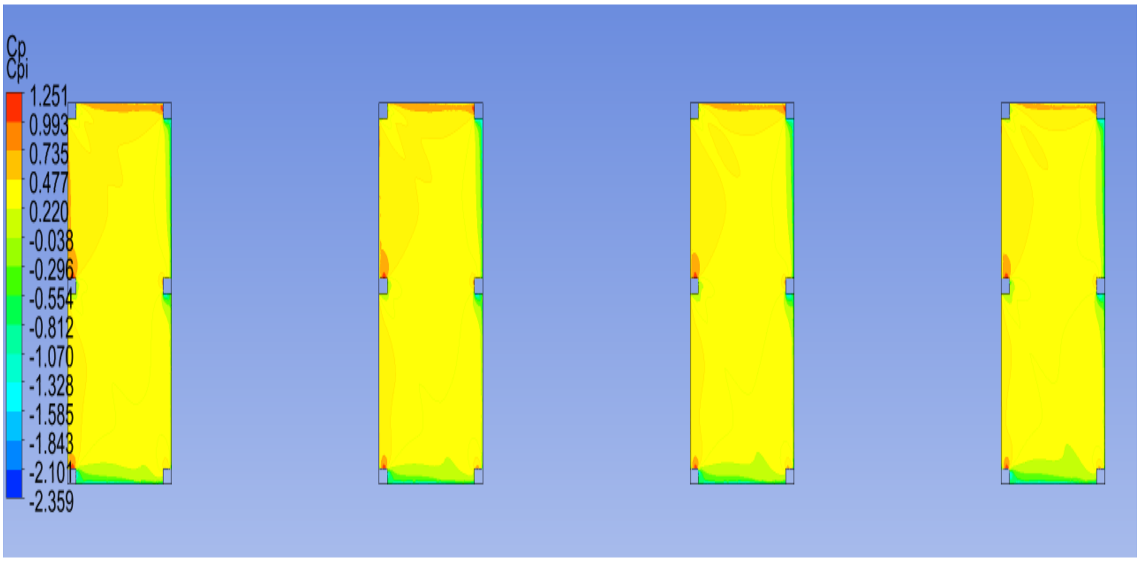

Fig. 3.158 Internal Pressure Coefficient at Wind Direction 135^0

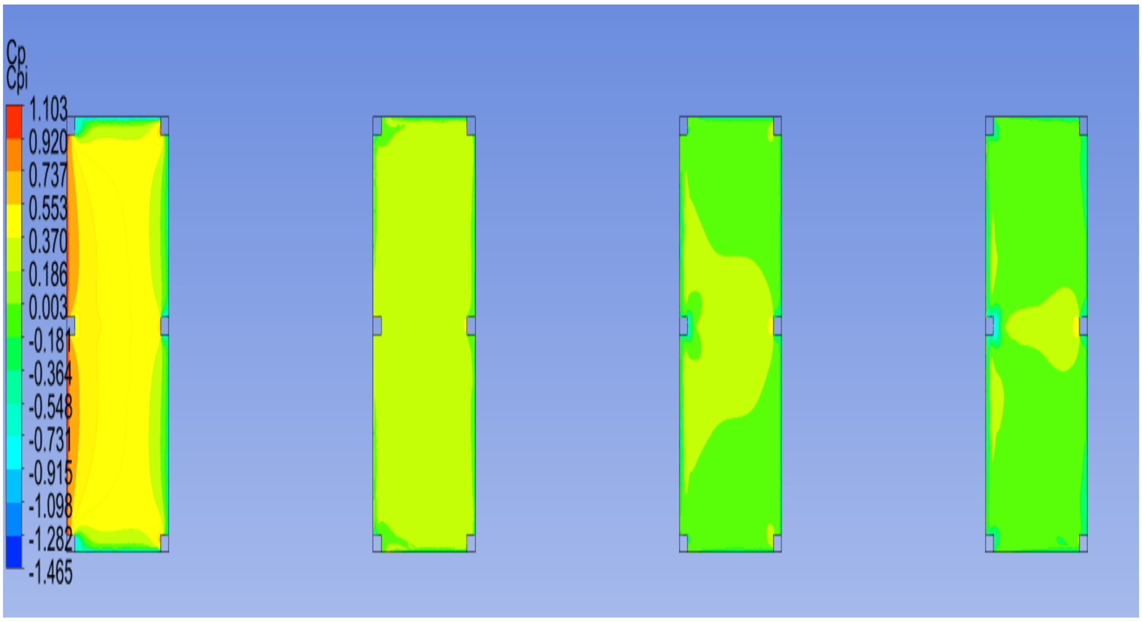

Fig. 3.159 Internal Pressure Coefficient at Wind Direction 180^0

3.9 STUDY OF INTERFERENCE EFFECT WITH VARIOUS SPACING AND HAVING DIFFERENT WIND DIRECTIONS

The interference effect between the roofs of the building is drawn by varying the relative positions of the buildings. The arrangement is done for different roof solves having angles 10, 20, and 30 respectively and by varying the spacing by 0,b/2,b,3b/2 and 2b respectively. In this study, for every arrangement the interference effect Among the four roofs of the building having different spacing (0,b/2,b,3b/2,2b) under different wind direction varying from 0^0 to 180^0.

a) Spacing=0
b) Spacing=b/2
c) Spacing=b
d) Spacing=3b/2
e) Spacing=2b

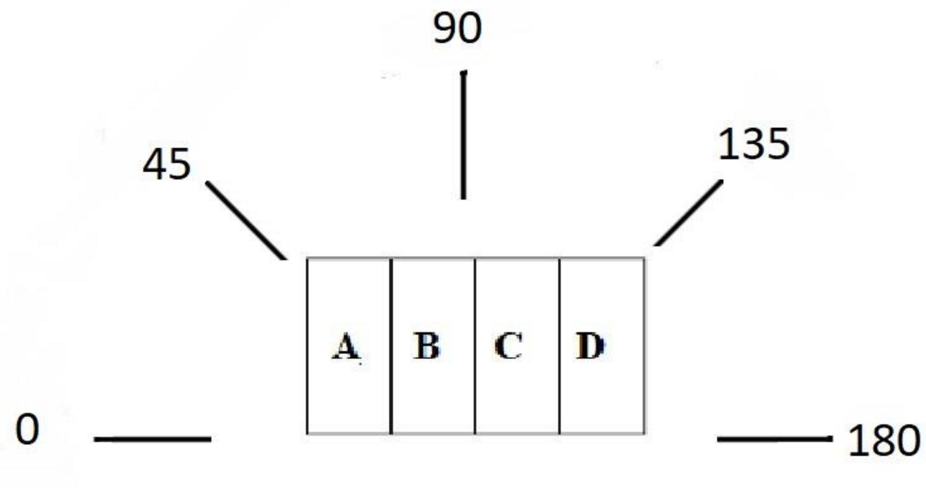

Fig. 3.160 Direction of Wind on the structure

The phenomenon of interference effect between the roofs of the building is drawn by varying the relative positions of the buildings. The arrangement is done for different roof solves having angles of 10^0, 20^0 and 30^0 respectively.

Slope Angle = 10°, Spacing =0

Table 3.3 Coefficient of Pressure (C_{pext}) at Slope Angle 10 , Spacing 0

C_{pext}	**Face A**	**Face B**	**Face C**	**Face D**
Ɵ = 0°	-0.0406527	-0.0658035	-0.0553772	-0.0807649
Ɵ =30°	-0.0627486	-0.0979344	-0.0960077	-0.102174
Ɵ = 45°	-0.110534	-0.150365	-0.150045	-0.14518
Ɵ =60 °	-0.155597	-0.20999	-0.219762	-0.193305
Ɵ =90°	-0.197928	-0.238643	-0.23525	-0.189833
Ɵ =120°	-0.360115	-0.334544	-0.311067	-0.313402
Ɵ =135°	-0.392668	-0.311759	-0.285808	-0.386189
Ɵ =150°	-0.386884	-0.254735	-0.195796	-0.427012
Ɵ =180 °	-0.194457	-0.0837728	-0.101008	-0.333214

Table 3.4 Coefficient of Pressure (C_{pint})at Slope Angle 10^0 , Spacing 0

C_{pint}	Face A	Face B	Face C	Face D
ϴ = 0°	-0.213134	-0.0526974	-0.0944811	-0.169352
ϴ =30°	-0.10032	-0.0899556	-0.10902	-0.197838
ϴ = 45°	-0.0799687	-0.13534	-0.153078	-0.229653
ϴ =60 °	-0.0534679	-0.09939	-0.102227	-0.158665
ϴ =90°	-0.141234	-0.168184	-0.166789	-0.138614
ϴ =120°	-0.0235534	0.0170151	0.0322886	0.102104
ϴ =135°	-0.031688	0.0267378	0.0483532	0.17935
ϴ =150°	-0.0199047	0.0309605	0.0308558	0.212011
ϴ =180 °	-0.0789545	-0.043463	-0.0670179	0.0816613

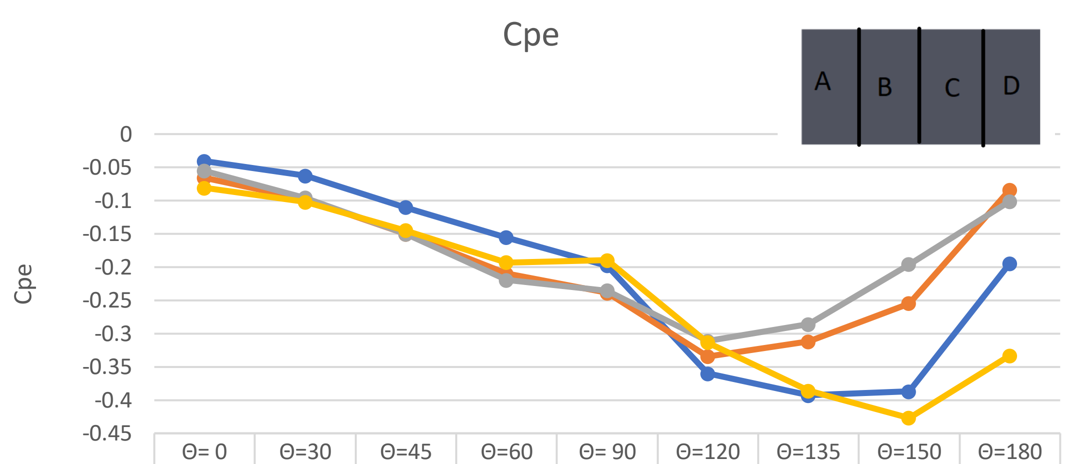

	Θ= 0	Θ=30	Θ=45	Θ=60	Θ= 90	Θ=120	Θ=135	Θ=150	Θ=180
Face A	-0.04065	-0.06275	-0.11053	-0.1556	-0.19793	-0.36012	-0.39267	-0.38688	-0.19446
Face B	-0.0658	-0.09793	-0.15037	-0.20999	-0.23864	-0.33454	-0.31176	-0.25474	-0.08377
Face C	-0.05538	-0.09601	-0.15005	-0.21976	-0.23525	-0.31107	-0.28581	-0.1958	-0.10101
Face D	-0.08076	-0.10217	-0.14518	-0.19331	-0.18983	-0.3134	-0.38619	-0.42701	-0.33321

Fig. 3.161 Cpe for roof angle 10° and zero spacing

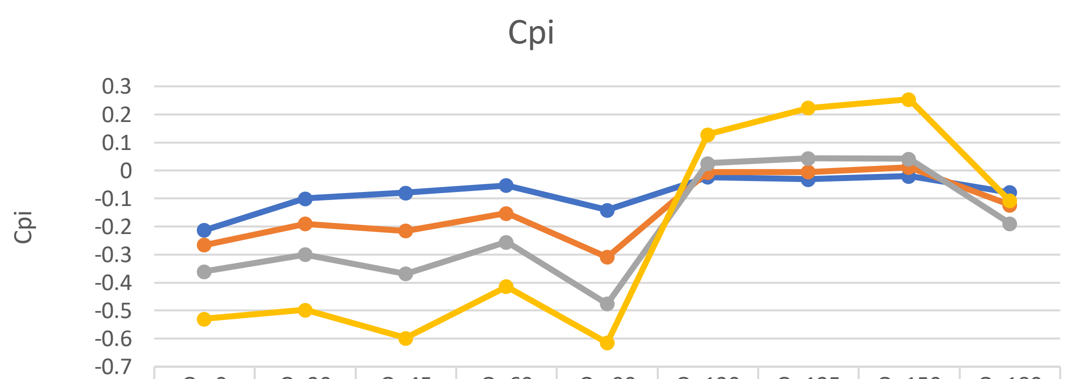

	Θ= 0	Θ=30	Θ=45	Θ=60	Θ= 90	Θ=120	Θ=135	Θ=150	Θ=180
Face D	-0.16935	-0.19784	-0.22965	-0.15867	-0.13861	0.102104	0.17935	0.212011	0.081661
Face C	-0.09448	-0.10902	-0.15308	-0.10223	-0.16679	0.032289	0.048353	0.030856	-0.06702
Face B	-0.0527	-0.08996	-0.13534	-0.09939	-0.16818	0.017015	0.026738	0.030961	-0.04346
Face A	-0.21313	-0.10032	-0.07997	-0.05347	-0.14123	-0.02355	-0.03169	-0.0199	-0.07895

Fig. 3.162 Cpi for roof angle 10° and zero spacing

Spacing =b/2

Table 3.5 Coefficient of Pressure (C_{pext}) at Slope Angle 10^0 , Spacing b/2

C_{pext}	**Face A**	**Face B**	**Face C**	**Face D**
ϴ = 0°	-0.0189732	-0.043275	-0.069678	-0.101154
ϴ =30°	-0.012219	-0.0316674	-0.0403217	-0.0676164
ϴ = 45°	-0.0484172	-0.0628325	-0.077128	-0.101063
ϴ =60 °	-0.0847324	-0.112516	-0.125931	-0.135044
ϴ =90°	-0.135285	-0.150915	-0.149216	-0.131855
ϴ =120°	-0.135285	-0.150915	-0.149216	-0.131855
ϴ =135°	-0.471723	-0.405728	-0.363121	-0.401984
ϴ =150°	-0.428857	-0.351309	-0.32141	-0.466242
ϴ =180 °	-0.18051	-0.140017	-0.117516	-0.38024

Table 3.6 Coefficient of Pressure (C_{pint}) at Slope Angle 10^0, Spacing b/2

C_{pint}	**Face A**	**Face B**	**Face C**	**Face D**
ϴ = 0°	-0.252884	-0.113522	-0.128346	-0.166913
ϴ =30°	-0.1722	-0.123953	-0.148624	-0.223028
ϴ = 45°	-0.114696	-0.116719	-0.148022	-0.217793
ϴ =60 °	-0.0767686	-0.0918147	-0.108621	-0.150506
ϴ =90°	-0.0876941	-0.0945232	-0.0942142	-0.0871751
ϴ =120°	-0.0876941	-0.0945232	-0.0942142	-0.0871751
ϴ =135°	0.073936	0.140916	0.162543	0.186576
ϴ =150°	0.0218095	0.087105	0.106378	0.223497
ϴ =180 °	-0.140934	-0.0651483	-0.0080348	0.107415

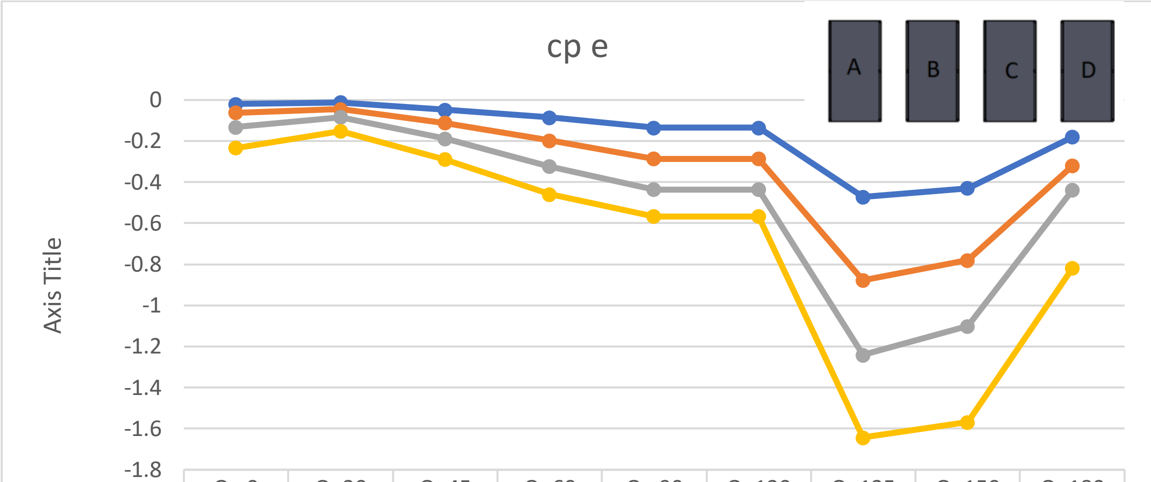

	Θ= 0	Θ=30	Θ=45	Θ=60	Θ= 90	Θ=120	Θ=135	Θ=150	Θ=180
Face D	-0.101154	-0.067616	-0.101063	-0.135044	-0.131855	-0.131855	-0.401984	-0.466242	-0.38024
Face C	-0.069678	-0.040322	-0.077128	-0.125931	-0.149216	-0.149216	-0.363121	-0.32141	-0.117516
Face B	-0.043275	-0.031667	-0.062833	-0.112516	-0.150915	-0.150915	-0.405728	-0.351309	-0.140017
Face A	-0.018973	-0.012219	-0.048417	-0.084732	-0.135285	-0.135285	-0.471723	-0.428857	-0.18051

Fig. 3.163 Cpe for roof angle 10° and spacing =b/2

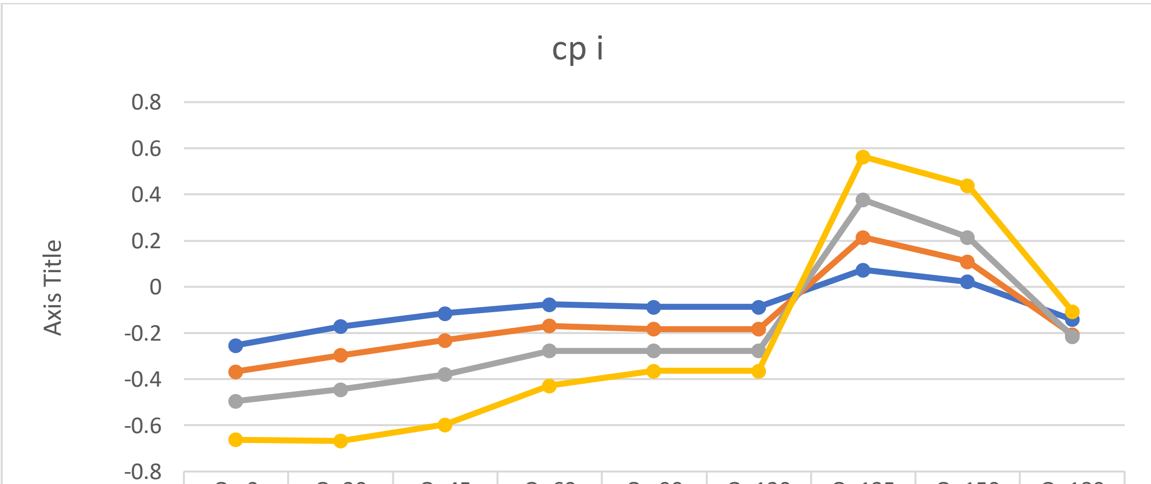

	Θ= 0	Θ=30	Θ=45	Θ=60	Θ= 90	Θ=120	Θ=135	Θ=150	Θ=180
Face D	-0.166913	-0.223028	-0.217793	-0.150506	-0.087175	-0.087175	0.186576	0.223497	0.107415
Face C	-0.128346	-0.148624	-0.148022	-0.108621	-0.094214	-0.094214	0.162543	0.106378	-0.008035
Face B	-0.113522	-0.123953	-0.116719	-0.091815	-0.094523	-0.094523	0.140916	0.087105	-0.065148
Face A	-0.252884	-0.1722	-0.114696	-0.076769	-0.087694	-0.087694	0.073936	0.0218095	-0.140934

Fig. 3.164 Cpi for roof angle 10° and spacing=b/2

Spacing =b

Table 3.7 Coefficient of Pressure (C_{pext}) at Slope Angle 10^0, Spacing b

C_{pext}	**Face A**	**Face B**	**Face C**	**Face D**
Ɵ = 0°	-0.0220074	-0.060434	-0.0747925	-0.100113
Ɵ =30°	-0.0117735	-0.0205237	-0.0301839	-0.0567267
Ɵ = 45°	-0.05236	-0.0556099	-0.0660068	-0.0831888
Ɵ =60 °	-0.0790726	-0.100016	-0.111976	-0.123667
Ɵ =90°	-0.124142	-0.133302	-0.132657	-0.121721
Ɵ =120°	-0.400142	-0.366594	-0.337113	-0.285312
Ɵ =135°	-0.507277	-0.458914	-0.426653	-0.422102
Ɵ =150°	-0.476283	-0.420974	-0.402851	-0.473696
Ɵ =180 °	-0.197022	-0.16475	-0.156524	-0.384228

Table 3.8 Coefficient of Pressure (C_{pint}) at Slope Angle 10^0 , Spacing b

C_{pint}	**Face A**	**Face B**	**Face C**	**Face D**
Ɵ = 0°	-0.291562	-0.129228	-0.12873	-0.156145
Ɵ =30°	-0.206792	-0.165706	-0.195925	-0.255894
Ɵ = 45°	-0.160601	-0.171905	-0.195765	-0.247961
Ɵ =60 °	-0.0905227	-0.108042	-0.124041	-0.155139
Ɵ =90°	-0.0836017	-0.0899653	-0.0903168	-0.0839482
Ɵ =120°	0.0457494	0.0737655	0.0849333	0.0837366
Ɵ =135°	0.0930144	0.140293	0.153472	0.148864
Ɵ =150°	0.0609244	0.105897	0.130761	0.195033
Ɵ =180 °	-0.155985	-0.0817369	0.000656	0.0815299

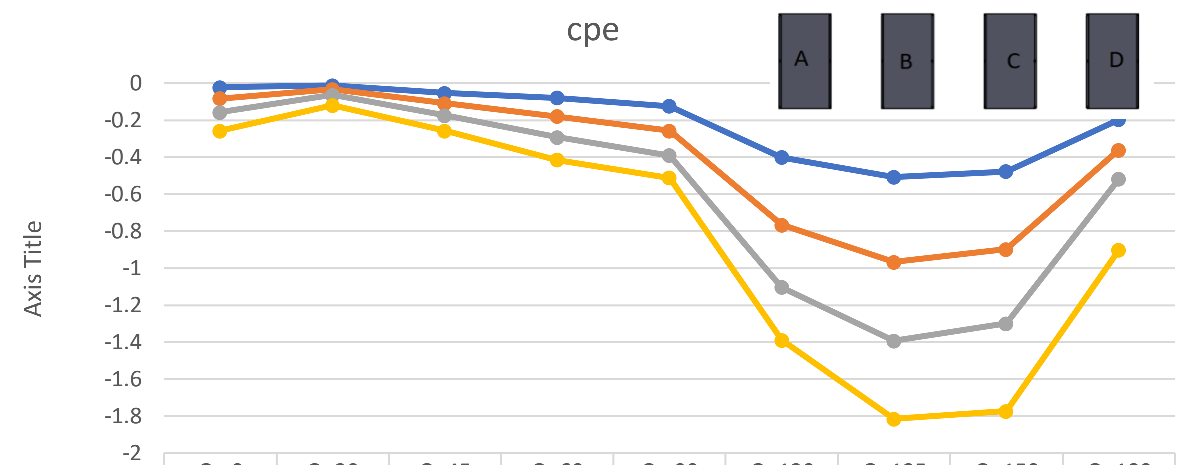

	Θ= 0	Θ=30	Θ=45	Θ=60	Θ= 90	Θ=120	Θ=135	Θ=150	Θ=180
Face D	-0.100113	-0.056727	-0.083189	-0.123667	-0.121721	-0.285312	-0.422102	-0.473696	-0.384228
Face C	-0.074793	-0.030184	-0.066007	-0.111976	-0.132657	-0.337113	-0.426653	-0.402851	-0.156524
Face B	-0.060434	-0.020524	-0.05561	-0.100016	-0.133302	-0.366594	-0.458914	-0.420974	-0.16475
Face A	-0.022007	-0.011774	-0.05236	-0.079073	-0.124142	-0.400142	-0.507277	-0.476283	-0.197022

Fig. 3.165 Cpe for roof angle 10° and spacing=b

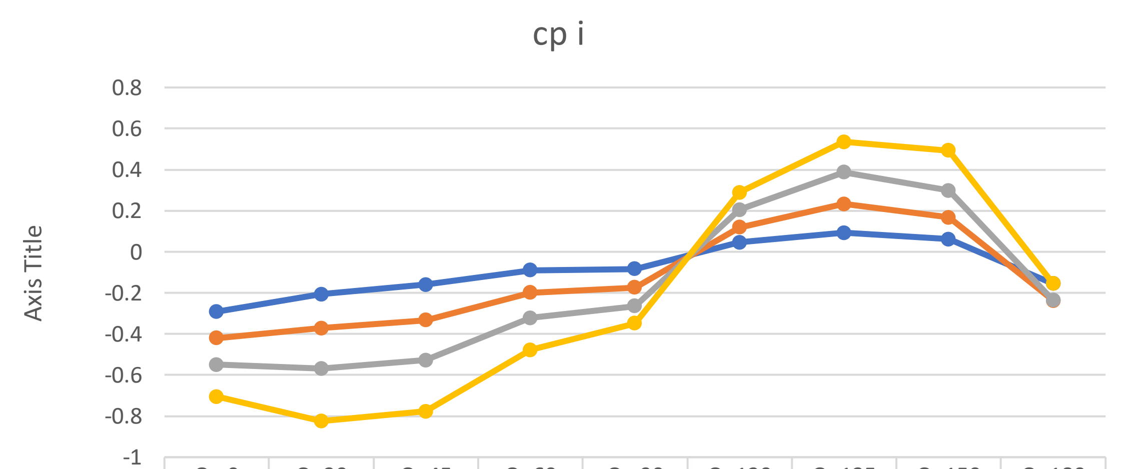

	Θ= 0	Θ=30	Θ=45	Θ=60	Θ= 90	Θ=120	Θ=135	Θ=150	Θ=180
Face D	-0.156145	-0.255894	-0.247961	-0.155139	-0.083948	0.0837366	0.148864	0.195033	0.0815299
Face C	-0.12873	-0.195925	-0.195765	-0.124041	-0.090317	0.0849333	0.153472	0.130761	0.000656
Face B	-0.129228	-0.165706	-0.171905	-0.108042	-0.089965	0.0737655	0.140293	0.105897	-0.081737
Face A	-0.291562	-0.206792	-0.160601	-0.090523	-0.083602	0.0457494	0.0930144	0.0609244	-0.155985

Fig. 3.166 Cpi for roof angle 10° and spacing=b

Spacing =3b/2

Table 3.9 Coefficient of Pressure (C_{pext}) at Slope Angle 10^0 , Spacing 3b/2

C_{pext}	**Face A**	**Face B**	**Face C**	**Face D**
ϴ = 0°	-0.025362	-0.0672899	-0.0869869	-0.105044
ϴ =30°	-0.014729	-0.0151532	-0.0242627	-0.0483414
ϴ = 45°	-0.0496838	-0.0504197	-0.0630646	-0.0776799
ϴ =60 °	-0.0765407	-0.0963128	-0.106829	-0.117665
ϴ =90°	-0.118622	-0.12468	-0.124224	-0.117196
ϴ =120°	-0.380013	-0.351399	-0.333127	-0.291339
ϴ =135°	-0.529491	-0.490308	-0.46009	-0.423517
ϴ =150°	-0.533848	-0.476381	-0.444539	-0.479779
ϴ =180 °	-0.22345	-0.202244	-0.197015	-0.416026

Table 3.10 Coefficient of Pressure (C_{pint}) at Slope Angle 10^0 , Spacing 3b/2

C_{pint}	Face A	Face B	Face C	Face D
ϴ = 0°	-0.321138	-0.149924	-0.136037	-0.156496
ϴ =30°	-0.232791	-0.220849	-0.252364	-0.303556
ϴ = 45°	-0.173822	-0.199517	-0.223163	-0.264262
ϴ =60 °	-0.0974666	-0.114925	-0.129207	-0.152628
ϴ =90°	-0.118622	-0.0846514	-0.0849226	-0.0828694
ϴ =120°	0.0409167	0.0623061	0.0721008	0.0753513
ϴ =135°	0.0969689	0.134926	0.145786	0.137871
ϴ =150°	0.0896174	0.131492	0.146871	0.181298
ϴ =180 °	-0.163962	-0.0936461	-0.0100906	0.0715095

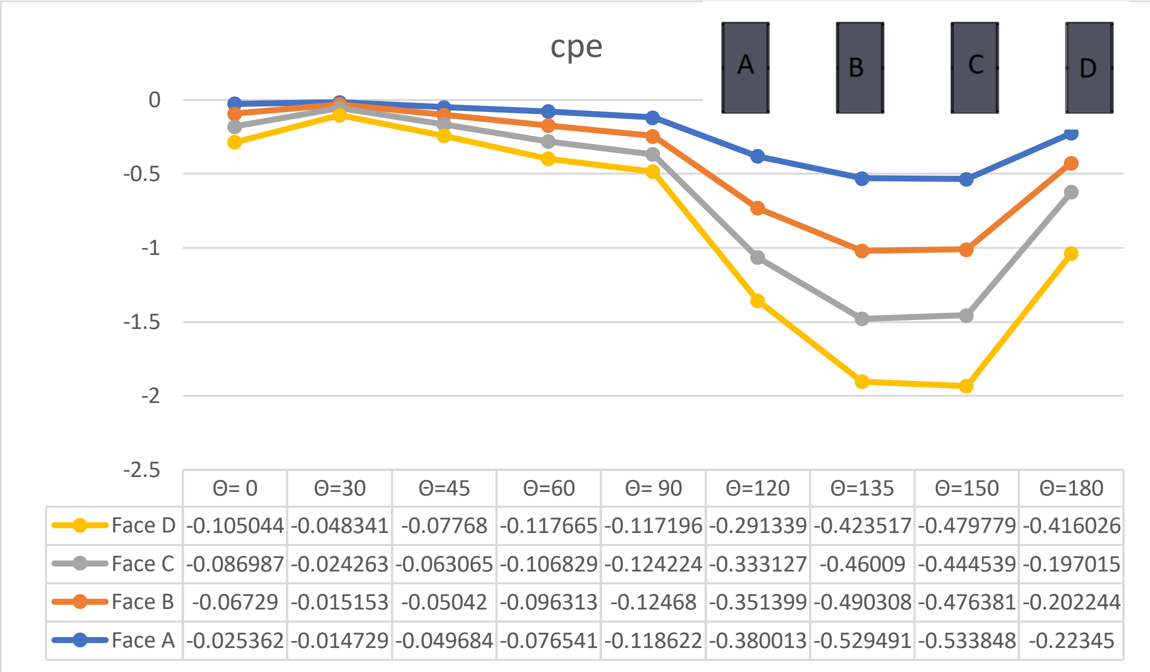

	Θ= 0	Θ=30	Θ=45	Θ=60	Θ= 90	Θ=120	Θ=135	Θ=150	Θ=180
Face D	-0.105044	-0.048341	-0.07768	-0.117665	-0.117196	-0.291339	-0.423517	-0.479779	-0.416026
Face C	-0.086987	-0.024263	-0.063065	-0.106829	-0.124224	-0.333127	-0.46009	-0.444539	-0.197015
Face B	-0.06729	-0.015153	-0.05042	-0.096313	-0.12468	-0.351399	-0.490308	-0.476381	-0.202244
Face A	-0.025362	-0.014729	-0.049684	-0.076541	-0.118622	-0.380013	-0.529491	-0.533848	-0.22345

Fig. 3.167 Cpe for roof angle 10° and spacing=3b/2

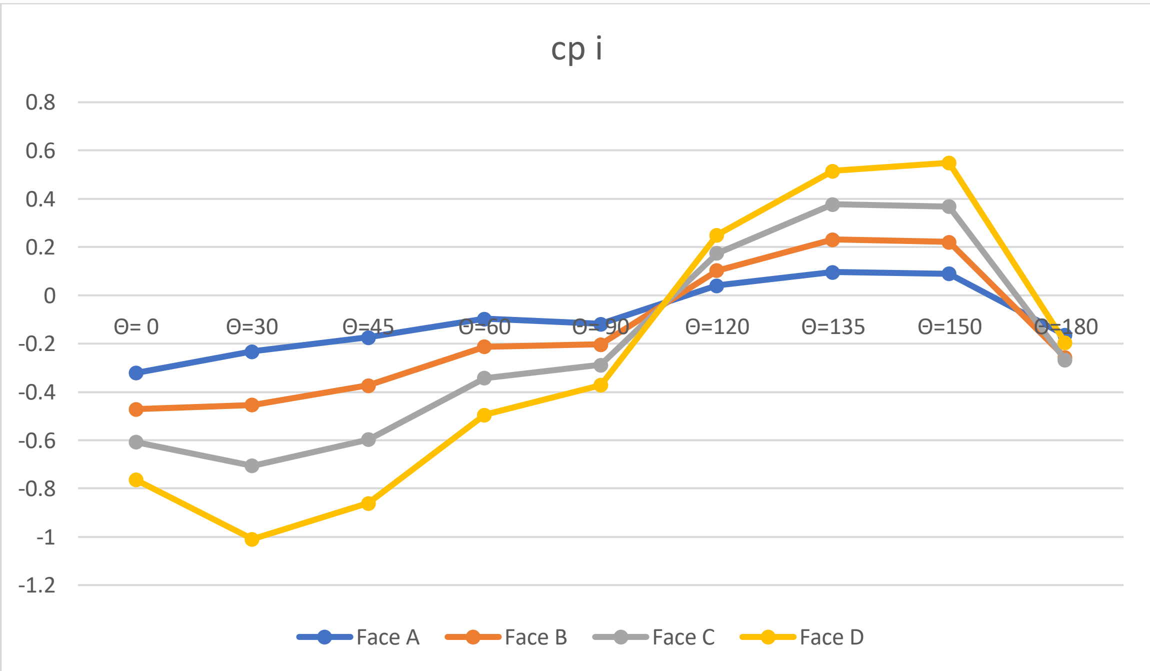

Fig. 3.168 Cpi for roof angle 10° and spacing=3b/2

Spacing =2b

Table 3.12 Coefficient of Pressure (C_{pext}) at Slope Angle 10^0 , Spacing 2b

C_{pext}	**Face A**	**Face B**	**Face C**	**Face D**
ϴ = 0°	-0.0267909	-0.0699779	-0.0909915	-0.104536
ϴ =30°	-0.0166106	-0.00872757	-0.0186813	-0.0394948
ϴ = 45°	-0.0490235	-0.0595814	-0.0692528	-0.0881416
ϴ =60 °	-0.0778516	-0.0938167	-0.104013	-0.11481
ϴ =90°	-0.116956	-0.12025	-0.120172	-0.116052
ϴ =120°	-0.367871	-0.344173	-0.329829	-0.299572
ϴ =135°	-0.534193	-0.499147	-0.477247	-0.431572
ϴ =150°	-0.526725	-0.480653	-0.455674	-0.486491
ϴ =180 °	-0.247388	-0.240327	-0.234489	-0.43538

Table 3.13 Coefficient of Pressure (C_{pint}) at Slope Angle 10^0 , Spacing 2b

C_{pint}	**Face A**	**Face B**	**Face C**	**Face D**
ϴ = 0°	-0.33741	-0.171047	-0.141167	-0.154475
ϴ =30°	-0.243895	-0.256793	-0.29024	-0.337933
ϴ = 45°	-0.186532	-0.212261	-0.23159	-0.262172
ϴ =60 °	-0.105434	-0.120963	-0.131995	-0.151998
ϴ =90°	-0.0836363	-0.0837859	-0.0836988	-0.082144
ϴ =120°	0.035212	0.0538692	0.063932	0.0711624
ϴ =135°	0.0856771	0.116753	0.126717	0.127461
ϴ =150°	0.0914679	0.1301	0.148919	0.168643
ϴ =180 °	-0.16859	-0.102853	-0.0210305	0.0651205

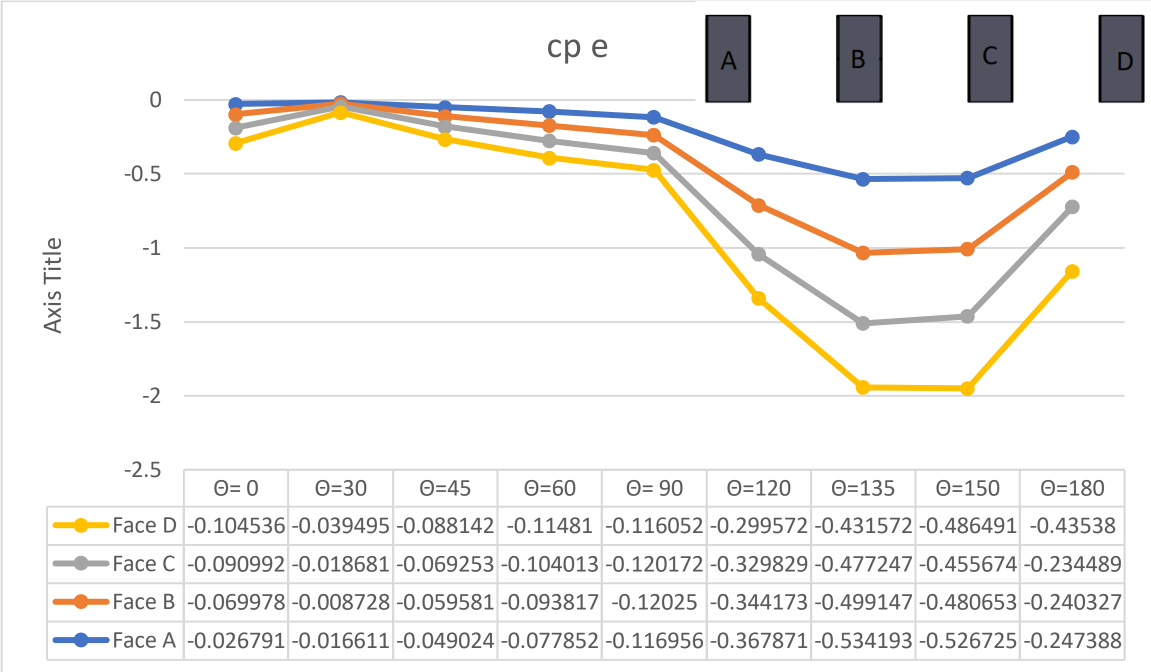

	Θ= 0	Θ=30	Θ=45	Θ=60	Θ= 90	Θ=120	Θ=135	Θ=150	Θ=180
Face D	-0.104536	-0.039495	-0.088142	-0.11481	-0.116052	-0.299572	-0.431572	-0.486491	-0.43538
Face C	-0.090992	-0.018681	-0.069253	-0.104013	-0.120172	-0.329829	-0.477247	-0.455674	-0.234489
Face B	-0.069978	-0.008728	-0.059581	-0.093817	-0.12025	-0.344173	-0.499147	-0.480653	-0.240327
Face A	-0.026791	-0.016611	-0.049024	-0.077852	-0.116956	-0.367871	-0.534193	-0.526725	-0.247388

Fig. 3.169 Cpe for roof angle 10° and spacing=2b

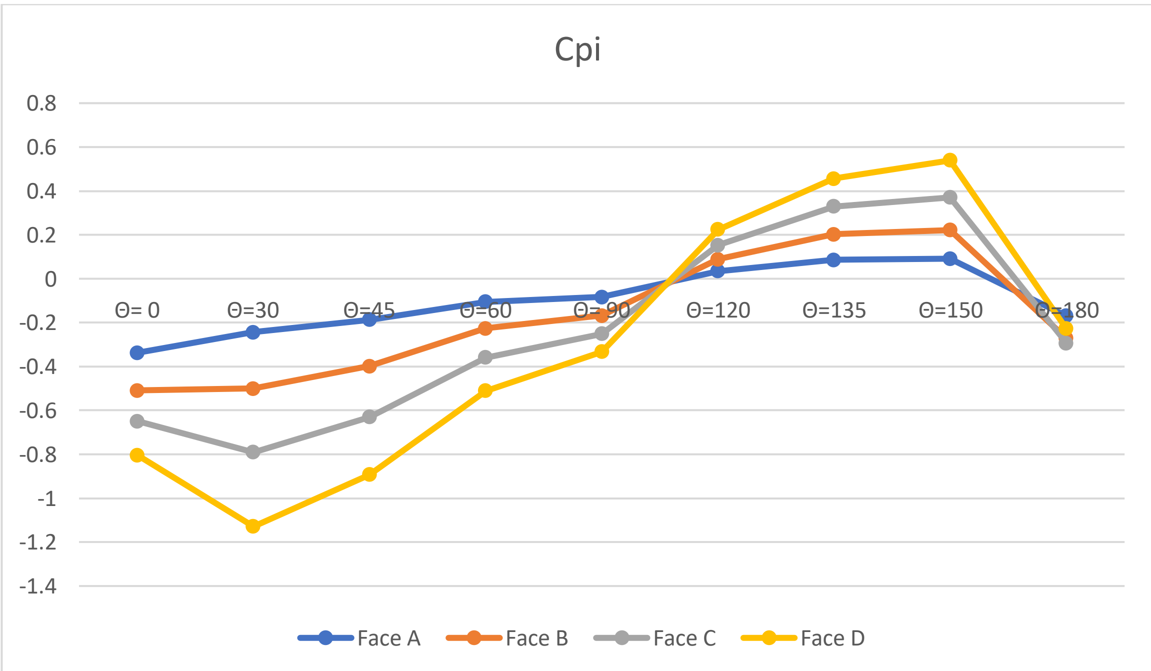

Fig. 3.170 Cpi for roof angle 10° and spacing=2b

Slope Angle = 20°, Spacing =0

Table 3.14 Coefficient of Pressure (C_{pext}) at Slope Angle = 20°, Spacing =0

C_{pint}	**Face A**	**Face B**	**Face C**	**Face D**
Ɵ = 0°	0.0863027	-0.178093	-0.0592644	-0.0936963
Ɵ =30°	0.139864	-0.0724153	-0.0595409	-0.0693963
Ɵ = 45°	0.0712778	-0.0701634	-0.0757581	-0.0940841
Ɵ =60 °	-0.0251125	-0.106281	-0.118576	-0.114044
Ɵ =90°	-0.18036	-0.208063	-0.202663	-0.167369
Ɵ =120°	-0.464298	-0.37422	-0.321807	-0.345216
Ɵ =135°	-0.482696	-0.359743	-0.3205	-0.493156
Ɵ =150°	-0.468376	-0.300577	-0.254667	-0.518357
Ɵ =180 °	-0.246742	-0.172897	-0.216059	-0.45424

Table 3.15 Coefficient of Pressure (C_{pint}) at Slope Angle = 20°, Spacing =0

C_{pint}	**Face A**	**Face B**	**Face C**	**Face D**
Ɵ = 0°	-0.400706	-0.118335	-0.174718	-0.252791
Ɵ =30°	-0.366006	-0.223951	-0.251017	-0.337261
Ɵ = 45°	-0.272871	-0.251519	-0.271381	-0.358948
Ɵ =60 °	-0.163781	-0.193701	-0.202048	-0.258634
Ɵ =90°	-0.14199	-0.173446	-0.172102	-0.139478
Ɵ =120°	-0.0120615	0.0429429	0.0564243	0.163965
Ɵ =135°	-0.0270345	0.0320867	0.073759	0.270256
Ɵ =150°	-0.0121363	0.0539396	-0.035892	0.314339
Ɵ =180 °	-0.0852934	-0.0221673	-0.207849	0.236617

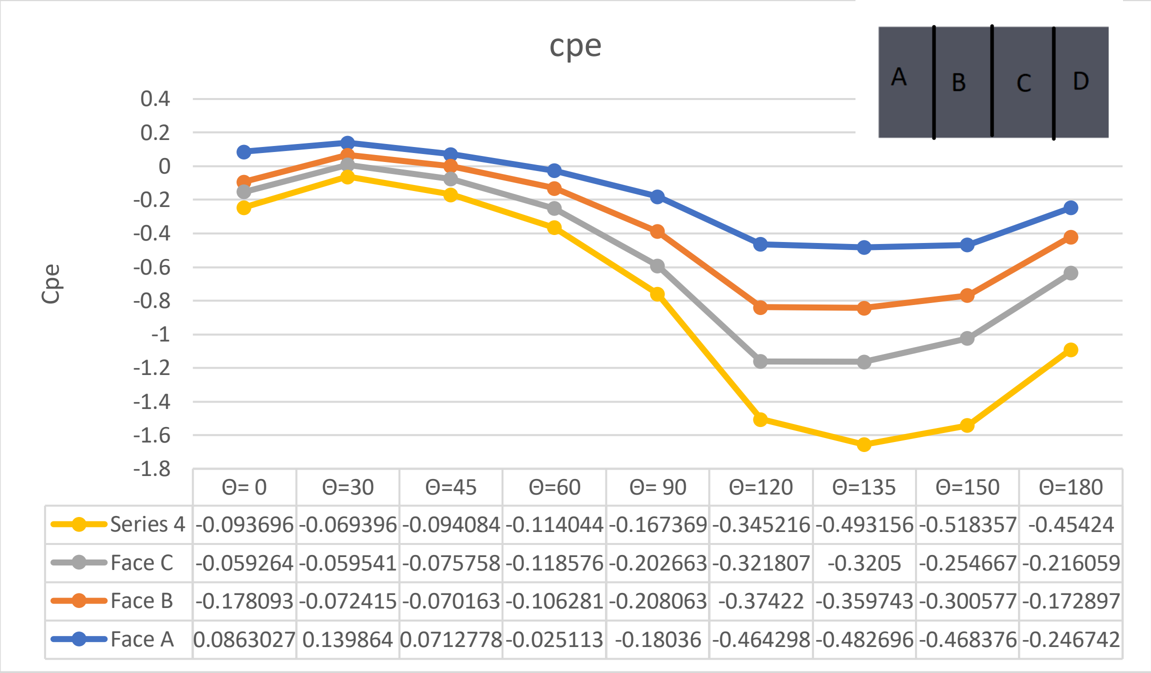

	Θ= 0	Θ=30	Θ=45	Θ=60	Θ= 90	Θ=120	Θ=135	Θ=150	Θ=180
Series 4	-0.093696	-0.069396	-0.094084	-0.114044	-0.167369	-0.345216	-0.493156	-0.518357	-0.45424
Face C	-0.059264	-0.059541	-0.075758	-0.118576	-0.202663	-0.321807	-0.3205	-0.254667	-0.216059
Face B	-0.178093	-0.072415	-0.070163	-0.106281	-0.208063	-0.37422	-0.359743	-0.300577	-0.172897
Face A	0.0863027	0.139864	0.0712778	-0.025113	-0.18036	-0.464298	-0.482696	-0.468376	-0.246742

Fig. 3.171 Cpe for roof angle 20° and spacing=zero

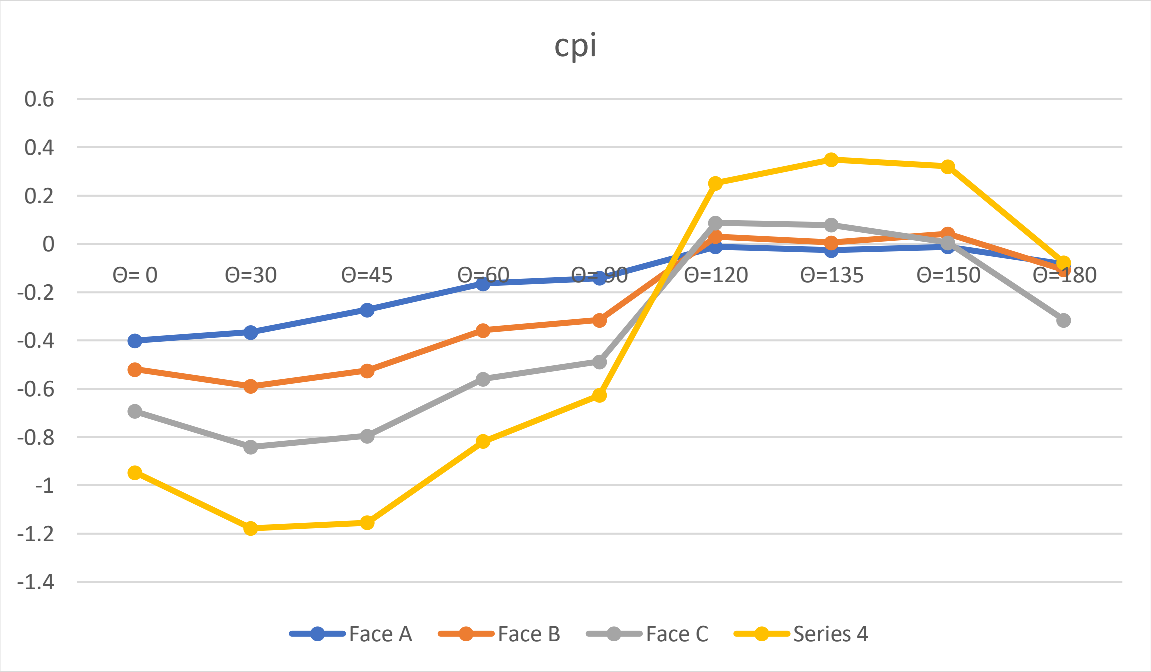

Fig. 3.172 Cpi for roof angle 20° and spacing=zero

Spacing =b/2

Table 3.16 Coefficient of Pressure (C_{pext}) at Slope Angle = 20°, Spacing b/2

C_{pint}	**Face A**	**Face B**	**Face C**	**Face D**
Ɵ = 0°	0.102019	-0.0646468	-0.0302147	-0.0842587
Ɵ =30°	0.160636	0.0373695	0.0358433	0.00702446
Ɵ = 45°	0.107046	0.0406406	0.0276804	0.00116386
Ɵ =60 °	0.0134252	-0.0224131	-0.0351143	-0.0474098
Ɵ =90°	-0.137042	-0.149604	-0.147735	-0.130934
Ɵ =120°	-0.516327	-0.426825	-0.374946	-0.345164
Ɵ =135°	-0.613471	-0.485319	-0.428903	-0.480638
Ɵ =150°	-0.532449	-0.367277	-0.320039	-0.524502
Ɵ =180 °	-0.275726	-0.212798	-0.147373	-0.468944

Table 3.17 Coefficient of Pressure (C_{pint}) at Slope Angle = 20°, Spacing b/2

C_{pint}	**Face A**	**Face B**	**Face C**	**Face D**
Ө = 0°	-0.383082	-0.133828	-0.199022	-0.259074
Ө =30°	-0.386063	-0.255432	-0.291321	-0.375387
Ө = 45°	-0.278949	-0.246093	-0.286994	-0.377142
Ө =60 °	-0.173682	-0.184415	-0.211571	-0.270184
Ө =90°	-0.0894703	-0.0964814	-0.0960365	-0.0895413
Ө =120°	0.0801983	0.113838	0.128088	0.15774
Ө =135°	0.1239	0.184352	0.209752	0.275494
Ө =150°	0.072515	0.131065	0.146281	0.3257
Ө =180 °	-0.139235	-0.0435988	-0.0683288	0.229285

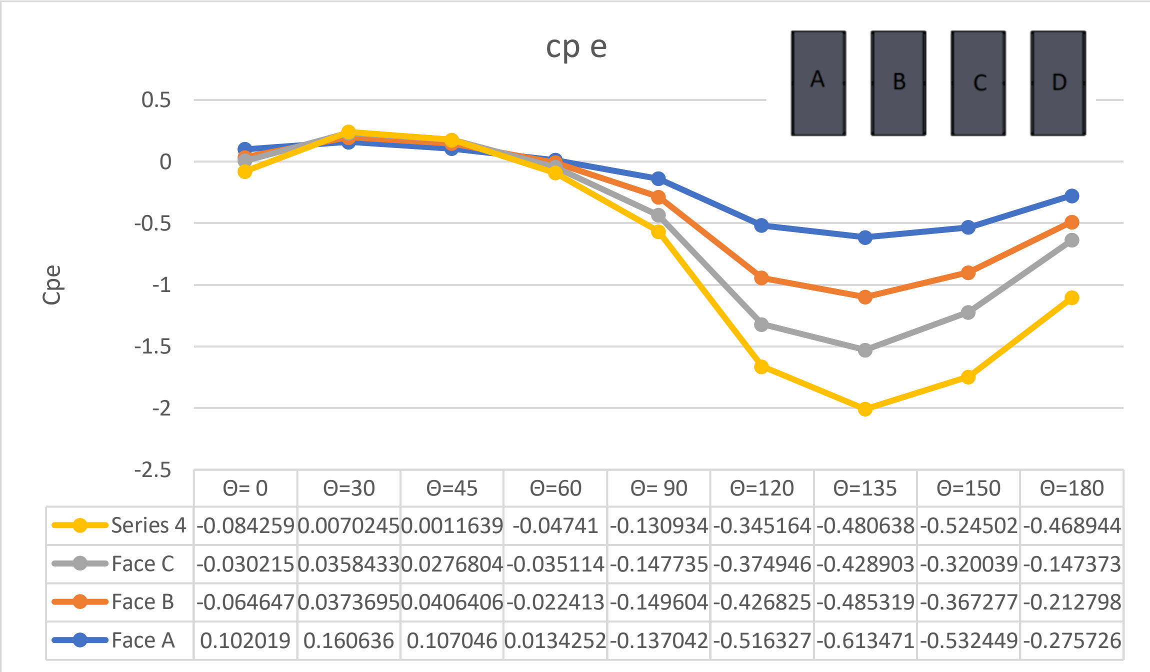

	Θ= 0	Θ=30	Θ=45	Θ=60	Θ= 90	Θ=120	Θ=135	Θ=150	Θ=180
Series 4	-0.084259	0.0070245	0.0011639	-0.04741	-0.130934	-0.345164	-0.480638	-0.524502	-0.468944
Face C	-0.030215	0.0358433	0.0276804	-0.035114	-0.147735	-0.374946	-0.428903	-0.320039	-0.147373
Face B	-0.064647	0.0373695	0.0406406	-0.022413	-0.149604	-0.426825	-0.485319	-0.367277	-0.212798
Face A	0.102019	0.160636	0.107046	0.0134252	-0.137042	-0.516327	-0.613471	-0.532449	-0.275726

Fig. 3.173 Cpe for roof angle 20° and spacing=b/2

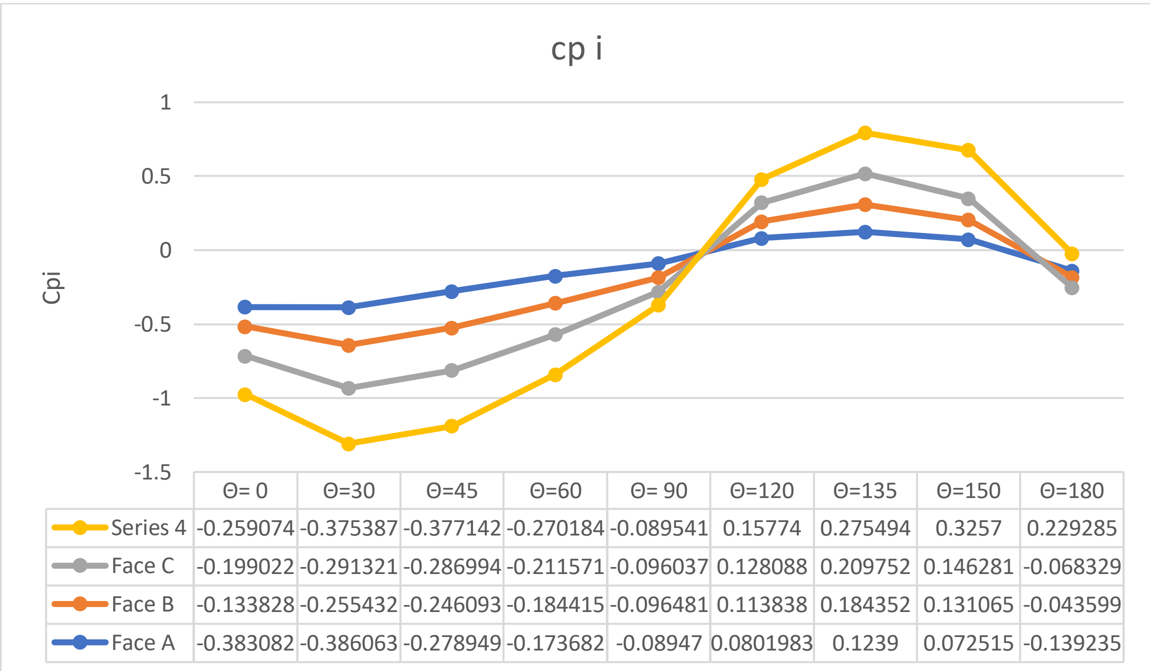

	Θ= 0	Θ=30	Θ=45	Θ=60	Θ= 90	Θ=120	Θ=135	Θ=150	Θ=180
Series 4	-0.259074	-0.375387	-0.377142	-0.270184	-0.089541	0.15774	0.275494	0.3257	0.229285
Face C	-0.199022	-0.291321	-0.286994	-0.211571	-0.096037	0.128088	0.209752	0.146281	-0.068329
Face B	-0.133828	-0.255432	-0.246093	-0.184415	-0.096481	0.113838	0.184352	0.131065	-0.043599
Face A	-0.383082	-0.386063	-0.278949	-0.173682	-0.08947	0.0801983	0.1239	0.072515	-0.139235

Fig. 3.174 Cpi for roof angle 20° and spacing=b/2

Spacing =b

Table 3.18 Coefficient of Pressure (C_{pext}) at Slope Angle = 20°, Spacing b

C_{pint}	**Face A**	**Face B**	**Face C**	**Face D**
ϴ = 0°	0.105985	-0.0140729	-0.0360056	-0.0851845
ϴ =30°	0.160213	0.0864928	0.0826515	0.0536125
ϴ = 45°	0.102617	0.082265	0.0742628	0.0516847
ϴ =60 °	0.0194392	-0.00324023	-0.0131014	-0.0236914
ϴ =90°	-0.124933	-0.133115	-0.13177	-0.12053
ϴ =120°	-0.532933	-0.47089	-0.431252	-0.375823
ϴ =135°	-0.669107	-0.5902	-0.545408	-0.538608
ϴ =150°	-0.62522	-0.477513	-0.42772	-0.535017
ϴ =180 °	-0.302418	-0.241464	-0.202383	-0.480584

Table 3.19 Coefficient of Pressure (C_{pint}) at Slope Angle = 20°, Spacing b

C_{pint}	**Face A**	**Face B**	**Face C**	**Face D**
Ɵ = 0°	-0.402715	-0.171426	-0.226445	-0.270877
Ɵ =30°	-0.414672	-0.324984	-0.359408	-0.441243
Ɵ = 45°	-0.325951	-0.322269	-0.359252	-0.431036
Ɵ =60 °	-0.193299	-0.224678	-0.246798	-0.291834
Ɵ =90°	-0.0870086	-0.0940876	-0.0942267	-0.0876481
Ɵ =120°	0.106012	0.133876	0.143519	0.151794
Ɵ =135°	0.172842	0.219907	0.235299	0.256433
Ɵ =150°	0.129359	0.189832	0.191146	0.303528
Ɵ =180 °	-0.15249	-0.0686301	0.0200784	0.231178

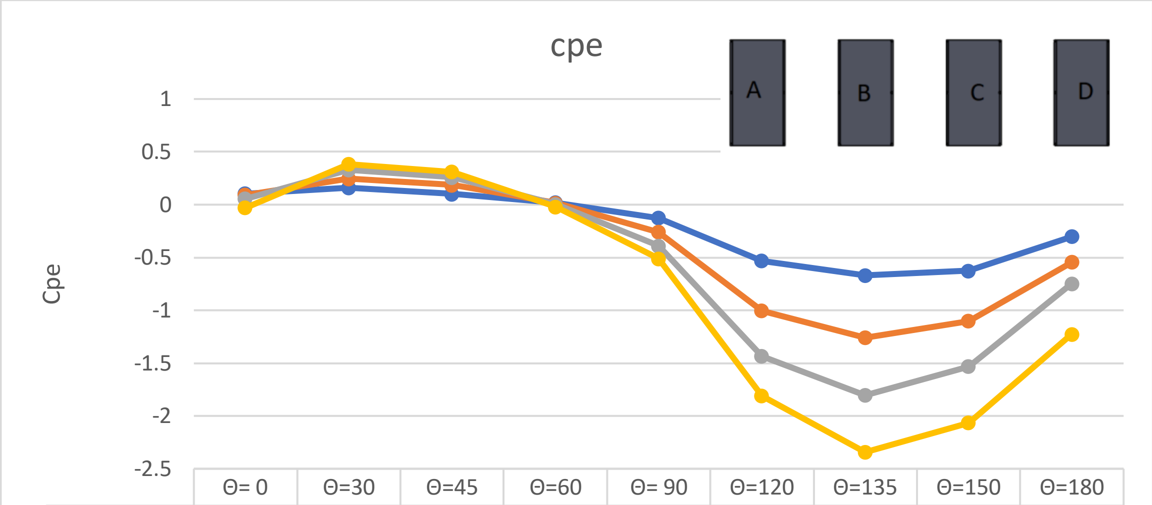

	Θ= 0	Θ=30	Θ=45	Θ=60	Θ= 90	Θ=120	Θ=135	Θ=150	Θ=180
Series 4	-0.085185	0.0536125	0.0516847	-0.023691	-0.12053	-0.375823	-0.538608	-0.535017	-0.480584
Face C	-0.036006	0.0826515	0.0742628	-0.013101	-0.13177	-0.431252	-0.545408	-0.42772	-0.202383
Face B	-0.014073	0.0864928	0.082265	-0.00324	-0.133115	-0.47089	-0.5902	-0.477513	-0.241464
Face A	0.105985	0.160213	0.102617	0.0194392	-0.124933	-0.532933	-0.669107	-0.62522	-0.302418

Fig. 3.175 Cpe for roof angle 20° and spacing=b

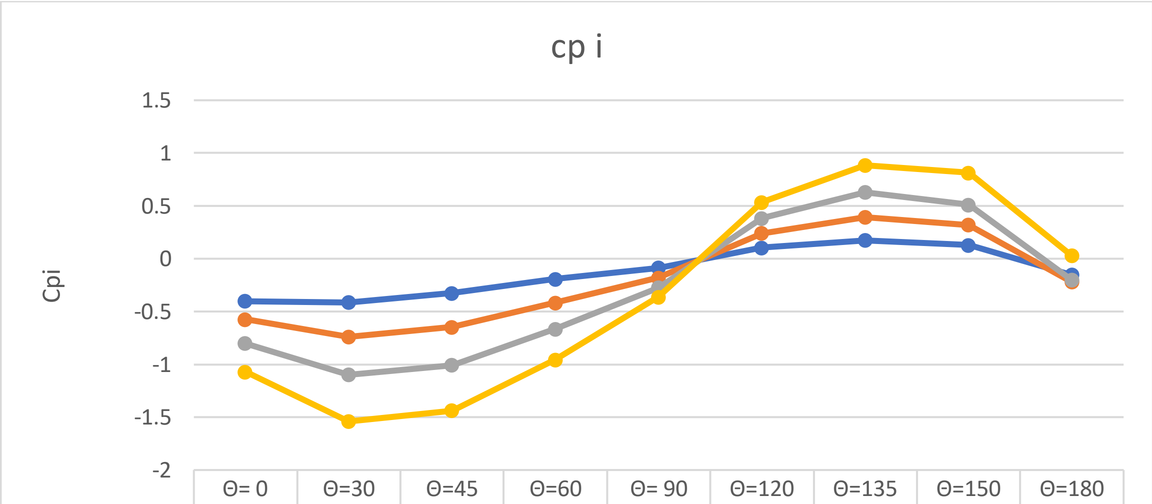

	Θ= 0	Θ=30	Θ=45	Θ=60	Θ= 90	Θ=120	Θ=135	Θ=150	Θ=180
Series 4	-0.270877	-0.441243	-0.431036	-0.291834	-0.087648	0.151794	0.256433	0.303528	0.231178
Face C	-0.226445	-0.359408	-0.359252	-0.246798	-0.094227	0.143519	0.235299	0.191146	0.0200784
Face B	-0.171426	-0.324984	-0.322269	-0.224678	-0.094088	0.133876	0.219907	0.189832	-0.06863
Face A	-0.402715	-0.414672	-0.325951	-0.193299	-0.087009	0.106012	0.172842	0.129359	-0.15249

Fig. 3.176 Cpi for roof angle 20° and spacing=b

Spacing =3b/2

Table 3.20 Coefficient of Pressure (C_{pext}) at Slope Angle = 20°, Spacing 3b/2

C_{pint}	**Face A**	**Face B**	**Face C**	**Face D**
Ɵ = 0°	0.10717	-0.00514585	-0.0477618	-0.0860735
Ɵ =30°	0.158837	0.117683	0.114986	0.0912538
Ɵ = 45°	0.103736	0.0996596	0.0910002	0.0726817
Ɵ =60 °	0.0201742	0.00273741	-0.00614141	-0.0163577
Ɵ =90°	-0.1194	-0.124296	-0.123808	-0.11539
Ɵ =120°	-0.516856	-0.470842	-0.44321	-0.395019
Ɵ =135°	-0.701368	-0.641392	-0.603883	-0.564955
Ɵ =150°	-0.649558	-0.540112	-0.532847	-0.537877
Ɵ =180 °	-0.339941	-0.302768	-0.253149	-0.518465

Table 3.21 Coefficient of Pressure (C_{pint}) at Slope Angle = 20°, Spacing 3b/2

C_{pint}	**Face A**	**Face B**	**Face C**	**Face D**
Ɵ = 0°	-0.432909	-0.216907	-0.257665	-0.277764
Ɵ =30°	-0.431869	-0.388231	-0.429117	-0.495974
Ɵ = 45°	-0.347218	-0.385718	-0.423093	-0.482308
Ɵ =60 °	-0.203546	-0.234286	-0.252699	-0.286893
Ɵ =90°	-0.0815556	-0.0864745	-0.0871823	-0.0825921
Ɵ =120°	0.105278	0.128704	0.137808	0.143357
Ɵ =135°	0.184348	0.226549	0.241726	0.245579
Ɵ =150°	0.158151	0.209462	0.235234	0.276813
Ɵ =180 °	-0.150554	-0.0791618	0.00977823	0.208287

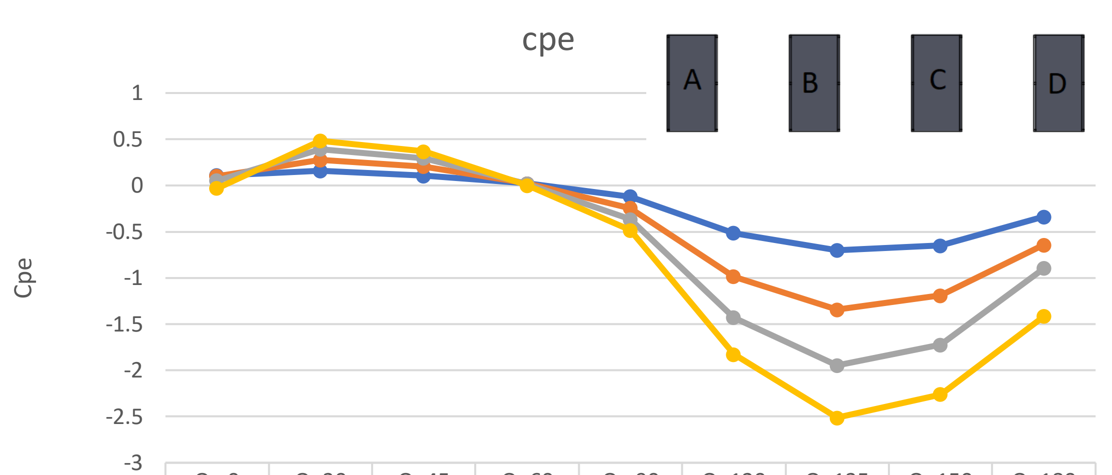

	Θ= 0	Θ=30	Θ=45	Θ=60	Θ= 90	Θ=120	Θ=135	Θ=150	Θ=180
Series 4	-0.086074	0.0912538	0.0726817	-0.016358	-0.11539	-0.395019	-0.564955	-0.537877	-0.518465
Face C	-0.047762	0.114986	0.0910002	-0.006141	-0.123808	-0.44321	-0.603883	-0.532847	-0.253149
Face B	-0.005146	0.117683	0.0996596	0.0027374	-0.124296	-0.470842	-0.641392	-0.540112	-0.302768
Face A	0.10717	0.158837	0.103736	0.0201742	-0.1194	-0.516856	-0.701368	-0.649558	-0.339941

Fig. 3.177 Cpe for roof angle 20° and spacing=3b/2

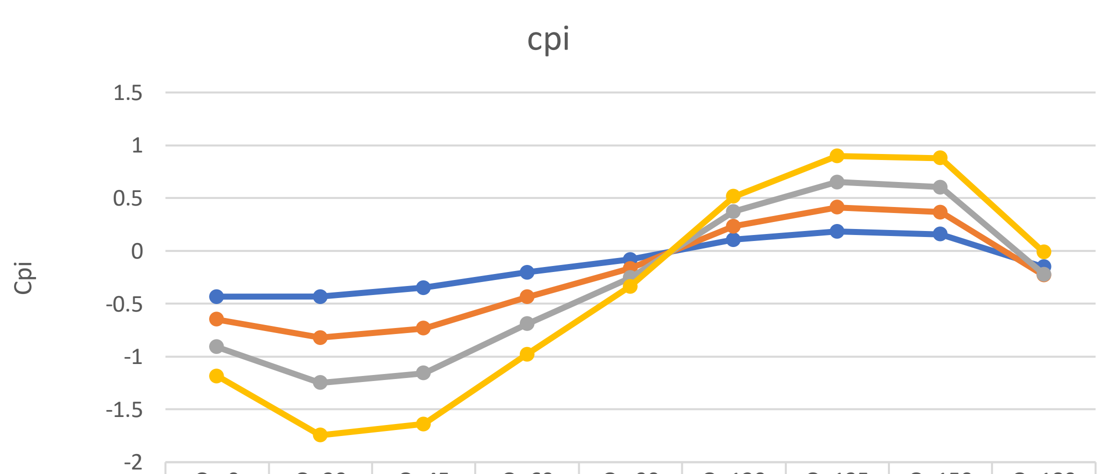

	Θ= 0	Θ=30	Θ=45	Θ=60	Θ= 90	Θ=120	Θ=135	Θ=150	Θ=180
Series 4	-0.277764	-0.495974	-0.482308	-0.286893	-0.082592	0.143357	0.245579	0.276813	0.208287
Face C	-0.257665	-0.429117	-0.423093	-0.252699	-0.087182	0.137808	0.241726	0.235234	0.0097782
Face B	-0.216907	-0.388231	-0.385718	-0.234286	-0.086475	0.128704	0.226549	0.209462	-0.079162
Face A	-0.432909	-0.431869	-0.347218	-0.203546	-0.081556	0.105278	0.184348	0.158151	-0.150554

Fig. 3.178 Cpi for roof angle 20° and spacing=3b/2

Spacing =2b

Table 3.22 Coefficient of Pressure (C_{pext}) at Slope Angle = 20°, Spacing 2b

C_{pint}	**Face A**	**Face B**	**Face C**	**Face D**
Ө = 0°	0.10699	-0.00536091	-0.0532852	-0.0793829
Ө =30°	0.15622	0.145842	0.143081	0.123769
Ө = 45°	0.10069	0.0955823	0.086808	0.0713189
Ө =60 °	0.0190646	0.00538179	-0.0041151	-0.0133549
Ө =90°	-0.116704	-0.119625	-0.119325	-0.114223
Ө =120°	-0.501048	-0.469226	-0.446046	-0.40767
Ө =135°	-0.702514	-0.655377	-0.626109	-0.580129
Ө =150°	-0.634852	-0.58408	-0.584032	-0.559212
Ө =180 °	-0.363445	-0.351943	-0.305348	-0.557307

Table 3.23 Coefficient of Pressure (C_{pint}) at Slope Angle = 20°, Spacing 2b

C_{pint}	**Face A**	**Face B**	**Face C**	**Face D**
Ɵ = 0°	-0.458831	-0.266532	-0.28406	-0.291735
Ɵ =30°	-0.444101	-0.44204	-0.482246	-0.544462
Ɵ = 45°	-0.36664	-0.406577	-0.440292	-0.490118
Ɵ =60 °	-0.211999	-0.239961	-0.256612	-0.281964
Ɵ =90°	-0.0811718	-0.0824952	-0.0825669	-0.079499
Ɵ =120°	0.100764	0.119825	0.129907	0.137768
Ɵ =135°	0.179896	0.213928	0.228029	0.233863
Ɵ =150°	0.183158	0.226283	0.250567	0.265595
Ɵ =180 °	-0.140512	-0.0774684	0.0032449	0.209256

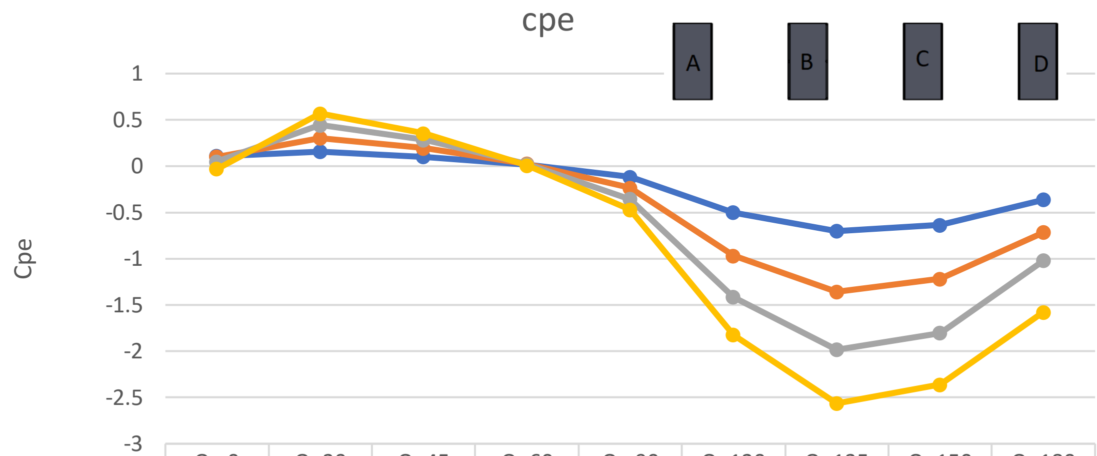

	Θ= 0	Θ=30	Θ=45	Θ=60	Θ= 90	Θ=120	Θ=135	Θ=150	Θ=180
Series 4	-0.079383	0.123769	0.0713189	-0.013355	-0.114223	-0.40767	-0.580129	-0.559212	-0.557307
Face C	-0.053285	0.143081	0.086808	-0.004115	-0.119325	-0.446046	-0.626109	-0.584032	-0.305348
Face B	-0.005361	0.145842	0.0955823	0.0053818	-0.119625	-0.469226	-0.655377	-0.58408	-0.351943
Face A	0.10699	0.15622	0.10069	0.0190646	-0.116704	-0.501048	-0.702514	-0.634852	-0.363445

Fig. 3.179 Cpe for roof angle 20° and spacing=2b

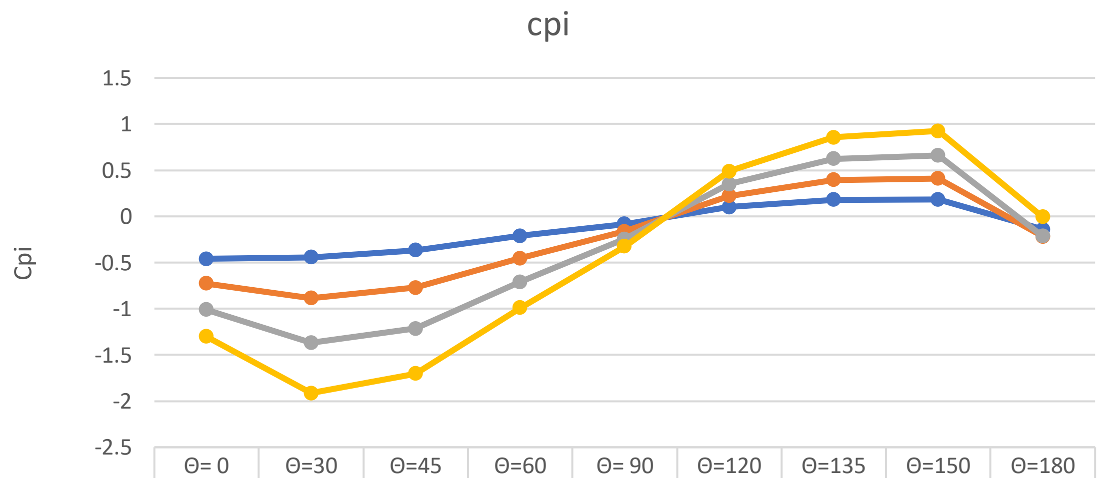

	Θ= 0	Θ=30	Θ=45	Θ=60	Θ= 90	Θ=120	Θ=135	Θ=150	Θ=180
Face D	-0.291735	-0.544462	-0.490118	-0.281964	-0.079499	0.137768	0.233863	0.265595	0.209256
Face C	-0.28406	-0.482246	-0.440292	-0.256612	-0.082567	0.129907	0.228029	0.250567	0.0032449
Face B	-0.266532	-0.44204	-0.406577	-0.239961	-0.082495	0.119825	0.213928	0.226283	-0.077468
Face A	-0.458831	-0.444101	-0.36664	-0.211999	-0.081172	0.100764	0.179896	0.183158	-0.140512

Fig. 3.180 Cpi for roof angle 20° and spacing=2b

Slope Angle = 30°, Spacing =0

Table 3.24 Coefficient of Pressure (C_{pext}) at Slope Angle = 30°, Spacing 0

C_{pint}	**Face A**	**Face B**	**Face C**	**Face D**
Ɵ = 0°	0.228643	-0.341633	-0.0956364	-0.0961126
Ɵ =30°	0.271225	-0.107991	-0.0418061	-0.0684861
Ɵ = 45°	0.199912	-0.0426258	-0.0437885	-0.0712388
Ɵ =60 °	0.0725576	-0.0438904	-0.0556783	-0.0648869
Ɵ =90°	-0.177468	-0.199607	-0.193115	-0.161541
Ɵ =120°	-0.558603	-0.413148	-0.34419	-0.374689
Ɵ =135°	-0.543812	-0.415895	-0.341607	-0.545555
Ɵ =150°	-0.479481	-0.385596	-0.299753	-0.50892
Ɵ =180 °	-0.275955	-0.234967	-0.235427	-0.499462

Table 3.25 Coefficient of Pressure (C_{pint}) at Slope Angle = 30°, Spacing 0

C_{pint}	**Face A**	**Face B**	**Face C**	**Face D**
ϴ = 0°	-0.518536	-0.163589	-0.195304	-0.307639
ϴ =30°	-0.479661	-0.307793	-0.350327	-0.431534
ϴ = 45°	-0.406031	-0.319277	-0.352951	-0.445775
ϴ =60 °	-0.240899	-0.251937	-0.272746	-0.352224
ϴ =90°	-0.1368	-0.168694	-0.169588	-0.145245
ϴ =120°	0.00387394	0.0657444	0.0854893	0.22246
ϴ =135°	-0.0405126	0.0514846	0.0733526	0.352289
ϴ =150°	-0.0362554	0.0294474	-0.10058	0.382461
ϴ =180 °	-0.0804993	-0.0320838	-0.40953	0.347724

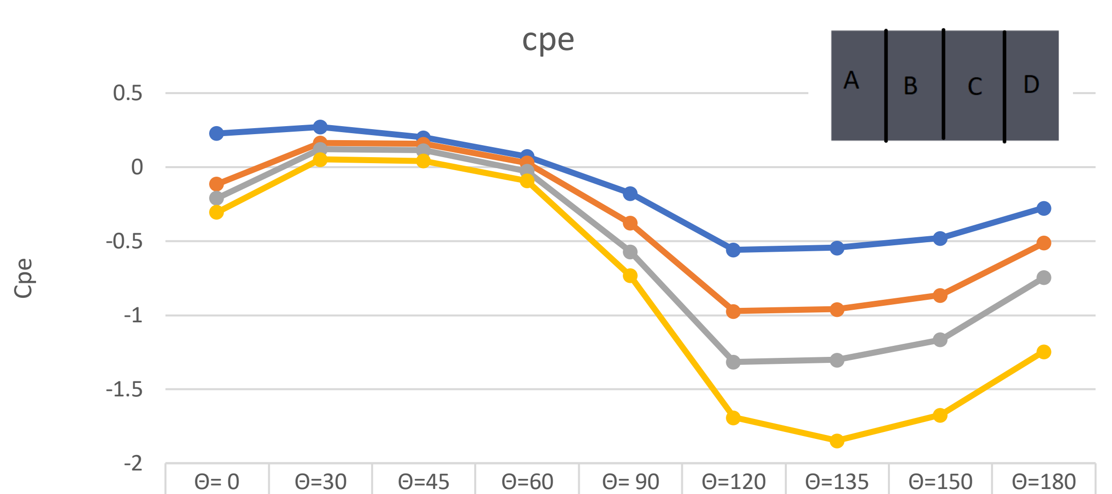

	Θ= 0	Θ=30	Θ=45	Θ=60	Θ= 90	Θ=120	Θ=135	Θ=150	Θ=180
Series 4	-0.096113	-0.068486	-0.071239	-0.064887	-0.161541	-0.374689	-0.545555	-0.50892	-0.499462
Face C	-0.095636	-0.041806	-0.043789	-0.055678	-0.193115	-0.34419	-0.341607	-0.299753	-0.235427
Face B	-0.341633	-0.107991	-0.042626	-0.04389	-0.199607	-0.413148	-0.415895	-0.385596	-0.234967
Face A	0.228643	0.271225	0.199912	0.0725576	-0.177468	-0.558603	-0.543812	-0.479481	-0.275955

Fig. 3.181 Cpe for roof angle 30° and spacing=0

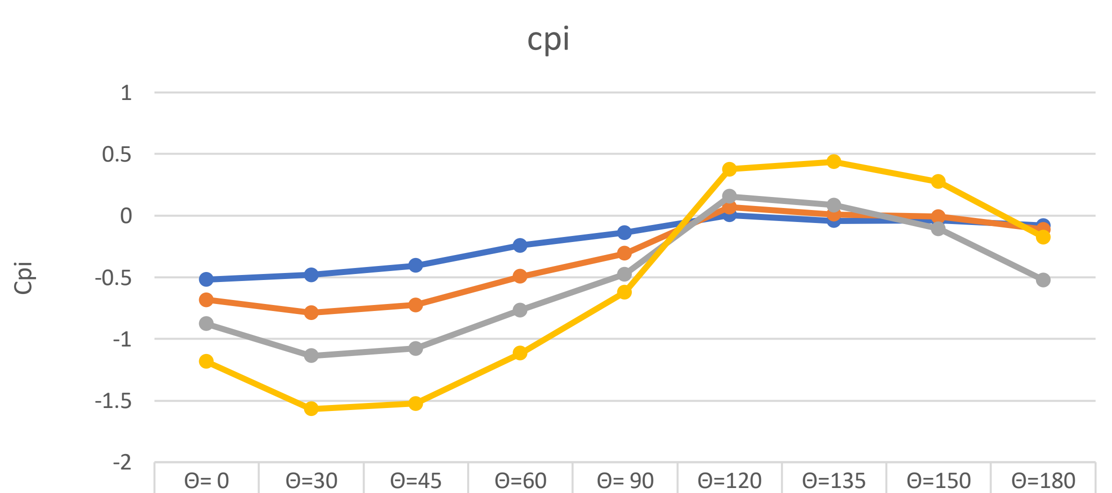

	Θ= 0	Θ=30	Θ=45	Θ=60	Θ= 90	Θ=120	Θ=135	Θ=150	Θ=180
Face D	-0.307639	-0.431534	-0.445775	-0.352224	-0.145245	0.22246	0.352289	0.382461	0.347724
Face C	-0.195304	-0.350327	-0.352951	-0.272746	-0.169588	0.0854893	0.0733526	-0.10058	-0.40953
Face B	-0.163589	-0.307793	-0.319277	-0.251937	-0.168694	0.0657444	0.0514846	0.0294474	-0.032084
Face A	-0.518536	-0.479661	-0.406031	-0.240899	-0.1368	0.0038739	-0.040513	-0.036255	-0.080499

Fig. 3.182 Cpi for roof angle 30° and spacing=0

Spacing =b/2

Table 3.26 Coefficient of Pressure (C_{pext}) at Slope Angle = 30°, Spacing b/2

C_{pext}	**Face A**	**Face B**	**Face C**	**Face D**
ϴ = 0°	0.238642	-0.183904	-0.00804907	-0.063099
ϴ =30°	0.28777	0.0514243	0.0716256	0.0388177
ϴ = 45°	0.23025	0.101931	0.0897	0.0585048
ϴ =60 °	0.0993307	0.0382477	0.0242101	0.0111746
ϴ =90°	-0.137634	-0.1467	-0.143329	-0.126609
ϴ =120°	-0.604965	-0.454459	-0.397078	-0.382005
ϴ =135°	-0.727279	-0.530289	-0.469087	-0.539077
ϴ =150°	-0.508239	-0.440206	-0.360349	-0.51626
ϴ =180 °	-0.324682	-0.21724	-0.153719	-0.449406

Table 3.27 Coefficient of Pressure (C_{pint}) at Slope Angle = 30°, Spacing b/2

C_{pint}	**Face A**	**Face B**	**Face C**	**Face D**
ϴ = 0°	-0.436066	-0.153669	-0.228832	-0.325917
ϴ =30°	-0.476408	-0.332334	-0.372721	-0.472368
ϴ = 45°	-0.408181	-0.342567	-0.390186	-0.507549
ϴ =60 °	-0.258983	-0.263297	-0.300194	-0.380451
ϴ =90°	-0.0847179	-0.0985513	-0.0989745	-0.0875265
ϴ =120°	0.0958442	0.13632	0.160538	0.219827
ϴ =135°	0.155822	0.222611	0.248112	0.364598
ϴ =150°	0.0874397	0.175441	0.13937	0.40573
ϴ =180 °	-0.085362	0.016397	-0.229483	0.366365

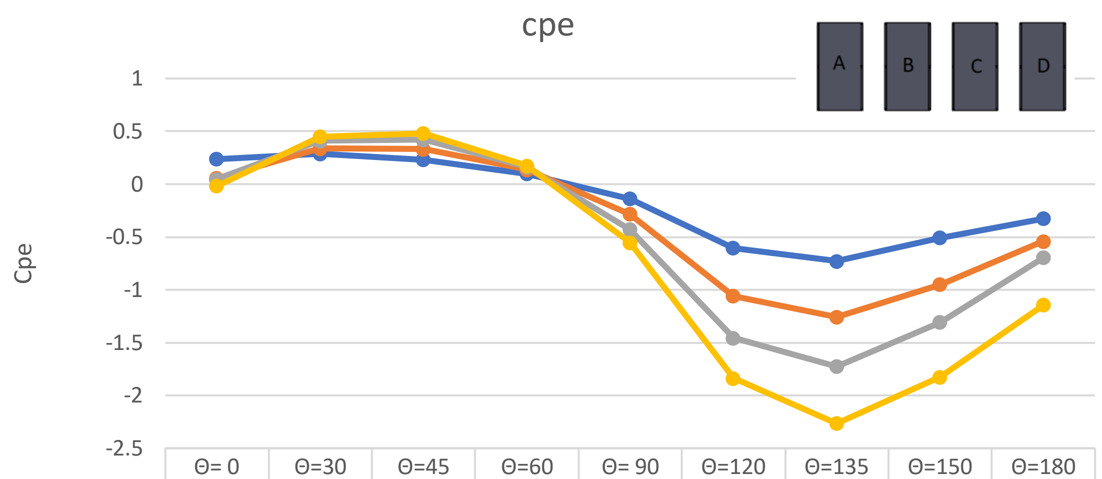

	Θ= 0	Θ=30	Θ=45	Θ=60	Θ= 90	Θ=120	Θ=135	Θ=150	Θ=180
Series 4	-0.063099	0.0388177	0.0585048	0.0111746	-0.126609	-0.382005	-0.539077	-0.51626	-0.449406
Face C	-0.008049	0.0716256	0.0897	0.0242101	-0.143329	-0.397078	-0.469087	-0.360349	-0.153719
Face B	-0.183904	0.0514243	0.101931	0.0382477	-0.1467	-0.454459	-0.530289	-0.440206	-0.21724
Face A	0.238642	0.28777	0.23025	0.0993307	-0.137634	-0.604965	-0.727279	-0.508239	-0.324682

Fig. 3.183 Cpe for roof angle 30° and spacing=b/2

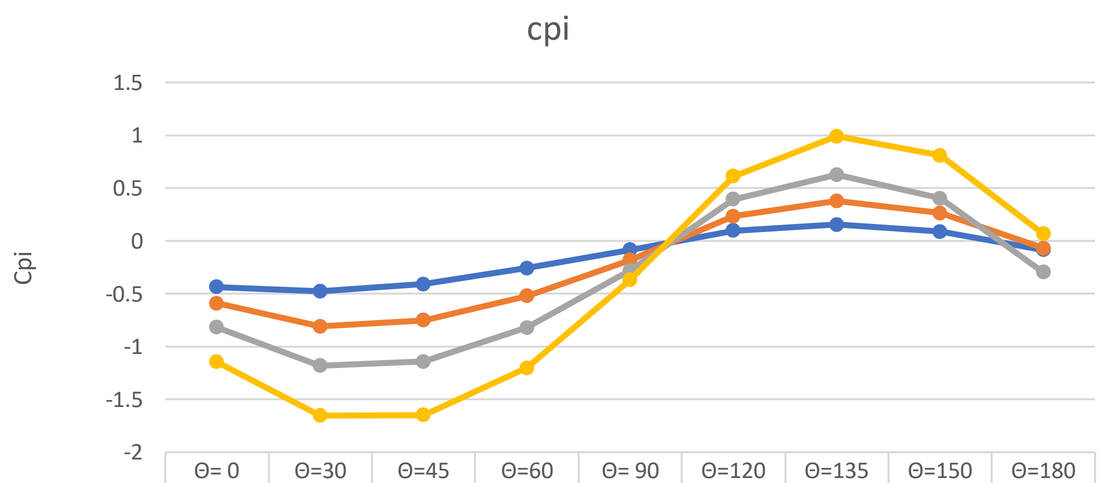

	Θ= 0	Θ=30	Θ=45	Θ=60	Θ= 90	Θ=120	Θ=135	Θ=150	Θ=180
Series 4	-0.325917	-0.472368	-0.507549	-0.380451	-0.087527	0.219827	0.364598	0.40573	0.366365
Series 3	-0.228832	-0.372721	-0.390186	-0.300194	-0.098975	0.160538	0.248112	0.13937	-0.229483
Series 2	-0.153669	-0.332334	-0.342567	-0.263297	-0.098551	0.13632	0.222611	0.175441	0.016397
Series 1	-0.436066	-0.476408	-0.408181	-0.258983	-0.084718	0.0958442	0.155822	0.0874397	-0.085362

Fig. 3.184 Cpi for roof angle 30° and spacing=b/2

Spacing =b

Table 3.28 Coefficient of Pressure (C_{pext}) at Slope Angle = 30°, Spacing b

C_{pint}	**Face A**	**Face B**	**Face C**	**Face D**
Ɵ = 0°	0.24555	-0.0518729	0.0132957	-0.0606838
Ɵ =30°	0.279001	0.13362	0.1435	0.115651
Ɵ = 45°	0.229821	0.167435	0.1577	0.132038
Ɵ =60 °	0.10614	0.0734022	0.0616132	0.0487008
Ɵ =90°	-0.126409	-0.133491	-0.13083	-0.120353
Ɵ =120°	-0.630036	-0.528831	-0.482365	-0.443262
Ɵ =135°	-0.77851	-0.666687	-0.618975	-0.602685
Ɵ =150°	-0.613934	-0.517664	-0.492052	-0.55196
Ɵ =180 °	-0.373394	-0.275287	-0.15453	-0.408943

Table 3.29 Coefficient of Pressure (C_{pint}) at Slope Angle = 30°, Spacing b

C_{pint}	**Face A**	**Face B**	**Face C**	**Face D**
ϴ = 0°	-0.404457	-0.171643	-0.285025	-0.361402
ϴ =30°	-0.478546	-0.383955	-0.424483	-0.532326
ϴ = 45°	-0.448482	-0.433396	-0.480192	-0.568835
ϴ =60 °	-0.284944	-0.320596	-0.351088	-0.41859
ϴ =90°	-0.0817141	-0.0884575	-0.0881645	-0.0832265
ϴ =120°	0.141617	0.171624	0.189246	0.210968
ϴ =135°	0.212634	0.266606	0.292742	0.342858
ϴ =150°	0.163668	0.236079	0.267073	0.395695
ϴ =180 °	-0.110352	0.0121067	-0.0458976	0.354541

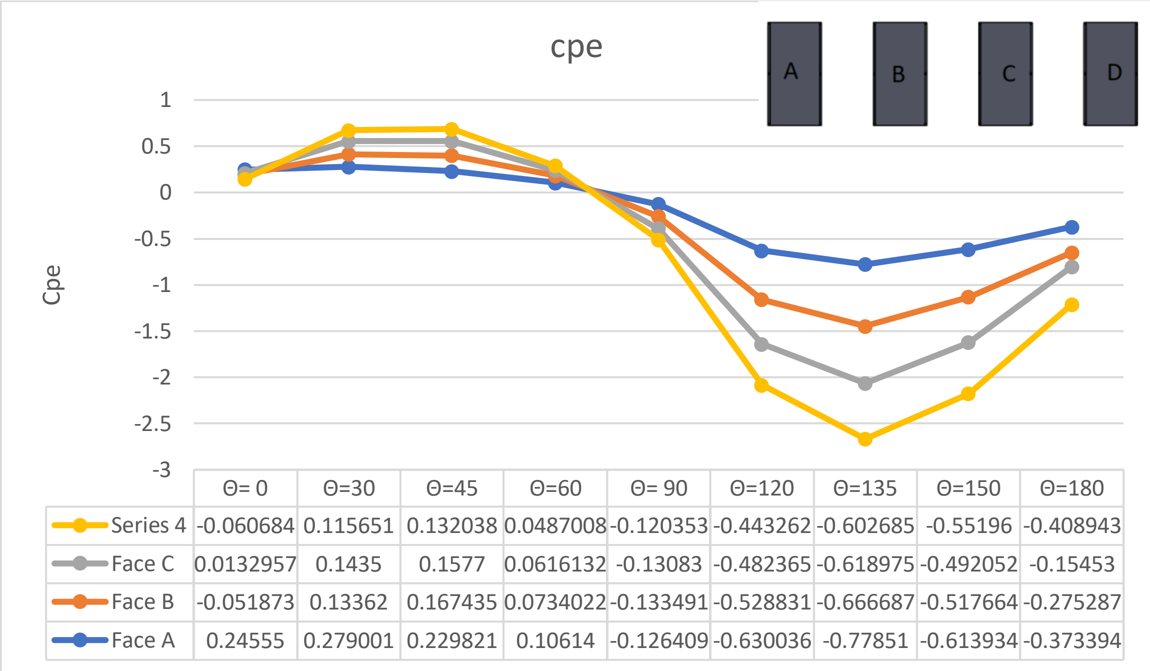

	Θ= 0	Θ=30	Θ=45	Θ=60	Θ= 90	Θ=120	Θ=135	Θ=150	Θ=180
Series 4	-0.060684	0.115651	0.132038	0.0487008	-0.120353	-0.443262	-0.602685	-0.55196	-0.408943
Face C	0.0132957	0.1435	0.1577	0.0616132	-0.13083	-0.482365	-0.618975	-0.492052	-0.15453
Face B	-0.051873	0.13362	0.167435	0.0734022	-0.133491	-0.528831	-0.666687	-0.517664	-0.275287
Face A	0.24555	0.279001	0.229821	0.10614	-0.126409	-0.630036	-0.77851	-0.613934	-0.373394

Fig. 3.185 Cpe for roof angle 30° and spacing=b

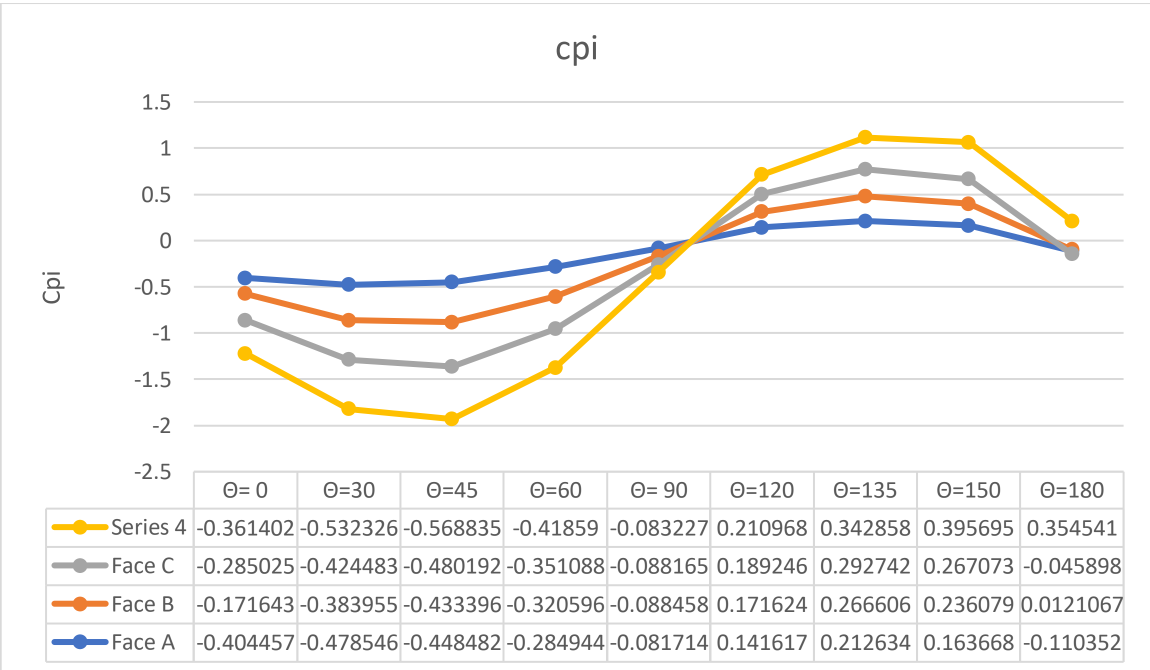

	Θ= 0	Θ=30	Θ=45	Θ=60	Θ= 90	Θ=120	Θ=135	Θ=150	Θ=180
Series 4	-0.361402	-0.532326	-0.568835	-0.41859	-0.083227	0.210968	0.342858	0.395695	0.354541
Face C	-0.285025	-0.424483	-0.480192	-0.351088	-0.088165	0.189246	0.292742	0.267073	-0.045898
Face B	-0.171643	-0.383955	-0.433396	-0.320596	-0.088458	0.171624	0.266606	0.236079	0.0121067
Face A	-0.404457	-0.478546	-0.448482	-0.284944	-0.081714	0.141617	0.212634	0.163668	-0.110352

Fig. 3.186 Cpi for roof angle 30° and spacing=b

Spacing =3b/2

Table 3.30 Coefficient of Pressure (C_{pext}) at Slope Angle = 30°, Spacing 3b/2

C_{pint}	**Face A**	**Face B**	**Face C**	**Face D**
Ɵ = 0°	0.250402	0.0438183	0.00480408	-0.0427009
Ɵ =30°	0.267231	0.181373	0.189702	0.170528
Ɵ = 45°	0.228624	0.201167	0.191809	0.168696
Ɵ =60 °	0.105604	0.0831962	0.0733143	0.0602771
Ɵ =90°	-0.118279	-0.123645	-0.121872	-0.113321
Ɵ =120°	-0.630906	-0.56166	-0.528385	-0.48171
Ɵ =135°	-0.800761	-0.713414	-0.671606	-0.631021
Ɵ =150°	-0.623318	-0.523329	-0.525724	-0.517236
Ɵ =180 °	-0.408153	-0.323728	-0.182615	-0.396753

Table 3.31 Coefficient of Pressure (C_{pint}) at Slope Angle = 30°, Spacing 3b/2

C_{pint}	**Face A**	**Face B**	**Face C**	**Face D**
Ɵ = 0°	-0.368142	-0.192928	-0.323595	-0.384051
Ɵ =30°	-0.481933	-0.434326	-0.475702	-0.567978
Ɵ = 45°	-0.469893	-0.510061	-0.554756	-0.634713
Ɵ =60 °	-0.30647	-0.346109	-0.374343	-0.423404
Ɵ =90°	-0.0764857	-0.0809966	-0.0813259	-0.0777732
Ɵ =120°	0.149027	0.175039	0.190176	0.202372
Ɵ =135°	0.239999	0.280856	0.302434	0.325681
Ɵ =150°	0.208747	0.268376	0.295638	0.365863
Ɵ =180 °	-0.112584	-0.0162677	0.0429218	0.347811

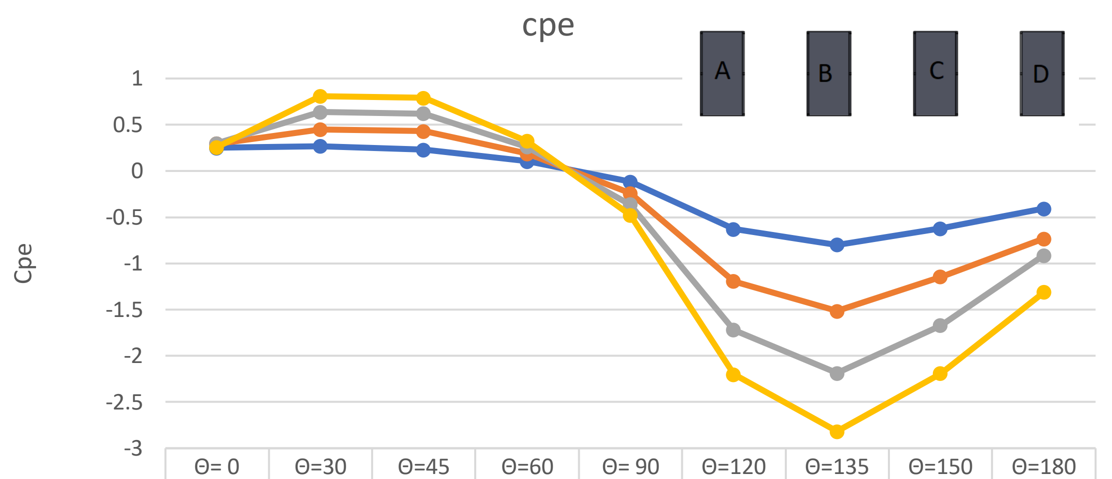

	Θ= 0	Θ=30	Θ=45	Θ=60	Θ= 90	Θ=120	Θ=135	Θ=150	Θ=180
Series 4	-0.042701	0.170528	0.168696	0.0602771	-0.113321	-0.48171	-0.631021	-0.517236	-0.396753
Face C	0.0048041	0.189702	0.191809	0.0733143	-0.121872	-0.528385	-0.671606	-0.525724	-0.182615
Face B	0.0438183	0.181373	0.201167	0.0831962	-0.123645	-0.56166	-0.713414	-0.523329	-0.323728
Face A	0.250402	0.267231	0.228624	0.105604	-0.118279	-0.630906	-0.800761	-0.623318	-0.408153

Fig. 3.187 Cpe for roof angle 30° and spacing=3b/2

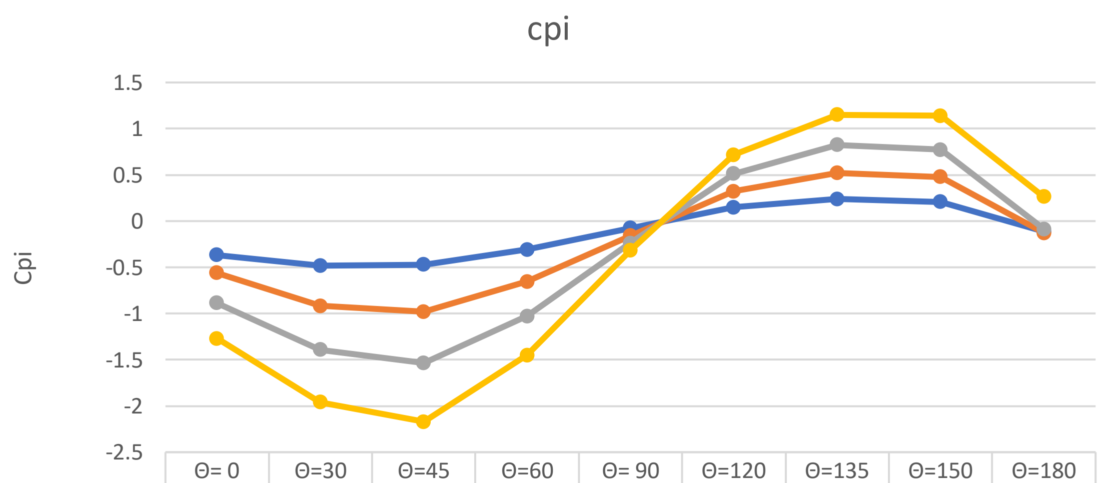

	Θ= 0	Θ=30	Θ=45	Θ=60	Θ= 90	Θ=120	Θ=135	Θ=150	Θ=180
Series 4	-0.384051	-0.567978	-0.634713	-0.423404	-0.077773	0.202372	0.325681	0.365863	0.347811
Face C	-0.323595	-0.475702	-0.554756	-0.374343	-0.081326	0.190176	0.302434	0.295638	0.0429218
Face B	-0.192928	-0.434326	-0.510061	-0.346109	-0.080997	0.175039	0.280856	0.268376	-0.016268
Face A	-0.368142	-0.481933	-0.469893	-0.30647	-0.076486	0.149027	0.239999	0.208747	-0.112584

Fig. 3.188 Cpi for roof angle 30° and spacing=3b/2

Spacing =2b

Table 3.32 Coefficient of Pressure (C_{pext}) at Slope Angle = 30°, Spacing 2b

C_{pint}	**Face A**	**Face B**	**Face C**	**Face D**
Ɵ = 0°	0.25111	0.0862572	0.00275376	-0.0227956
Ɵ =30°	0.256916	0.21791	0.21924	0.201359
Ɵ = 45°	0.22273	0.208554	0.196752	0.175402
Ɵ =60 °	0.10357	0.0851471	0.0747086	0.0641068
Ɵ =90°	-0.114405	-0.117879	-0.117073	-0.0758244
Ɵ =120°	-0.623507	-0.572543	-0.544818	-0.503577
Ɵ =135°	-0.812496	-0.737221	-0.70053	-0.661404
Ɵ =150°	-0.566988	-0.518417	-0.540827	-0.534329
Ɵ =180 °	-0.428671	-0.357567	-0.239453	-0.397392

Table 3.33 Coefficient of Pressure (C_{pint}) at Slope Angle = 30°, Spacing 2b

C_{pint}	**Face A**	**Face B**	**Face C**	**Face D**
Ɵ = 0°	-0.370666	-0.258456	-0.361625	-0.400739
Ɵ =30°	-0.48089	-0.476244	-0.513508	-0.594987
Ɵ = 45°	-0.490588	-0.541777	-0.579964	-0.639476
Ɵ =60 °	-0.322418	-0.357193	-0.379812	-0.417671
Ɵ =90°	-0.0748972	-0.078592	-0.0800433	-0.0758244
Ɵ =120°	0.149992	0.172887	0.184668	0.196455
Ɵ =135°	0.247616	0.280157	0.300061	0.317754
Ɵ =150°	0.22047	0.273858	0.302678	0.347785
Ɵ =180 °	-0.0916455	-0.0288517	0.070679	0.346976

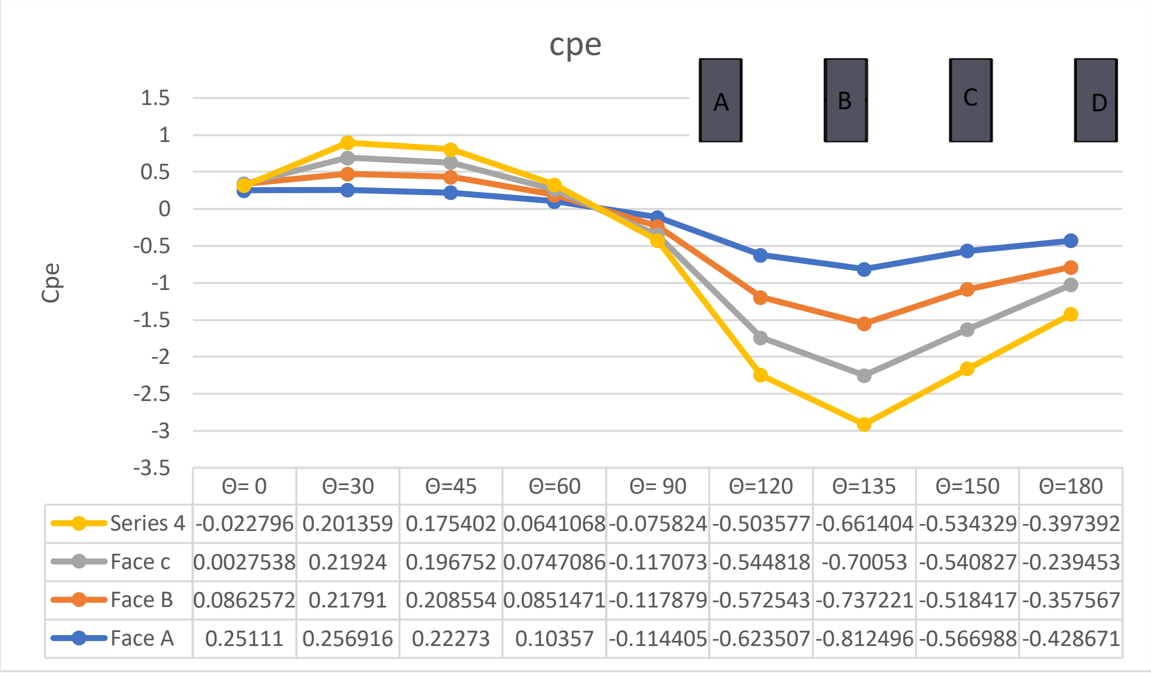

	Θ= 0	Θ=30	Θ=45	Θ=60	Θ= 90	Θ=120	Θ=135	Θ=150	Θ=180
Series 4	-0.022796	0.201359	0.175402	0.0641068	-0.075824	-0.503577	-0.661404	-0.534329	-0.397392
Face c	0.0027538	0.21924	0.196752	0.0747086	-0.117073	-0.544818	-0.70053	-0.540827	-0.239453
Face B	0.0862572	0.21791	0.208554	0.0851471	-0.117879	-0.572543	-0.737221	-0.518417	-0.357567
Face A	0.25111	0.256916	0.22273	0.10357	-0.114405	-0.623507	-0.812496	-0.566988	-0.428671

Fig. 3.189 Cpe for roof angle 30° and spacing=2b

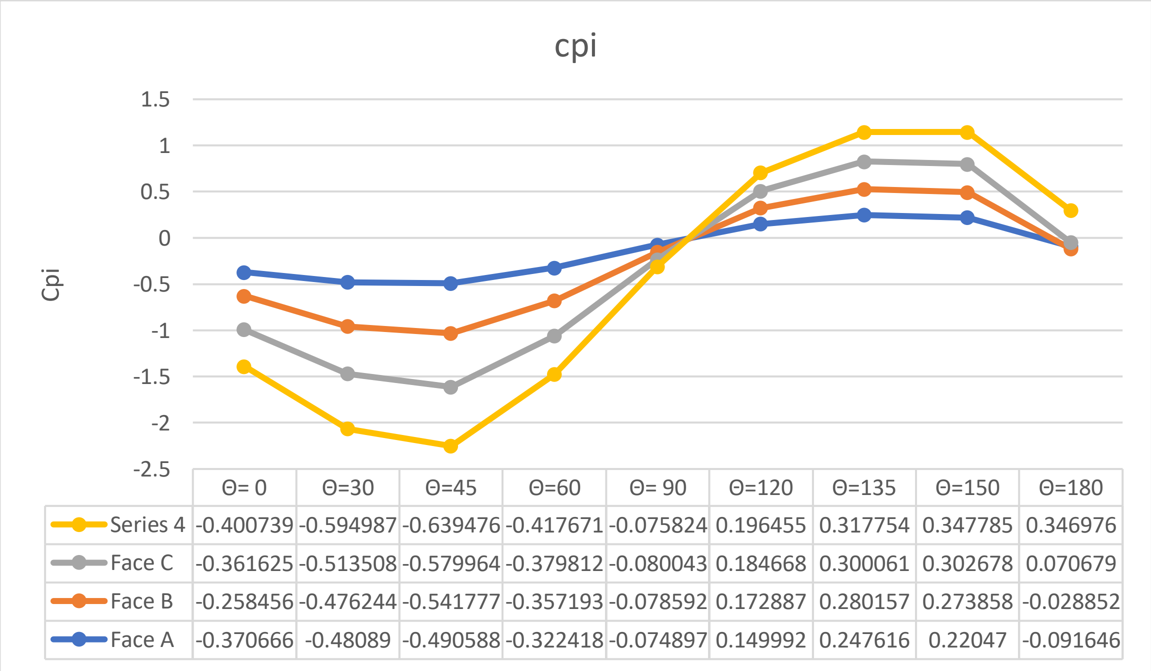

	Θ= 0	Θ=30	Θ=45	Θ=60	Θ= 90	Θ=120	Θ=135	Θ=150	Θ=180
Series 4	-0.400739	-0.594987	-0.639476	-0.417671	-0.075824	0.196455	0.317754	0.347785	0.346976
Face C	-0.361625	-0.513508	-0.579964	-0.379812	-0.080043	0.184668	0.300061	0.302678	0.070679
Face B	-0.258456	-0.476244	-0.541777	-0.357193	-0.078592	0.172887	0.280157	0.273858	-0.028852
Face A	-0.370666	-0.48089	-0.490588	-0.322418	-0.074897	0.149992	0.247616	0.22047	-0.091646

Fig. 3.190 Cpi for roof angle 30° and spacing=2b

CHAPTER
CONCLUSION

- By varying the roof slope angle, a considerable increase in the coefficient of pressure can be seen. Thus increase in the Cp can be seen from the roof slope from 10^0 to 20^0 and then from 20^0 to 30^0 accordingly.
- The coefficient of pressure due to interference effect can be comparatively higher from wind direction 90^0 to 180^0 as compared to wind direction 0^0 to 90^0 can be seen due to shielding effect.
- Value of Cp increases with roof slope angle.
- The coefficient of internal pressure is maximum for the front building as compared to other ones. The value of internal Cp is maximum for the wind direction 0^0 and minimum for the wind direction 90^0 and then increases from there.

REFERENCES

[1] Adam B. Smith, "A landmark decade of U.S. Billion-Dollar Weather and climatic Disasters", *NOAA's National Center for Environmental Information*, (2019).

[2] Storm Severe, Winter Storm and Severe Storm, National Climatic Data Billion-Dollar Weather and Climate Disasters : *Summary Stats, https://www.ncdc.noaa.gov/billions/summarystats*/US/2000-2017 (2017).

[3] J.D. Holmes (1988). "DISTRIBUTION OF PEAK WIND LOADS ON A LOW-RISE BUILDING". *Journal of Wind Engineering and Industrial Aerodynamics*, 29 (1988) 59-67.

[4] Hoxey, R.P., Robertson, A.P., Basara, B., and Younis, B.A. (1993). "Geometric parameters that affect wind loads on low-rise buildings: full-scale and CFD experiments." *Journal of Wind Engineering and Industrial Aerodynamics*, 50: 243-252.

[5] Krishna, P. (1995). "Wind loads on low rise buildings". *Journal of Wind Engineering and Industrial Aerodynamics*, 54-55: 383-396.

[6] T. Stathopoulos, (1996). "Design wind pressure coefficients for mono-slope roofs: A time series approach". *Journal of Wind Engineering and Industrial Aerodynamics* 65 (1996) 143-153.

[7] Masanao Nakayama, (1998). "An efficient method for selection of vibration modes contributory to wind response on dome-like roofs". *Journal of Wind Engineering*, 73 (1998) 31-43.

[8] C.W. Letchford, (2000). “Mean wind loads on porous canopy roofs”. *Journal of Wind Engineering and Industrial Aerodynamics*. 84 (2000) 197-213.

[9] P. Montes, (2001). “Behaviour of a hemispherical dome subjected to wind loading”. *Journal of Wind Engineering and Industrial Aerodynamics* 89 (2001) 911–924.

[10] C.M. Chen, (2010). “Characteristic of wind loads on a hemispherical dome in smooth flow and turbulent boundary layer flow”. *J. Wind Eng. Ind. Aerodyn*. 98 (2010) 328–344.

[11] Augusto Poitevin, (2013). “Pressures on open canopy structures with parapets under wind loading”. *Engineering Structures*. 56 (2013) 850-867.

[12] Yan Zhang, (2014). “Comparison of microburst-wind loads on low-rise structures of various geometric shapes”. *J. Wind Eng. Ind. Aerodyn*. 133 (2014) 181–190.

[13] ASTHA VERMA and ASHOK KUMAR AHUJA (2015). “WIND PRESSURE DISTRIBUTION ON LOW-RISE BUILDINGS WITH CYLINDRICAL ROOFS”. *ISEC* ISBN: 978-0-9960437-1-7.

[14] Rocky Patel, (2015). “Determination of Optimum Domain Size for 3D Numerical Simulation in ANSYS CFX”. *IJIRST* Vol. 4, Issue 6, June 2015.

[15] Singh, J., and Roy, A.K. (2021). “Wind loads on roof of low-rise buildings.” *Disaster Advances* 14(5):83-98.

[16] Jagbir Singh and Amrit Kumar Roy, “CFD simulation of the wind field around pyramidal roofed single-story buildings.” *Springer Nature Switzerland AG* 2019.

[17] Roy, A.K., Ahuja, A.K., and Gupta, V.K. (2010). "Variation of wind pressure on Canopy-Roofs." *International Journal of Earth Sciences and Engineering* 03(02):19-30.

[18] Alireza Fiouz, (2012). "Effect of wind loading on spherical single layer space truss steel domes". *International Journal of Physical Sciences* Vol. 7(16), pp. 2493 - 2505, 16 April, 2012.

[19] Xingqian Peng, (2012). "Analysis of wind load effect on the roof of low-rise building in the mountain Terrain". *Advanced Materials Research* Vol. 382 (2012) pp 176-182.

[20] Ashish Agarwal, (2017). "Numerical study of lift and drag coefficients on a ground-mounted photo-voltaic solar panel". *Science Direct.* Proceedings 4 (2017) 9822–9827.

[21] Fabio Rizzo, (2017). "Design pressure coefficients for circular and elliptical plan structures with hyperbolic paraboloid roof". *Engineering Structures* 139 (2017) 153–169.

[22] Gang Li, (2017). "Wind-induced interference effects on low-rise buildings with gable roof". *Journal of Wind Engineering & Industrial Aerodynamics*. 170(2017) 94-106.

[23] Majdi Yousef (2017). "A Comparison of Force and Pressure Coefficients on Dome, Cube and Prism Shaped Buildings due to Straight and Tornadic Wind Using Three Dimensional Computational Fluids Dynamics". *Ph. D Thesis*, University of Al- Mukhtar.

[24] Rani, N., and Ahuja, A.K. (2017). "Wind Loads on Multi-Span Mono-Slope Canopy Roof". *Urbanization Challenges in Emerging Economies, ASCE India Conference*, December 12–14, 2017, New Delhi, India.

[25] Verma, A., and Ahuja, A.K. (2015). “Wind Pressure Distribution on Rectangular Plan Buildings with Multiple Domes.” *International Journal of Engineering and Technical Research*, 3(7): 129-133.

[26] Singh, J., and Roy, A.K. (2019). “Effects of roof slope and wind direction on wind pressure distribution on the roof of a square plan pyramidal low-rise building using CFD simulation.” *International Journal of Advanced Structural Engineering*, 11: 231–254.

[27] Tiantian Li, (2019). “Dynamic structural responses of long-span dome structures induced by tornadoes”. *Journal of Wind Engineering & Industrial Aerodynamics*. 190(2019) 293-308.

[28] Zhixiang Liu, (2019). “An investigation on external airflow around low-rise building with various roof types: PIV measurements and LES simulations”. *Building and Environment*, https://doi.org/10.1016/j.buildenv.2019.106583.

[29] M.B. Natalini, C. Morel and B. Natalini (2013). “Mean loads on vaulted canopy roofs”. *Journal of Wind Engineering and Industrial Aerodynamics*, 119(2013) 102-113.

[30] Bo Chen, (2018). “Wind interference effects of high-rise building on low-rise building with flat roof”. *Journal of Wind Engineering & Industrial Aerodynamics* 183 (2018) 88-113.

[31] Singh, J., and Roy, A.K. (2018). “Wind Pressure Coefficients on Pyramidal Roof of Square Plan Low Rise Double Storey Building.” *Computational Engineering and Physical Modeling*, 2(1): 1-16.

[32] Nourhan Sayed Fouad, (2018). “Comparative study of international codes wind loads and CFD results for low rise buildings”. *Alexandria Engineering Journal*.

[33] Juliya Mironova (2020). “Wind impact on low-rise buildings when placing high-rises into the existing development”. *Materials Science and Engineering* 890 (2020) 012055.

[34] Sakib, F.A., Stathopoulos, T., and Bhowmick, A.K. (2021). “A review of wind loads on canopies attached to walls of low-rise buildings.” *Engineering Structures*, 230(9): 111656

[35] Sanyal, P., and Dalui, S.K. (2020). “Effects of side ratio for ‘Y’ plan shaped tall building under wind load.” *Wind and Structures An International Journal* 30(3):145-160

[36] R.H. Ong, (2020). “Numerical simulation of wind-induced mean and peak pressures around a low-rise structure”. *Engineering Structures.* 214 (2020)110583.

[37] Suman Kumar Laha, (2020). “Analysis of mechanical stress and structural deformation on a solar photovoltaic panel through various wind loads”. *Springer-Verlag GmbH Germany*. https://doi.org/10.1007/s00542-020-05142-8.